

The Preston Geothermal Prospect:
Re-examining a Previously Studied Geothermal Area

A Thesis

Presented in Partial Fulfillment of the Requirements for the

Degree of Master of Science

with a

Major in Hydrology

in the

College of Graduate Studies

University of Idaho

by

Wade C. Worthing

Major Professor: Thomas R. Wood, Ph.D.

Committee Members: Jerry Fairley, Ph.D, James St. Clair, Ph.D.

Department Administrator: Mickey Gunter, Ph.D.

June 2016

AUTHORIZATION TO SUBMIT

This thesis of Wade Worthing, submitted for the degree of Master of Science with a Major in Hydrology and titled “The Preston Geothermal Prospect, Re-examining a Previously Studied Geothermal Area,” has been reviewed in final form. Permission, as indicated by the signatures and dates below, is now granted to submit final copies to the College of Graduate Studies for approval.

Major Professor: _____ Date: _____
Thomas R. Wood, Ph.D.

Committee Members: _____ Date: _____
Jerry Fairley, Ph.D.

_____ Date: _____
James St. Clair, Ph.D.

Department
Administrator: _____ Date: _____
Mickey Gunter, Ph.D.

ABSTRACT

The Preston geothermal prospect is centered on Clifton Hill, located in the Cache Valley, a north-south trending structural graben of the northeastern portion of the Basin and Range Province, just south of the border with the Eastern Snake River Plain (ESRP). Though studied previously during the 1970s and 80s, interests were abandoned. Today, the local geothermal system in the area remains poorly defined. To better define the local fault system, high resolution potential field (gravity and magnetic) studies were conducted, including data along several profiles across Clifton Hill. These data were combined with a survey of the local aquifer and analyzed to better understand the geothermal system. Updated fault interpretation and temperatures indicate upwelling thermal fluids interact with local groundwater in the southwest portion of the study area, and that thermal waters may be traveling along additional undefined faults.

ACKNOWLEDGEMENTS

I would like to thank Dr. Tom Wood for his guidance, support and expertise throughout the last two years. The assistance of Dr. Jonathan Glen and Brent Ritzinger of the United States Geological Survey have also been invaluable in the planning of geophysical surveys and analysis of data. I would also like to thank Travis McLing, Dr. James St. Clair, Dr. Hari Neupane and Dr. Patrick F. Dobson for their support and technical advice and guidance. I thank David Bosen for allowing me to hike all over his property and Clifton Hill to collect data.

DEDICATION

For my mother and father who have always supported me.

TABLE OF CONTENTS

AUTHORIZATION TO SUBMIT	ii
ABSTRACT.....	iii
ACKNOWLEDGEMENTS.....	iv
DEDICATION.....	v
TABLE OF CONTENTS.....	vi
LIST OF FIGURES	viii
LIST OF TABLES.....	xiii
CHAPTER 1 : HISTORY, GEOLOGY AND GEOCHEMISTRY.....	1
SCIENTIFIC HISTORY.....	2
GEOLOGIC SETTING.....	10
LOCAL GEOLOGY	13
GEOCHEMISTRY.....	20
CHAPTER 2 : NEW RESEARCH.....	23
NEW SURVEYS.....	23
MAGNETICS.....	24
GRAVITY.....	29
SHALLOW AQUIFER SURVEY	32
CHAPTER 3 DATA AND DISCUSSION.....	35
MAGNETIC DATA.....	36
GRAVITY DATA.....	37
SHALLOW AQUIFER DATA.....	38
MAGNETIC AND GRAVITY MODELS.....	41
STRUCTURAL ANALYSIS.....	56
AQUIFER TEMPERATURE AND WATER LEVEL DATA.....	58

PERMEABLE FAULT STRUCTURES.....	71
CHAPTER 4 SUMMARY AND RECOMMENDATIONS	77
SUMMARY	77
RECOMMENDATIONS	79
REFERENCES	82
APPENDIX A : GRAVITY BASE STATION ESTABLISHMENT.....	88
APPENDIX B : ROCK SAMPLING AND SUSCEPTIBILITY FIELD MEASUREMENTS	93
SUSCEPTIBILITY FIELD MEASUREMENTS	113
APPENDIX C : LABORATORY DENSITY MEASUREMENTS.....	116

LIST OF FIGURES

Figure 1.1. The Cache Valley of Southeastern Idaho and Northern Utah.	1
Figure 1.2. The North Cache Valley of Southeastern Idaho with local communities and range-bounding faults.	2
Figure 1.3. Sunedco deep test wells from the late 1970's, and vicinity to local hot springs and the newly drilled Bosen well.....	4
Figure 1.4. Sunedco deep temperature boreholes from the late 1970s.	5
Figure 1.5. Chevron deep temperature boreholes of the late 1970's.	6
Figure 1.6. Corresponding data for wells and springs compiled by Wood et al (2015) from previous studies. Wood et al, 2011	8
Figure 1.7. Extent of the Sevier fold-thrust belt (Sevier orogenic belt) in relation to the western United States and Canadian Provinces. The North Cache Valley lies within a range of the fold-thrust belt referred to locally as the Idaho Thrust belt, following the eastern border of Idaho with the western borders of Wyoming and Montana. Abbreviations are as follows: CRO, Coast Range ophiolite; LFTB, Luning-Fencemaker thrust belt; CNTB, Central Nevada thrust belt; WH, Wasatch hinge line; UU, Uinta Mountains uplift; CMB, Crazy Mountains basin; PRB, Powder River basin; DB, Denver basin; RB, Raton basin. Modified from DeCelles, 2004.....	10
Figure 1.8. Extent and borders of the Basin and Range Province, nearby bordering geologic provinces and the Intermountain Seismic Zone in the Western USA. The Intermountain Seismic Zone extends from Canada south to southern Nevada.....	12
Figure 1.9. Geologic map of the North Cache Valley. Study area indicated by red oval. After Wood et al, 2015.....	14
Figure 1.10. Extent of the Mink Creek-Bear River Lineament in the NCV.....	15
Figure 1.11. Geologic map of Clifton Hill. Modified from Link and LeFebre, 1983.	17
Figure 1.12. Piper diagram mapping the springs and wells of the NCV. Wayland and Battle Creek hot springs are hidden by the cluster of samples plotting on the extreme right hand side of the diagram (Wood et al, 2015).....	21
Figure 1.13. Giggenbach diagram depicting spring and well water of the NCV (Wood et al, 2015).....	22

Figure 2.1. Cross-sectional diagram depicting horst and graben structure and behavior typical of the Basin and Range province. Source: http://geology.isu.edu/Alamo/devonian/basin_range.php	24
Figure 2.2. Location of the magnetics base station used for the duration of the magnetics survey.....	27
Figure 2.3. Locations and extent of magnetics lines collected for analysis.....	28
Figure 2.4. Locations of gravity stations occupied during the gravity survey.....	31
Figure 2.5. Wells chosen for new water level and temperature survey.	33
Figure 2.6. Wells previously measured for temperature and water level, McGreevey & Bjorklund, 1970.	34
Figure 3.1. Gridded magnetic data collected across the survey area. Additional lines are included in the southwestern portion of the study area which were did not cross any structures of interest and so were analyzed for the purposes of this thesis.....	36
Figure 3.2. Gridded isostatic gravity data collected over the survey area. Additional lines are included in the southwestern portion of the study area which were did not cross any structures of interest and so were analyzed for the purposes of this thesis.....	38
Figure 3.3. Contoured water level map of the study area. Water level values are in meters above mean sea level (AMSL). Ground water flow in the valley is towards the Bear River. Fault system layout has been updated based on interpretation of geophysical models.....	39
Figure 3.4. Well temperatures from the shallow depth range (1,439 to 1,354 m). Red dots indicate temperatures measured in wells (with the exception of two hot springs temperatures included along the Bear River) and are graduated based on the temperature value, i.e. higher temperatures corresponds to a larger circle. Fault system layout has been updated based on interpretation of geophysical models.....	40
Figure 3.5. Well temperatures from the shallow depth range (1,439 to 1,354 m). Red dots indicate temperatures measured in wells (with the exception of two hot springs temperatures included along the Bear River) and are graduated based on the temperature value, i.e. higher temperatures corresponds to a larger circle. Fault system layout has been updated based on interpretation of geophysical models.....	41
Figure 3.6. Geophysical model fitted to the magnetic and gravity data for line 2. Magnetic error: 4.74 nT; Gravity error: 0.091 mGal. Vertical Exageration = 0.75.....	44

Figure 3.7. Geophysical model fitted to the magnetic and gravity data for line 3. Magnetic error: 2.395 nT; Gravity error: 1.045 mGal. Vertical Exageration = 1.25.....	46
Figure 3.8. Geophysical model fitted to the magnetic and gravity data for line 4. Magnetic error: 0.855 nT; Gravity error: 2.388 mGal. Vertical Exageration = 0.75.....	48
Figure 3.9. Geophysical model fitted to the magnetic and gravity data for line 6. Magnetic error: 0.229 nT; Gravity error: 1.48 mGal. Vertical Exageration = 0.75.....	50
Figure 3.10. Geophysical model fitted to the magnetic and gravity data for line 7. Magnetic error: 9.189 nT; Gravity error: 0.894 mGal. Vertical Exageration = 3.5.....	52
Figure 3.11. Geophysical model fitted to the magnetic and gravity data for line 8. Magnetic error: 1.245 nT; Gravity error: 0.313 mGal. Vertical Exageration = 1.5.....	54
Figure 3.12. Updated fault layout for the Clifton Hill bounding faults based on interpretation and modeling of potential field measurements taken from the area.	56
Figure 3.13. Position of the Stock 1 and Stocks 1-A wells and the distances separating them perpendicularly from the Clifton Hill bounding faults.	57
Figure 3.14. Temperature (Celsius) contours in the Shallow depth range of the Clifton Hill geothermal prospect. Deflection of the toe of the plume to the sw may be caused by the flux of ground water down the axis of the Bear River Valley.	61
Figure 3.15. Temperature contours in the deep depth range of the Clifton Hill geothermal prospect. Deflection of the toe of the plume to the sw may be caused by the flux of ground water down the axis of the Bear River Valley.	62
Figure 3.16. Temperature gradient profile for Sunedco test well 2-78-7.	64
Figure 3.17. Temperature gradient exemplifying an outflow plume pattern and temperature reversal at approximately 350 ft. The inflection point at which the temperature reaches a maximum is indicative of the depth at which a permeable lateral flow layer exists. After Shevenell et al, 2012.	66
Figure 3.18. Temperature gradient profile for the Stock 1 well (2-78-1001).	67
Figure 3.19. Temperature gradient profile for Sunedco test well 2-78-9.	68
Figure 3.20. Temperature gradient profile for Sunedco test well 2-78-1002.	69
Figure 3.21. Temperature gradient profile for Sunedco test well 2-78-8.	70
Figure 3.22. Example of step-over faults, a favorable structure of permeability caused by small faults translating stress from one fault to another. Modified from Faulds et al, 2011..	72

Figure 3.23. Yellow ovals indicates possible location of step-over faults. These faults increase permeability in the shallow subsurface while translating stress from one fault to another. Geothermal fluids often use these permeable zones as flow conduits. Labels correspond to the faults: NW – Northwest fault, Middle West – Middle West fault, SW – Southwest fault, NE – Northeast fault, SE – Southeast fault, W-E – West-East trending bounding fault, W – West bounding fault, E – East bounding fault.	73
Figure 3.24. Conceptual model of the interaction of the Mink Creek-Bear River lineament with the southern extension of the Clifton Hill bounding faults. Here the structure of the lineament is depicted as being nearly vertical, and the type and direction of movement is unknown. After Mitchell, 1976.....	74
Figure 4.1. Current interpretation of fault positions and orientations surrounding Clifton Hill. Yellow circle indicates recommended location of new shallow temperature wells.	81
Figure A.1. Locations of the Preston, ID Federal Post Office and the Salt Lake City BM8 base station, relative to one another.....	89
Figure A.2. Information sheet for the Salt Lake City BM8 gravity base station.....	90
Figure A.3. Information sheet for Preston, ID gravity base station.....	91
Figure B.1. Locations where rock samples (RS-####) and pictures (Pic#####) were taken and descriptions incorporated into the appendix were observed (Desc-###).....	94
Figure B.2. Meta-dabase, samples 001, 002 & 003 are of this type (Figure B.1: picture 2508).	95
Figure B.3. Meta-dabase, samples 001, 002 & 003 are of this type (Figure B.1: picture 2509).	96
Figure B.4. Meta-dabase, samples 001, 002 & 003 are of this type (Figure B.1: picture 2511).	97
Figure B.5. Emplaced Argillite of the Scout Mountain Member of the Pocatello Formation (Figure B.1: picture 2513).....	98
Figure B.6. Meta-dabase float and possible outcrop along ridgeline of Clifton Hill (Figure B.1: picture 2514).	99
Figure B.7. Close up of Meta-dabase along ridgeline of Clifton Hill (Figure B.1: picture 2515).	99

Figure B.8. Small pieces of slate scattered among larger chunks of meta-d diabase (Figure B.1: picture 2516).	100
Figure B.9. Large chunk of slate (Figure B.1: picture 2517).	101
Figure B.10. Broken piece of slate that sample 006A&B were taken from (Figure B.1: picture 2519).	102
Figure B.11. Basalt of the Bannock Volcanic member of the Pocatello Formation, southernmost outcrop seen on Clifton Hill (Figure B.1: picture 2520).	103
Figure B.12. Argillite (Figure B.1: picture 2521).	103
Figure B.13. Argillite with iron pyrite crystals (Figure B.1: picture 2522).	104
Figure B.14. Bannock Volcanic Member outcrop near the ridgeline where magnetic and gravity line 3 crosses over Clifton Hill (Figure B.1: picture 2523).	105
Figure B.15. Bannock Volcanic member boulder (Figure B.1: picture 2524).	105
Figure B.16. Bannock Volcanic Member outcrop (Figure B.1: picture 2525).	106
Figure B.17. Bannock Volcanic Member outcrop (Figure B.1: picture 2526).	106
Figure B.18. Close up of Bannock volcanic member outcrop (Figure B.1: picture 2527).	107
Figure B.19. Bannock Volcanic member outcrop (Figure B.1: picture 2528).	108
Figure B.20. Metagreywacke or Argillite (Figure B.1: picture 2529).	109
Figure B.21. Basalt (Figure B.1: picture 2531).	110
Figure B.22. Basalt (Figure B.1: picture 2532).	111
Figure B.23. Basalt (Figure B.1: picture 2533).	111
Figure B.24. Basalt displaying "hummocky" surface texture (Figure B.1: picture 2534).	112
Figure B.25. Basalt displaying "hummocky" surface texture (Figure B.1: picture 2535).	112
Figure B.26. Locations of susceptibility field measurements taken along Clifton Hill.	114
Figure C.1. Denver Instrument XL6100 scale modified to make saturated mass measurements.	117
Figure C.2. Suspension linking the platform holding the saturated, submerged sample to a connection hook on the underside of the scale.	118
Figure C.3. Equation used to calculate the density of rock samples, where m_{dry} is the mass of the dry sample and m_{wet} is the mass of the saturated sample. Value of water density used was 1.0 g/cm^3 .	119

LIST OF TABLES

Table 1.1. Temperatures and chemical data for wells and springs of the North Cache Valley.	9
Table 3.1. Magnetic susceptibility ranges from measurements collected in the field, and density ranges from values measured in the laboratory. Density units are Kg/m ³ and susceptibility units are x10 ⁻³ SI. See Appendix B and C for more information.	35
Table 3.2. Names of wells and respective temperatures and elevations included in the deep temperature range.....	75
Table 3.3. Names of wells and respective temperatures and elevations included in the shallow temperature range.....	76
Table A.1. Base station tie-in data. Time is in military time, Reading, Tidal Correction and Corrected Reading values are in mGal.	92
Table B.1. Susceptibility measurements and average measurements organized by unit, taken in the field. The diabase rock type refers to the meta-diabase intrusive seen in the area. Color codes are green for meta-diabase, blue for Scout Mountain member of the Pocatello formation and red for the Bannock member of the Pocatello formation. Susceptibility units are SI.	115
Table C.1. Density values calculated for rock samples collected from Clifton Hill, near Preston, ID.	120

CHAPTER 1 : HISTORY, GEOLOGY AND GEOCHEMISTRY

The Cache Valley is a north trending valley stretching across the Idaho-Utah border in the northeastern extent of the Basin and Range province (Figure 1.1).

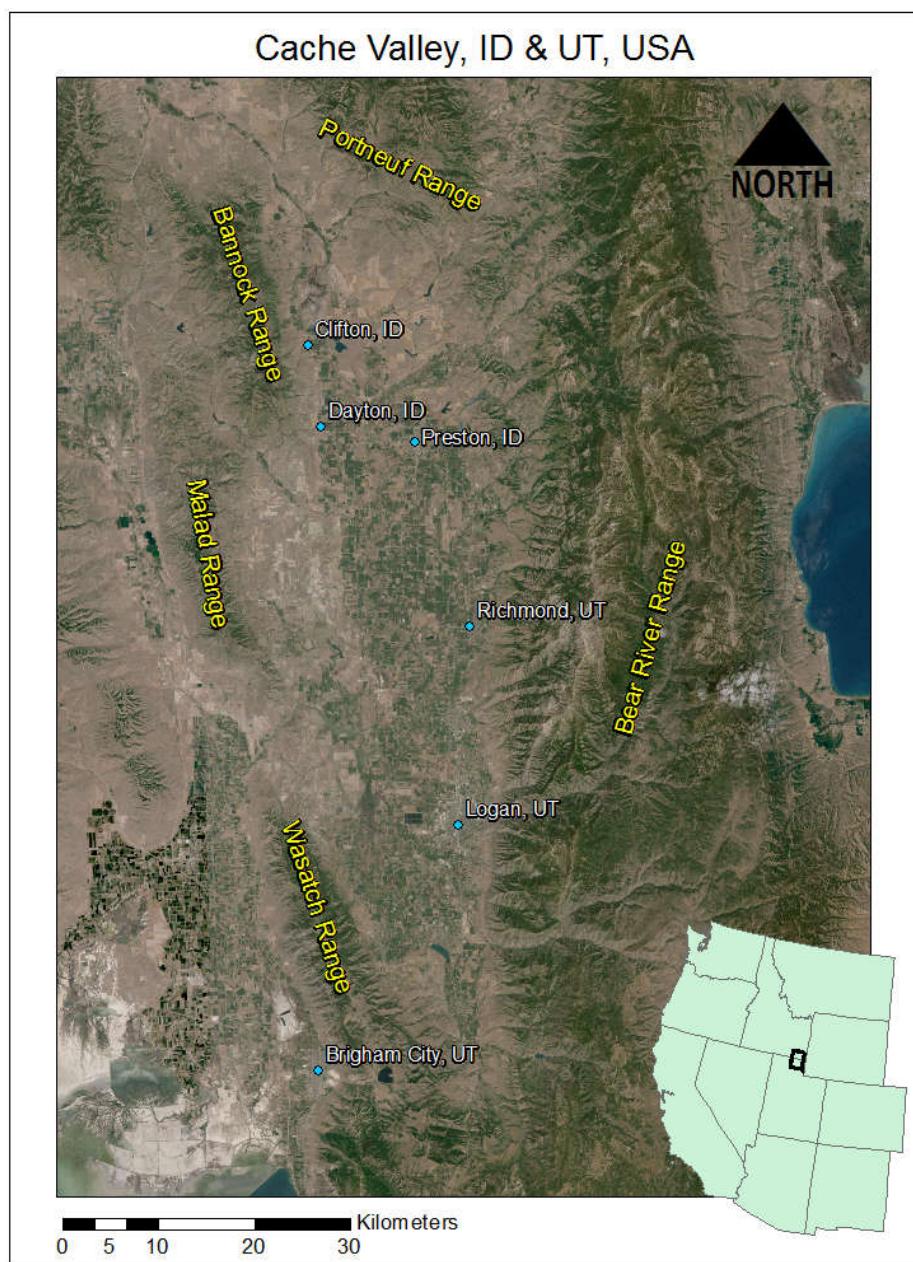


Figure 1.1. The Cache Valley of Southeastern Idaho and Northern Utah.

The North Cache Valley (NCV) is a portion of the Cache Valley that extends from Idaho's southern border with Utah to Red Rock Pass between the Portneuf and Bannock mountain ranges (Figure 1.2). The NCV displays hallmarks of a typical Basin and Range horst-graben complex, bounded on the east and west by large systems of normal faults, filled partially with quaternary sediments. The valley also possesses other common Basin and Range characteristics such as thermal springs.

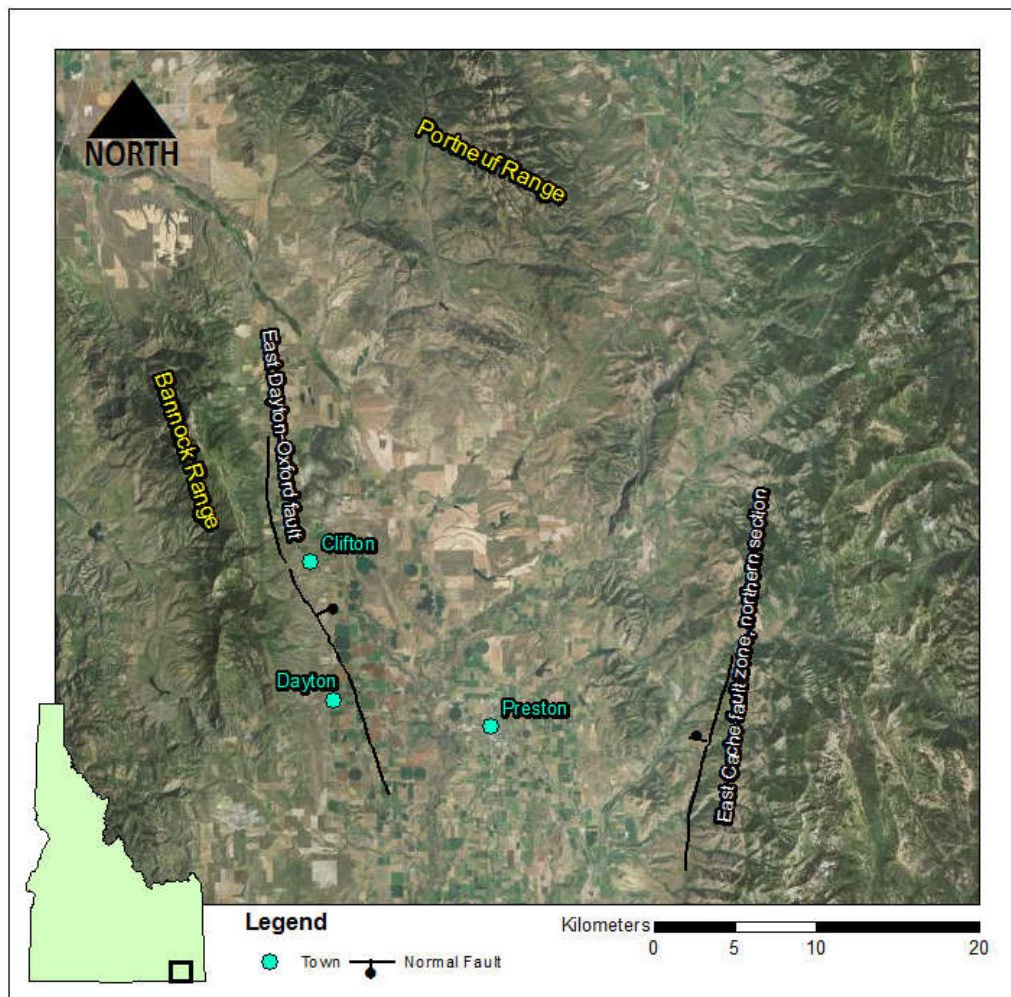


Figure 1.2. The North Cache Valley of Southeastern Idaho with local communities and range-bounding faults.

SCIENTIFIC HISTORY

Over 150 years ago, in the 1870s, the lithology of the North Cache Valley (NCV) and the presence of thermal springs were documented by the Hayden expedition while en route to the Yellowstone area (Hayden, 1872). This study, while important, was observational, and

intended to serve as a record of the expedition's experiences and encounters of the previously unexplored country being traveled through. Modern scientific study began over fifty years later, when Henry W. Coulter documented the stratigraphy and geology of the Bear River Range and the Cache Valley for a Yale University study (Coulter, 1956). This study was one of the first comprehensive investigations and records of the geological makeup of southeastern Idaho, and was recognized by the Idaho Bureau of Mines and Geology and adopted into their collection of geological literature on Idaho.

In 1962 Williams described the lasting influence of the prehistoric Lake Bonneville and its' role in the geomorphological development of the southern portion of the valley, extending into Utah (Williams, 1962). Lake Bonneville's lasting effects on the area and its' method of evacuation were later studied by Janecke and Oaks (2011) (Janecke & Oaks, 2011).

McGreevy and Bjorklund authored two papers for the U.S. Geological Survey summarizing the valley's hydrogeological data from hydrothermal expressions in 1970 and 1971 (McGreevy & Bjorklund, 1970; McGreevy & Bjorklund, 1971). Peterson and Oriel explored the subsurface of the valley using gravity (Peterson & Oriel, 1970). Between 1970 and 1981, samples of wells and springs were taken from the NCV as part of three separate reports, Young and Mitchell (1973), Mitchell (1976) and Ralston (1981). Robert Mitchell's 1976 Idaho Department of Water Resources (IDWR) report is the most comprehensive and detailed reference for thermal waters in the NCV. In the Mitchell (1976) study, seventeen samples were collected from the thermal waters of eight sites. The measured temperatures ranged from 35° C to 84° C with a mean temperature of 61° C.

Geothermal exploration of the valley began in earnest during the first geothermal boom of the 1970s. During this time, The Sunoco Energy Development Company (Sunedco) took a commercial interest in the valley, drilling two deep test wells in the central portion of the valley, near Clifton Hill (also known as Little Mountain), and 12 deep temperature boreholes in the surrounding area 10 of which will be discussed here (Figures 1.3, 1.4). Chevron also drilled a number of deep temperature holes in the area, though their exploration of the prospect was not as extensive as Sunedco's (Figure 1.5).

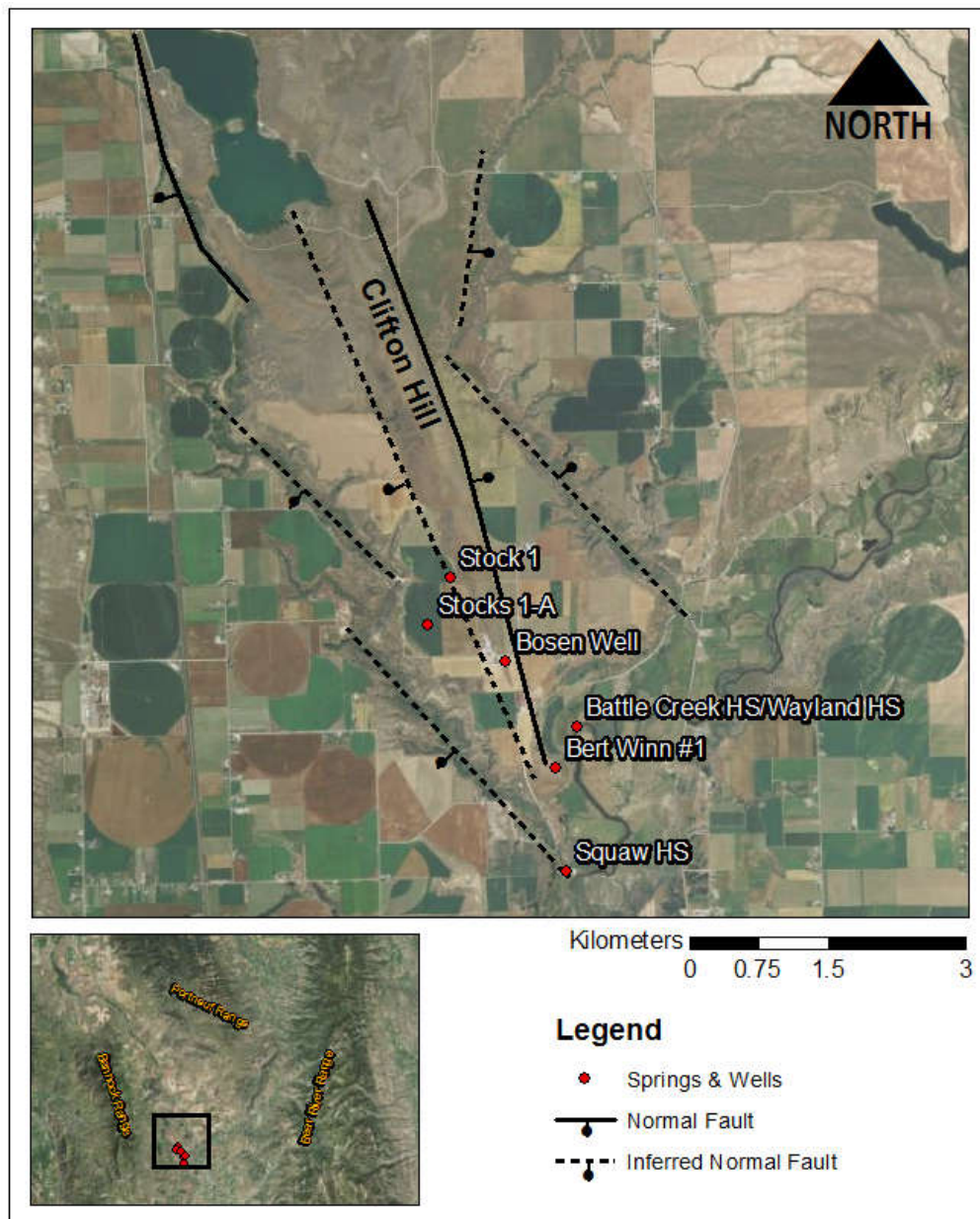


Figure 1.3. Sunedco deep test wells from the late 1970's, and vicinity to local hot springs and the newly drilled Bosen well.

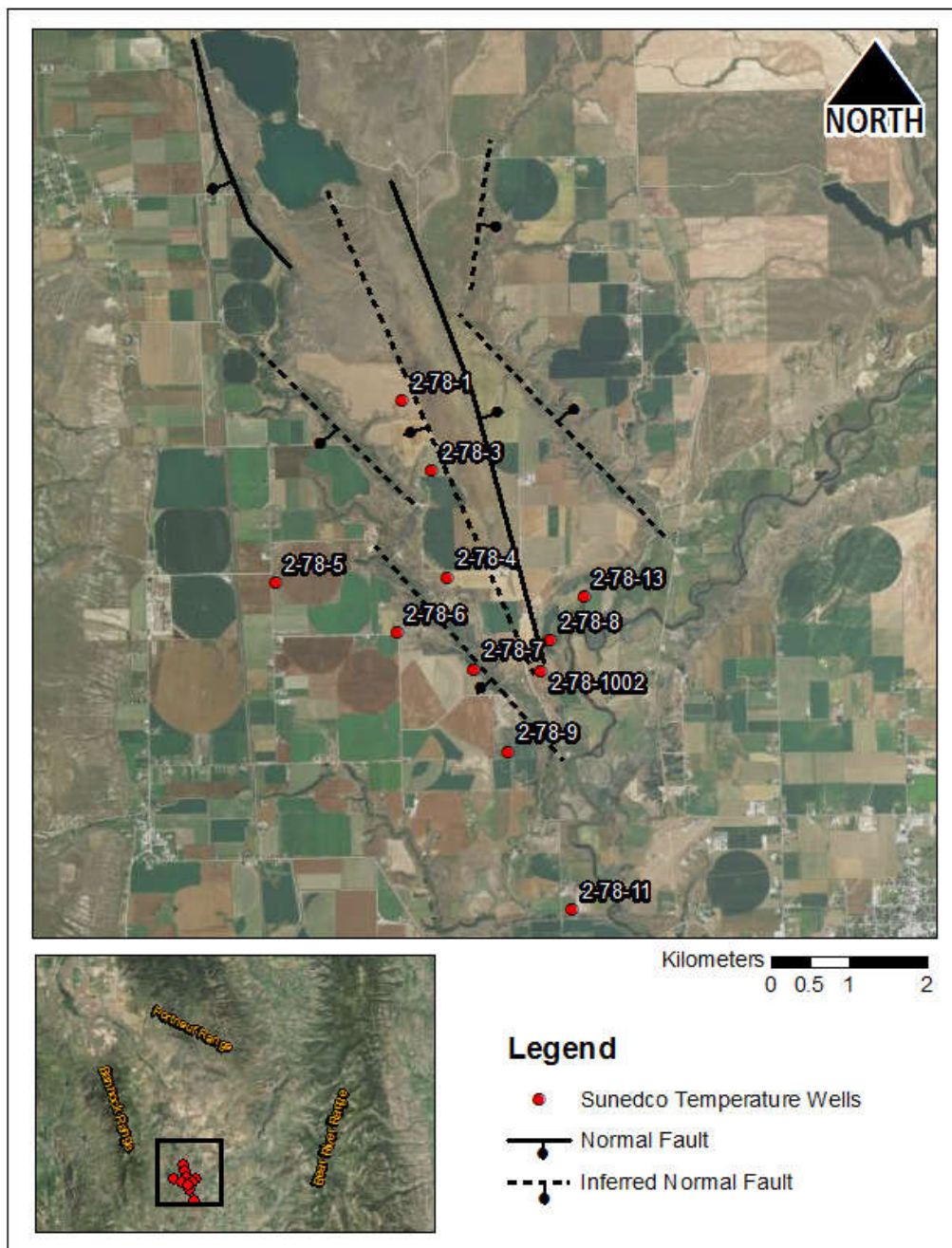


Figure 1.4. Sunedco deep temperature boreholes from the late 1970s.

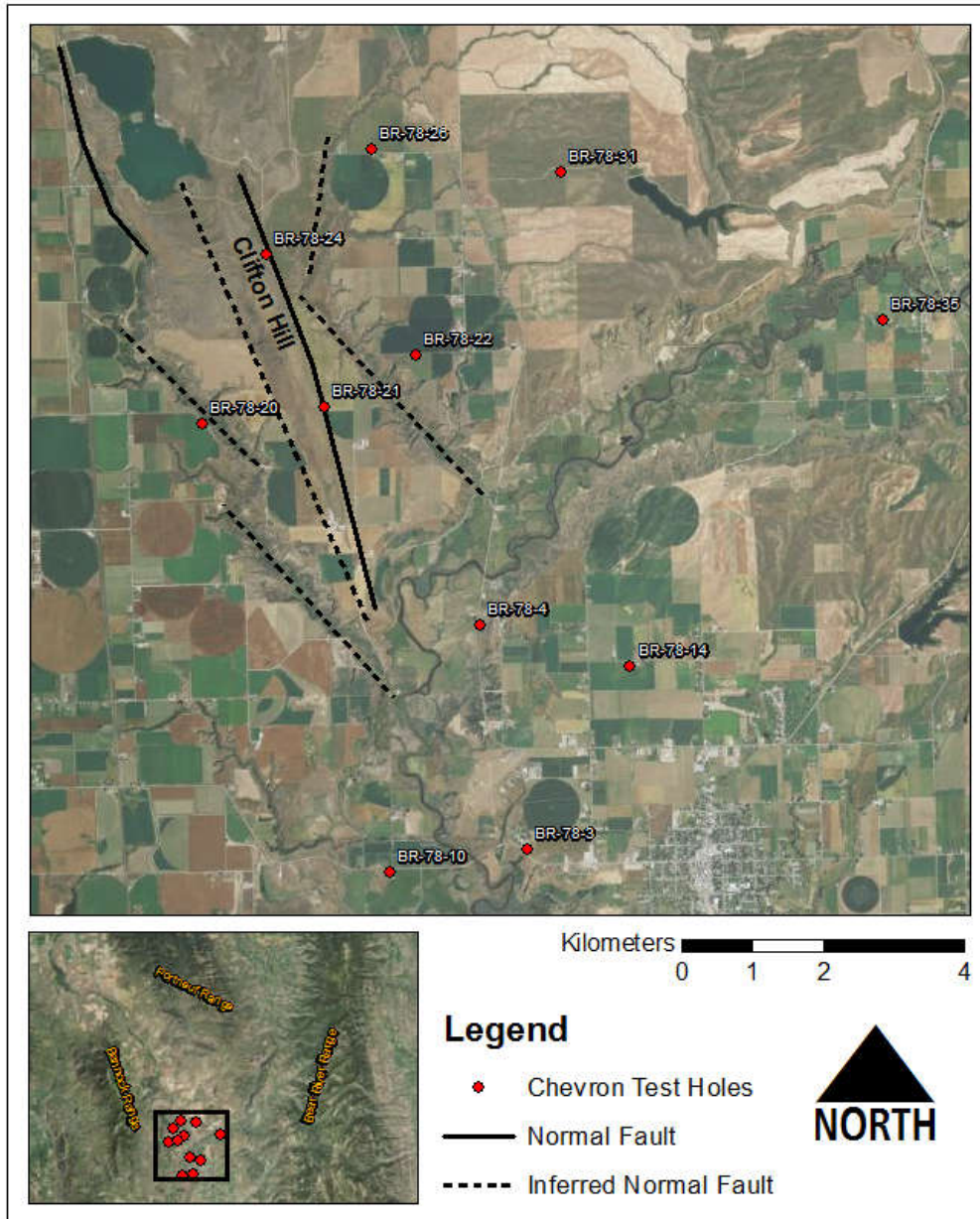


Figure 1.5. Chevron deep temperature boreholes of the late 1970's.

In this episode of exploration, the data and conclusions from Peterson & Oriol (1970) figured in heavily in the consideration of locations for test wells. The data collected by Peterson & Oriol (1970) is fairly low resolution, with large measurement spacing and valley wide data lines, but was nonetheless an important aid in the geothermal exploration of the Clifton Hill area. Test results and data from the Sunoco C. H. Stocks 1-A and Bert Winn #1 test wells are summarized by McIntyre and Koenig (McIntyre & Koenig, 1978; McIntyre & Koenig, 1980). It was determined that Bert Winn #1 did intersect the targeted bounding fault but no

permeable zone carrying large quantities of thermal fluids was discovered (McIntyre & Koenig, 1980). Further, Bert Winn #1 did not reach temperatures hot enough for power production, nor did Stocks 1-A, and that if temperatures did exist in the area the wells would need to be much deeper or new wells would need to be drilled (McIntyre & Koenig, 1978; McIntyre & Koenig, 1980). Development was not pursued though, citing temperatures too low for commercial power production. However, these deep test wells and investigations were the first comprehensive looks at the possibility of commercial scale geothermal power production in the valley.

The low-temperature geothermal potential of the valley was investigated in 1982 by Janey de Vries (de Vries, 1982), wherein samples and measurements of pH, temperature, alkalinity and conductivity were taken from a number of wells and thermal springs from the Utah portion of the valley. Thermal waters were sampled and characterized in 1987 when Avery examined the thermal waters of southeastern Idaho, northern Utah and southwestern Wyoming. Avery's aim was to predict reservoir temperatures using traditional geothermometers, and identify any wide-ranging trends or relationships between thermal waters in those areas. Though Avery was unable to define or identify any trends, the water samples taken near Preston, ID, in the northern Cache Valley yielded some of the highest predicted reservoir temperatures in the study.

For the next couple of decades, interest waned in the valley's geothermal possibilities. Then in 2008, Carl Austin, a geologist local to southern Idaho, was hired by a group of investors to author a consultant's report detailing the possibility of power production using a subsurface heat source near Preston, ID. Austin revisited existing data, and examined claims and stories from locals involving accelerated snow melt occurring regularly near Clifton Hill. More recently, in 2013, a portion of the valley was included in an analysis of the structural controls influencing thermal springs in Southeastern Idaho by Young and others (Young et al., 2013).

Most recently, a particularly hot and shallow well (217°F at 215 ft) was drilled at the southern toe of Clifton Hill. This well, called the Bosen Well, was sampled by Cannon et al (2014) as part of a project aimed at predicting geothermal reservoir temperatures in southern Idaho using both traditional methods and a newly developed multi-component equilibrium geothermometer (MEG) (Figure 1.3). The related data from this investigation, as well as

those by Young and Mitchell (1973), Mitchell (1976) and Ralston (1981) were compiled by Wood et al (2015) and analyzed to gain an idea of reservoir temperatures in the vicinity of Clifton Hill (Table 1.1, Figure 1.6). This compilation included data from Battle Creek (also known as Wayland), Squaw, Cleveland, Maple and Treasureton hot springs along with other numerous wells. Battle Creek and Squaw hot springs are located in the central portion of the valley, just south of the southern tip of Clifton Hill and northwest of Preston, ID, while Cleveland, Maple and Treasureton hot springs are located near the Oneida Reservoir. Water temperatures tend to be hottest in the central valley, with the Bosen well, Battle Creek, Squaw hot springs yielding the warmest samples (Table 1.1; Chapter 1: Geochemistry).

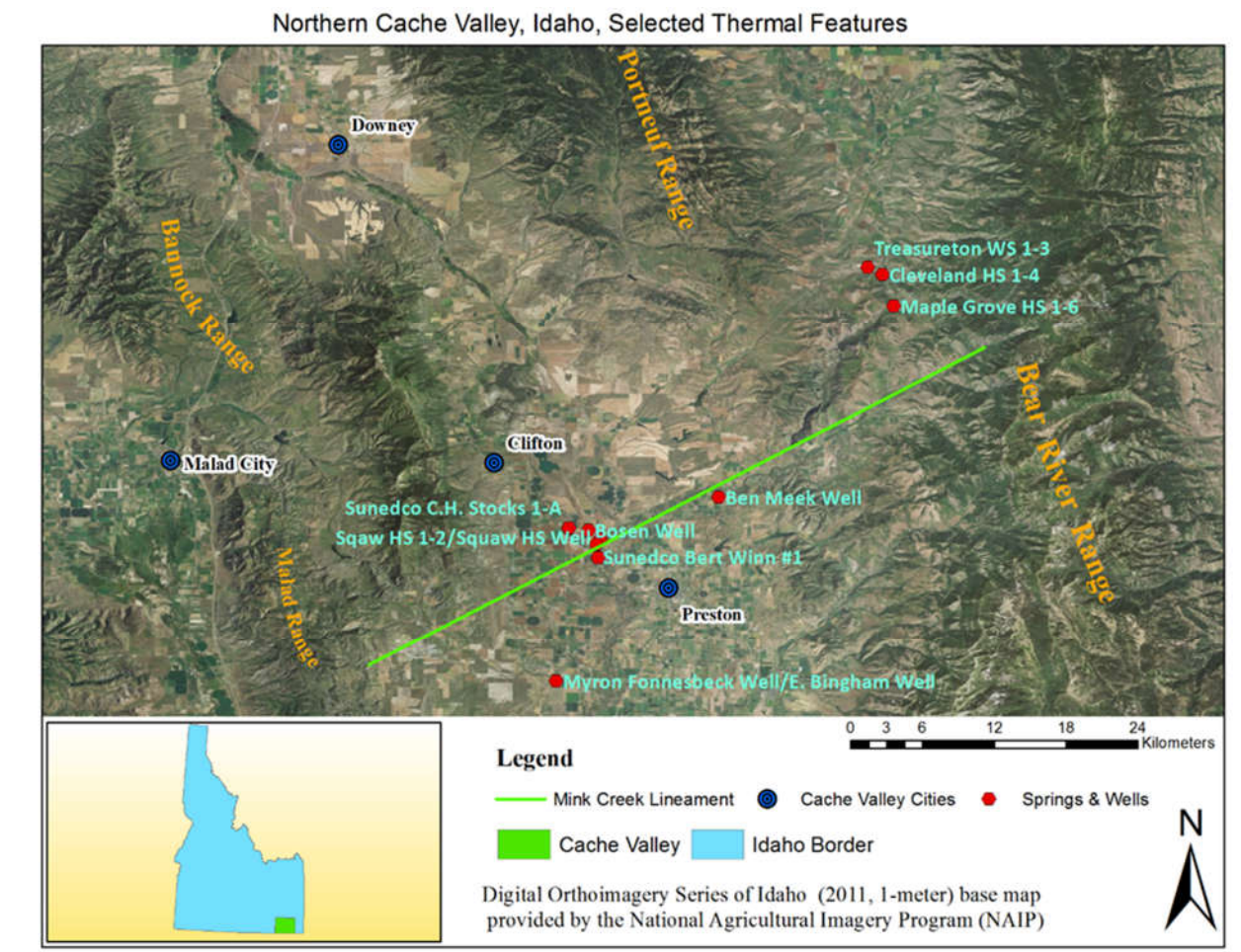


Figure 1.6. Corresponding data for wells and springs compiled by Wood et al (2015) from previous studies. Wood et al, 201

Table 1.1. Temperatures and chemical data for wells and springs of the North Cache Valley.

Springs/Wells	T (°C)	pH	Ca	Na	Mg	K	Cl	SiO2	SO4	HCO3	F	Units	Reference
Treasureton Warm Springs 1	35	6.6	265	563	68	127	632	54	788	704	2.2	mg/L	Mitchell, 1976
Treasureton Warm Springs 2	40	6.4	336	542	48	110	626	54	735	726	2	mg/L	Ralston, 1981
Treasureton Warm Springs 3	33	6.6	259	517	64	137	633	52	755	704	1.9	mg/L	Mitchell, 1976
Cleveland Hot Springs 1	55	6.2	259	444	41	90	574	62	517	565	1.7	mg/L	Ralston, 1981
Cleveland Hot Springs 2	66	6.4	208	458	50	98	532	60	533	718	1.9	mg/L	Mitchell, 1976
Cleveland Hot Springs 3	61	6.5	178	460	50	102	530	64	530	576	1.9	mg/L	Mitchell, 1976
Cleveland Hot Springs 4	56	6.5	172	460	50	100	532	63	532	583	1.9	mg/L	Mitchell, 1976
Maple Grove Hot Springs 1	76	7.3	89	490	24	110	630	55	260	491	1.1	mg/L	Young & Mitchell, 1973
Maple Grove Hot Springs 2	72	6.8	93	501	29	82	601	85	261	495	1.1	mg/L	Mitchell, 1976
Maple Grove Hot Springs 3	60	6.8	93	492	25	80	584	86	251	494	1	mg/L	Mitchell, 1976
Maple Grove Hot Springs 4	71	7.8	69	494	31	76	595	52	255	424	0.9	mg/L	Dion, 1969
Maple Grove Hot Springs 5	78	6.6	85	492	30	82	596	84	256	494	1.1	mg/L	Mitchell, 1976
Maple Grove Hot Springs 6	62	5.9	82	499	22	77	585	64	323	454	1	mg/L	Ralston, 1981
Ben Meek Well	40	6.9	24	368	6.6	22	322	89	13	513	9.6	mg/L	Mitchell, 1976
Battle Creek Hot Springs 1	82	6.7	174	3161	19	552	5241	109	35	696	6	mg/L	Mitchell, 1976
Battle Creek Hot Springs 2	43	6.5	166	3071	15	535	5048	107	29	697	6	mg/L	Mitchell, 1976
Battle Creek Hot Springs 3	81	6.5	162	3053	19	533	5034	109	37	757	6	mg/L	Mitchell, 1976
Battle Creek Hot Springs 4	84	6.8	215	4184	24	686	6967	97	33	610	6.4	mg/L	Mitchell, 1976
Wayland HS 1	77	7	160	3100	16	660	5400	80	50	699	12	mg/L	Young & Mitchell, 1973
Wayland HS 2	77	6.5	179	2985	16	493	5092	90	39	681	6	mg/L	Ralston, 1981
Squaw Hot Springs Well	84	6.5	279	4368	24	782	7398	124	35	791	4.3	mg/L	Mitchell, 1976
Squaw Hot Springs 1	69	6.5	135	4184	23	708	6877	126	27	816	4.3	mg/L	Mitchell, 1976
Squaw Hot Springs 2	73	6.6	241	3844	26	533	6396	126	23	866	4.8	mg/L	Mitchell, 1976
E. Bingham Well	23	6.2	320	4600	36	770	7800	68	48	930	3.9	mg/L	Ralston, 1981
Bosen Well	90	6.7	207	4523	18	795	7129	95	49	583	5	mg/L	Wood et al., 2015
Myron Fonnesbeck Well	23	6.8	78	68	27	18	91	74	4.3	418	0.5	mg/L	Mitchell, 1976

GEOLOGIC SETTING

The NCV is situated at the confluence of several geologic terranes on the northeastern extent of the Basin and Range Province where it meets the Sevier orogenic belt and Rocky Mountains. The juncture of these provinces is characterized by frequent seismic activity and clusters of hot springs (Sbar et al., 1972; Figure 1.7).

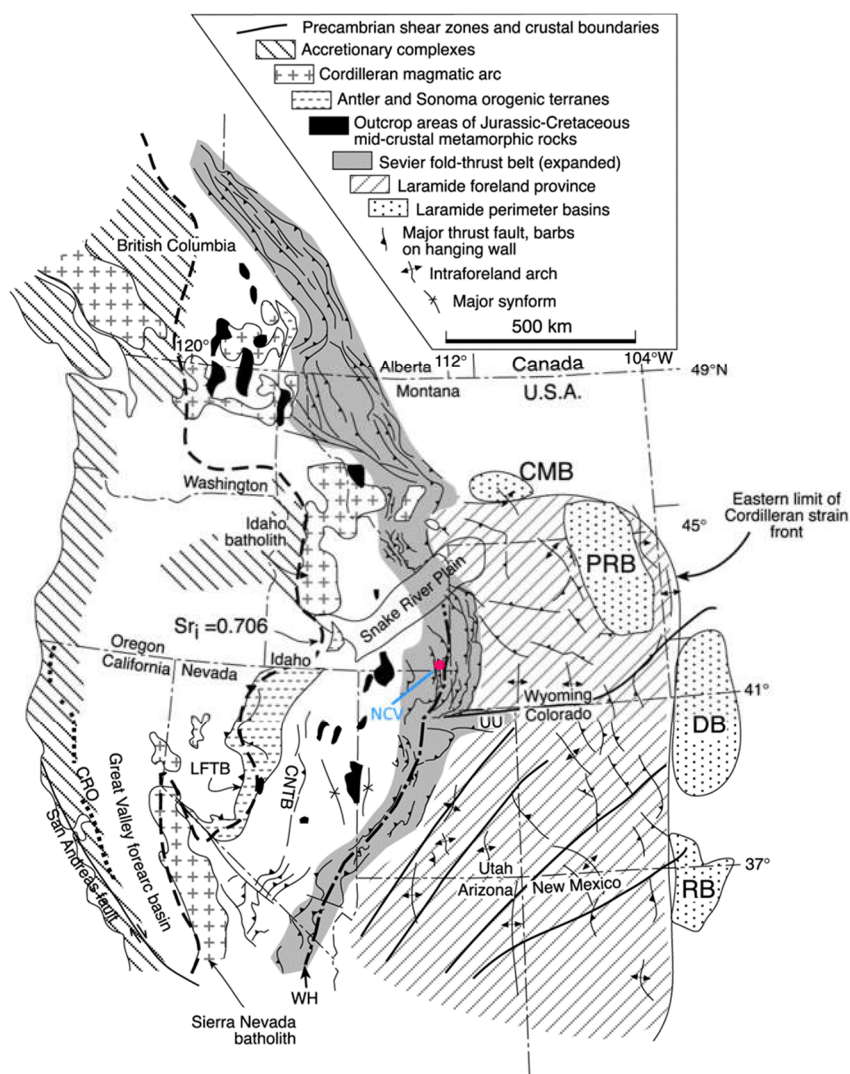


Figure 1.7. Extent of the Sevier fold-thrust belt (Sevier orogenic belt) in relation to the western United States and Canadian Provinces. The North Cache Valley lies within a range of the fold-thrust belt referred to locally as the Idaho Thrust belt, following the eastern border of Idaho with the western borders of Wyoming and Montana. Abbreviations are as follows: CRO, Coast Range ophiolite; LFTB, Luning-Fencemaker thrust belt; CNTB, Central Nevada thrust belt; WH, Wasatch hinge line; UU, Uinta Mountains uplift; CMB, Crazy Mountains basin; PRB, Powder River basin; DB, Denver basin; RB, Raton basin. Modified from DeCelles, 2004.

The NCV is underlain by the western portion of the Idaho Thrust belt, which formed in the Sevier orogeny, active from late Jurassic to the late Eocene, 140 - 70 million years ago (m.y.a.) (Grubbs & Van Der Voo, 1976). During the compressional Sevier orogeny, folding and faulting of the predominantly Paleozoic marine sediments occurred along the western edge of the North American plate as the oceanic Farallon plate was subducted at a shallow angle; this created a zone of deformation stretching from central British Columbia to southeastern California. As the North American plate moved further west, the subduction angle of the underlying Farallon plate lessened, initiating a period of mountain building known as the Laramide orogeny, lasting from the late Cretaceous (70-80 m.y.a.) to the early/late Eocene (35-55 m.y.a.), resulting in the formation of the Rocky Mountains (Liu, 2008).

Basin and Range extension began in the early Eocene, approximately 45 m.y.a., and continues to the present. The province is characterized by repeating sequences of paired normal faults (i.e. graben forming), accommodating the extensional forces and stretching the area to double that of its original width. These paired normal faults allow for the formation of successive series of valleys and mountains. The valleys, or grabens, move downward in relation to the mountains, or horsts. As these extensional forces and mechanics thin the continental crust, it may be predicted that the crust would subside. This is not the case however, as the northern Basin and Range remains relatively high above sea level. This is possibly the result of long term subduction of the Farallon plate and others beneath the North American plate, effectively buoying the continental crust with lower density mantle and helping to keep it floating higher on the mantle (Parsons, 1995). Another theory suggests the higher elevation may be the result of the Yellowstone Hot Spot emplacing buoyant asthenosphere underneath the northern section of the Great Basin (Parsons, 1995).

Because the NCV is located at the convergence of structurally distinct and active provinces, it is influenced by many forces and processes that may influence the occurrence of sources of geothermal energy and secondary sources of permeability. Crust that was deformed and shortened during the Sevier orogeny has been reshaped and stretched by Basin and Range extension to form the mountains bounding the NCV on the east and west. The border of the Basin and Range with the Rocky Mountains and the Colorado Plateau runs from southeastern

Idaho to southern Nevada (Figure 8). This area makes up a large portion of the Intermountain Seismic Belt (ISB) and the seismicity seen along it may indicate that the Rocky Mountains are still rising with respect to the Basin and Range province (Smith & Sbar, 1974; Parsons, 1995). The potential impacts of mountain building forces at the scale of a geothermal prospect are discussed in the following sections.

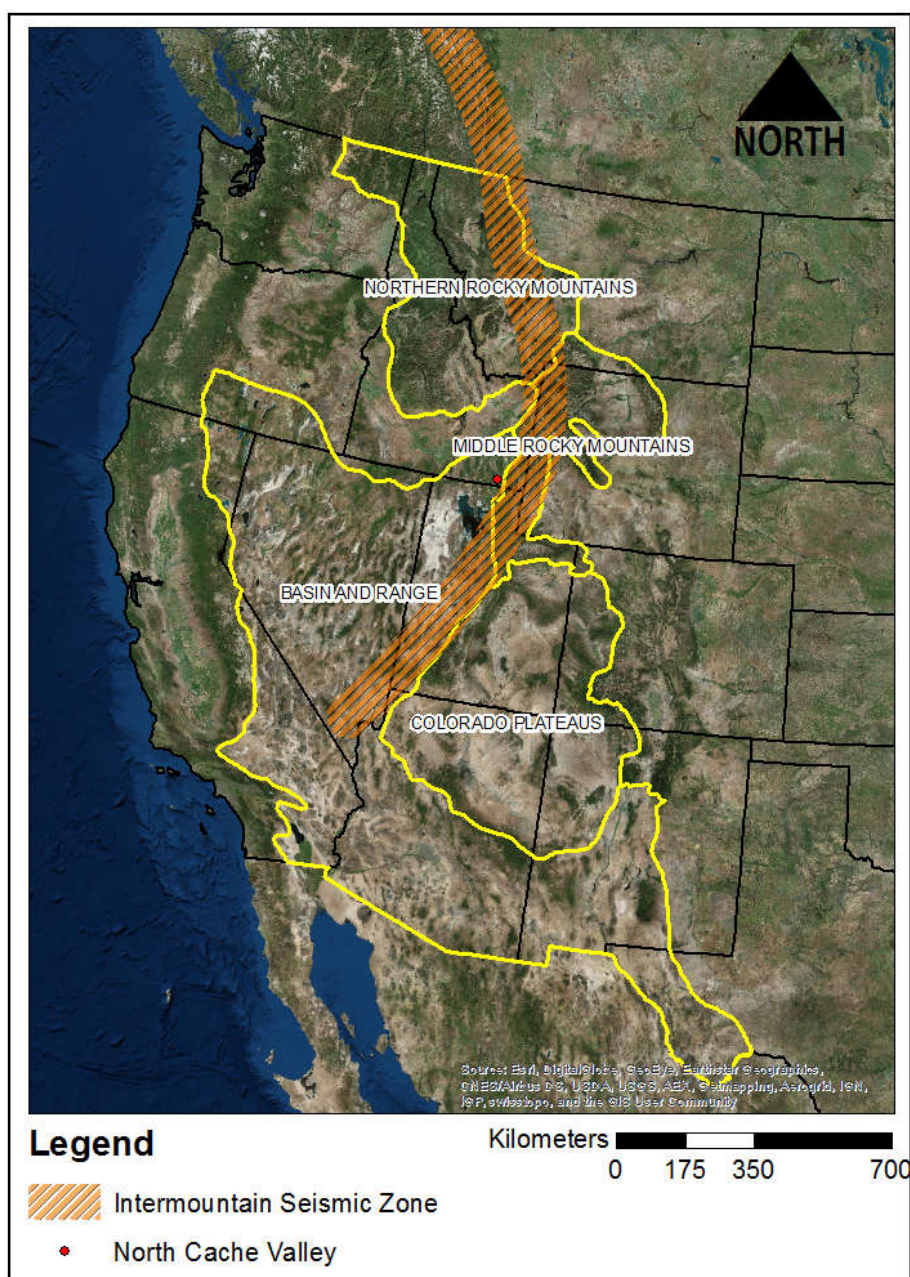


Figure 1.8. Extent and borders of the Basin and Range Province, nearby bordering geologic provinces and the Intermountain Seismic Zone in the Western USA. The Intermountain Seismic Zone extends from Canada south to southern Nevada.

LOCAL GEOLOGY

The Portneuf, Bear River and Bannock mountain ranges are horst complexes bounding the NCV (Figures 1.1, 1.2, 1.5, 1.9). The Bannock mountain range is made up primarily of the Precambrian Scout Mountain member of the Pocatello formation. This member is characterized by diamictite featuring angular, silt and sand sized grains of quartz and feldspar within a chloritic or sericitic groundmass punctuated by large granule to boulder sized clasts. Less prominent units associated with the Scout Mountain member include a purer quartzite, phyllite, fine-grained green-schist and thin beds of calcite and dolomite marble (McIntyre and Koenig, 1978). On the west side of the valley, the Oxford-Dayton fault stretches along the base of the Bannock mountain range (Figure 1.2). This east-dipping, north-trending normal fault is the dominant structure in the North end of the valley and acts as the master fault of the local active Basin and Range system (Janecke & Evans, 1999).

Along the northeastern and eastern edge of the valley are low rolling foothills overlying the base of the Portneuf and the Bear River mountain ranges. These foothills are comprised of Miocene to Pliocene aged, east-northeast dipping Salt Lake formation deposits overlying Cambrian to Ordovician aged carbonates, which have been faulted overtop Neoproterozoic to Cambrian aged Brigham group quartzite (McIntyre and Koenig, 1978; Figure 1.9).

Separating the foothills on the east side of the valley from the Bear River range is a system of inactive, northeast trending, west to southwest dipping normal faults which flatten at shallow depths (Janecke & Evans, 1999). The stratigraphy of the Bear River range consists of marine sedimentary units of Ordovician through Silurian age situated atop large sequences of Cambrian aged carbonates. These in turn are underlain by upper Precambrian and lower Cambrian meta-sedimentary rocks of the Brigham group. Structures found in these mountains are complex, complicated by fold structures such as roll over anticlines to the northeast and east-northeast plunging synclines and anticlines (Janecke and Evans, 1999).

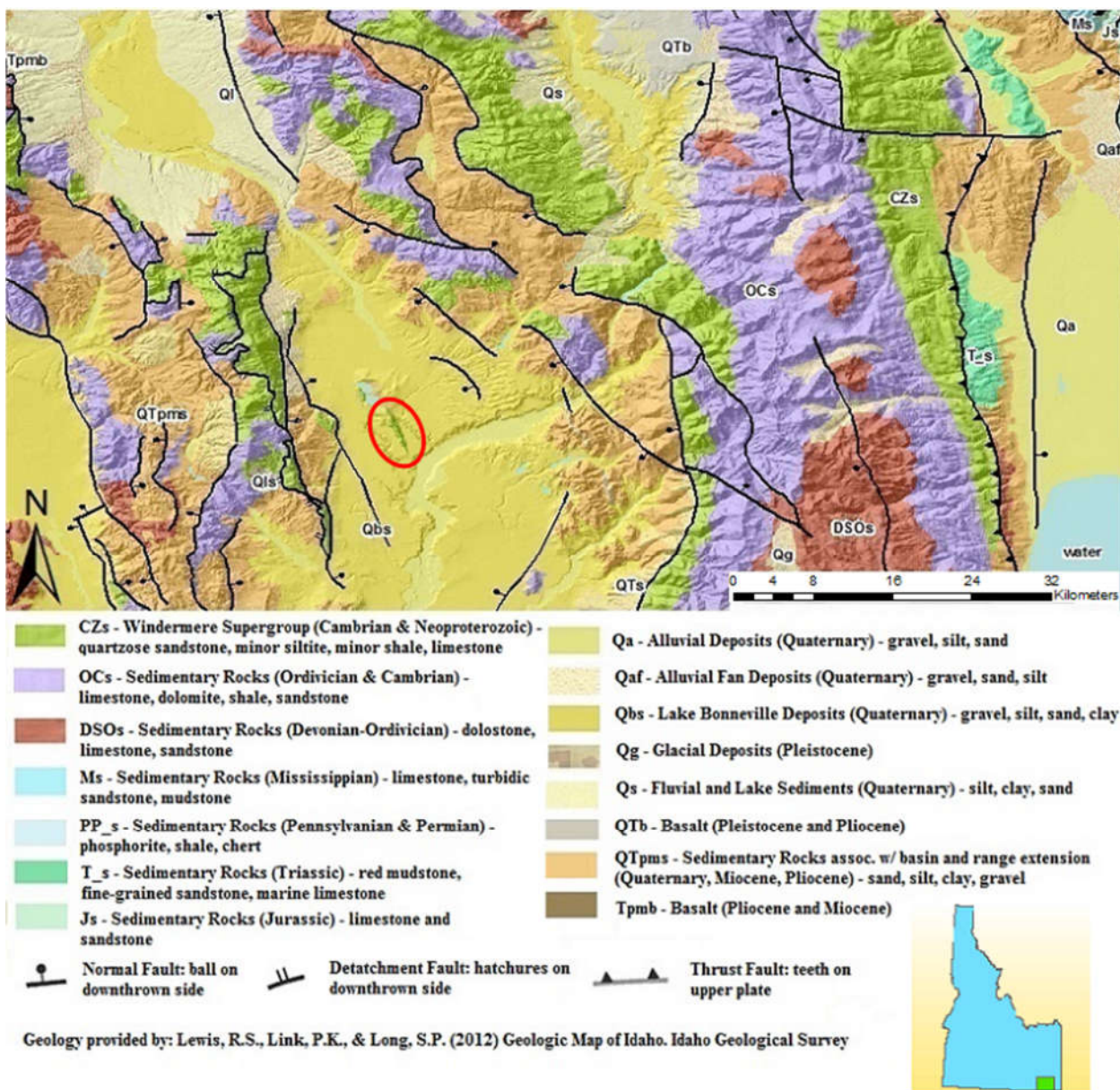


Figure 1.9. Geologic map of the North Cache Valley. Study area indicated by red oval. After Wood et al, 2015.

Two major north-trending normal faults run along the east and west flanks of the valley at the base of the Bannock and Bear River mountain ranges (Figure 1.2). The displacement of these faults may be between 2,400 and 3,000 meters, while smaller subsidiary faults, such as those associated with the Clifton Hill Horst complex, run throughout the graben (McIntyre and Koenig, 1978). Also present is a linear structure described by Mitchell (1976) as the “Mink Creek-Bear River Lineament” (Figure 1.6, 1.10). The lineament is consistent with the trend

of the Bear River northeast of Battle Creek Hot Springs. Austin (2008) postulates the lineament may be a vertical structure accommodating shear stresses or another type of fault (Austin, 2008). Further information on this structure is sparse, though the positioning of the recently drilled Bosen thermal well and Battle Creek and Squaw hot springs are coincident with the lineament's inferred path. In his report, Mitchell (1976) speculated on the possible interaction of the feature with the Battle Creek and Squaw hot springs of the central valley, noting, "The intersection of this Mink Creek-Bear River lineament and the Clifton Hill boundary faults could be the controlling structure or focal point for the hot spring activity in this area." (Mitchell, 1976).

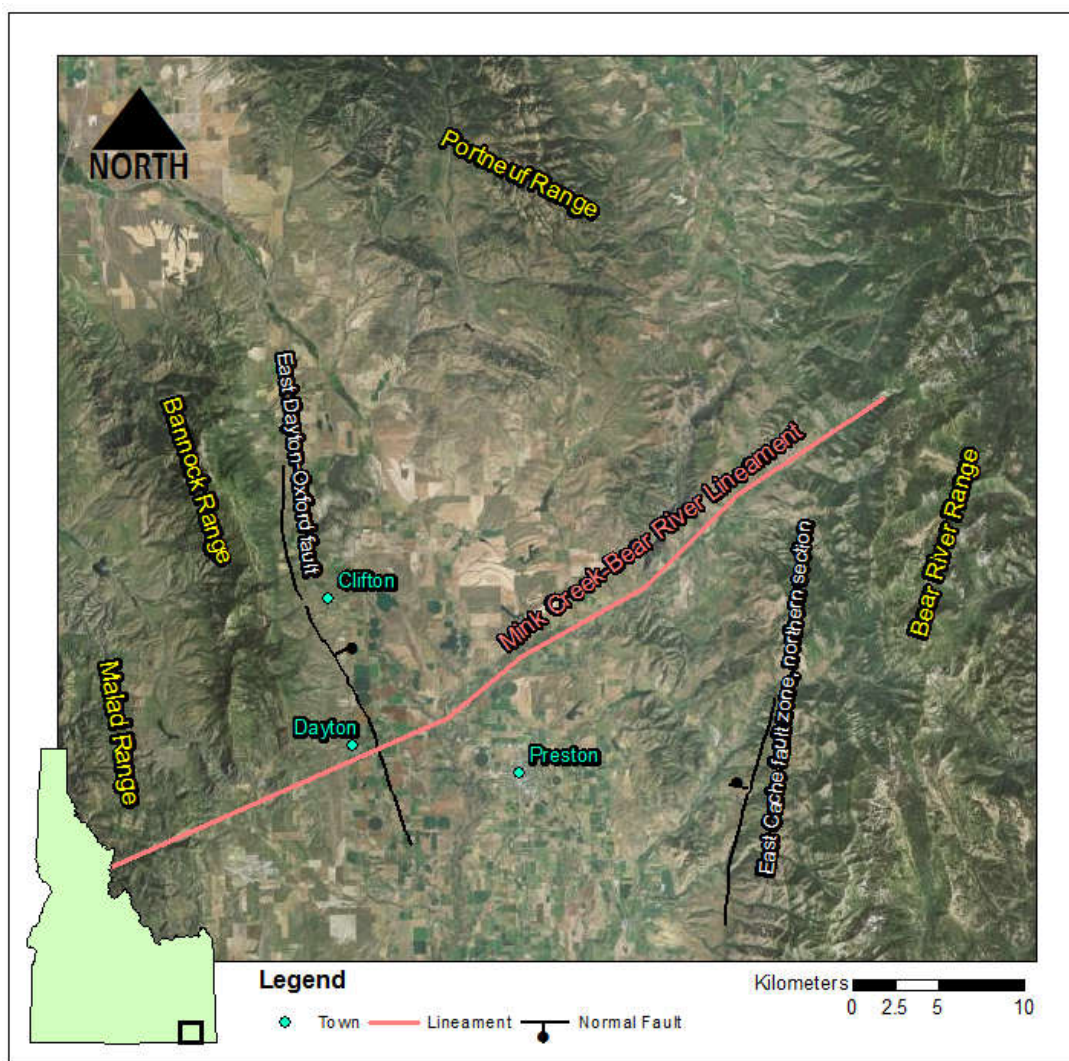


Figure 1.10. Extent of the Mink Creek-Bear River Lineament in the NCV.

During the Pleistocene the Salt Lake Valley was filled by a large inland lake, Lake Bonneville; which also inundated the NCV and left behind numerous lacustrine deposits and layers of unconsolidated sediment. The thickness of this sediment varies widely, nearing 100 meters in some portions of the valley. A Sunoco Energy development test well, located approximately 6 miles northeast of Preston, encountered 104 meters of these sediments (McIntyre & Koenig, 1978). Underlying the Lake Bonneville sediments is a thick sedimentary sequence of Tertiary age Salt Lake formation. Gravity data near Preston, ID suggest these deposits are in excess of 1,675 meters thick, and thicken to more than 2,400 meters further south near the Idaho-Utah border (Peterson & Oriel, 1970). These late Tertiary deposits are of a fluvial and lacustrine origin and comprised of silt and bentonitic clay thinly interbedded with sand. The formation also contains a tuffaceous material which may be the product of Snake River Plain (SRP) volcanism. Locally, the Salt Lake Formation sits atop the Precambrian basement rock of the Pocatello formation.

Several hills are expressed on the floor of the NCV. Of particular interest is Clifton Hill, a narrow ridge that extends from Twin Lakes reservoir 8 km to the southeast (Figures 1.3 and 1.4). The genesis of Clifton Hill is attributed to high angle faulting on both its east and west sides (Petersen & Oriel, 1970, and Oriel and Platt, 1968). Situated between two normal faults, Clifton hill represents a small secondary horst complex located within the larger Cache Valley graben. The west bounding fault trends towards a bend in the Bear River and the locations of hot springs including Squaw hot springs (Figure 1.3). Gravity data indicate that the bounding faults may extend southward as far as Squaw and Battle Creek hot springs (Mitchell, 1976).

Clifton Hill is composed of the Bannock Volcanic and Scout Mountain members of the Pocatello formation (Link and LeFebre, 1983; Figure 1.3) from field observations and sampling, these units seem to be intruded by a slightly metamorphosed metadiabase intrusion (Appendix B).

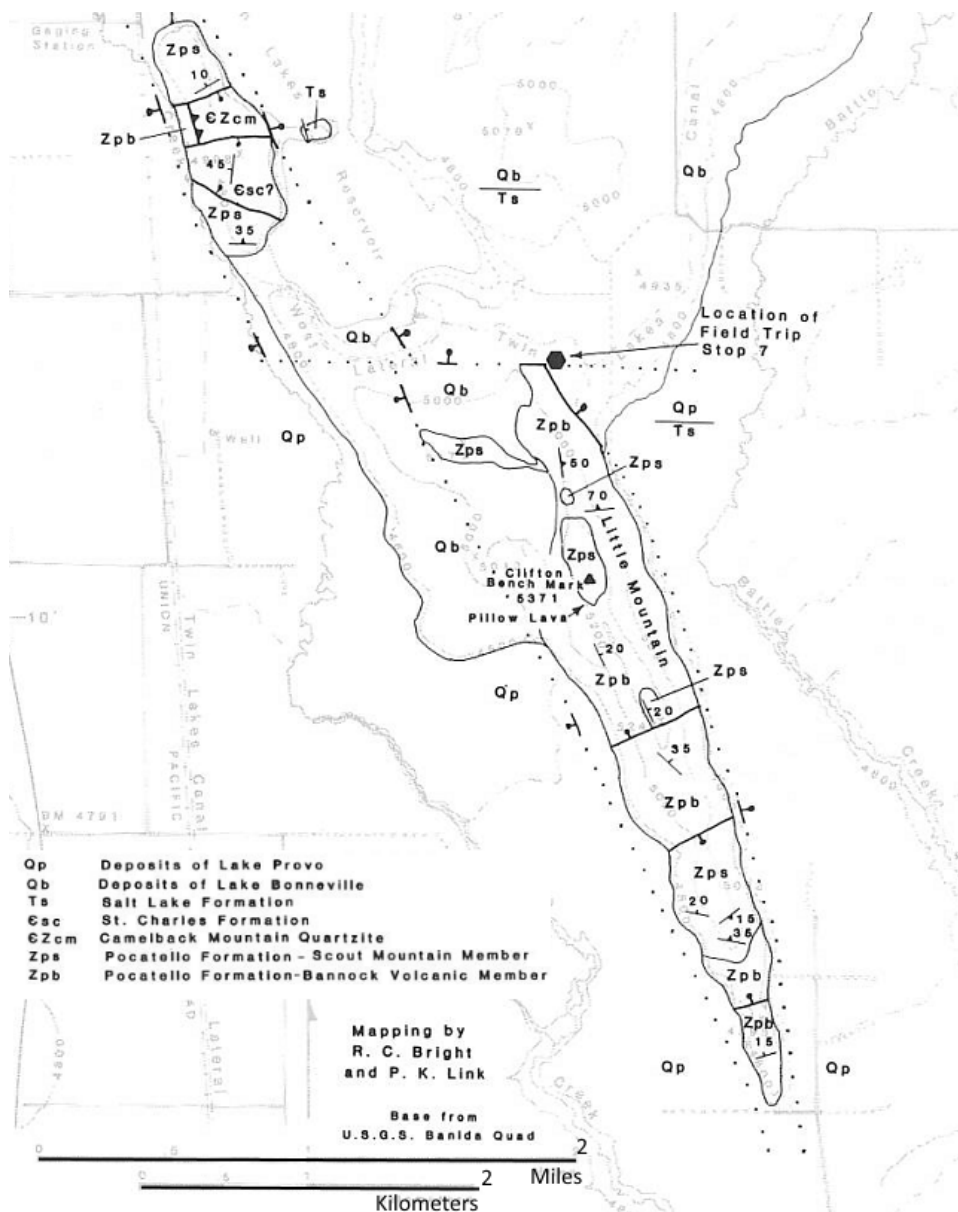


Figure 1.11. Geologic map of Clifton Hill. Modified from Link and LeFebre, 1983.

Drilling in the late 1970's by Sunedco included the C.H. Stocks 1, C.H. Stocks 1-A and Bert Winn #1 wells (Figure 1.3). The C.H. Stocks 1-A well was drilled first in the summer of 1978 to a depth of 1.7 km (5,479 ft) at a location about 0.6 km west of Clifton Hill (Figure 1.3). The location was picked based on magnetotelluric mapping. The well penetrated less than 104 m (340 ft) of Tertiary Salt lake Formation and terminated in Precambrian Pocatello Formation. The highest temperatures obtained were 122° C (252° F) and 1600 m (5,250 ft), 60 hours after breaking circulation and, the following day, 118° C (245° F) at 1530 m (5,015 ft) about 6 hours after breaking circulation (McIntyre and Koenig, 1978). Although a drilling

problem prevented the hole from being drilled deeper, it was concluded that the depth was sufficient to test the upper part of the magnetotelluric anomaly. Two possible anomalous conditions were found: 1) elevated concentrations of pyrite and other metallic minerals at several horizons in the Precambrian; and 2) the occurrence of moderately saline warm water in fractures in the same section (McIntyre and Koenig, 1978).

The Bert Winn #1 well was drilled in the spring of 1980 to a depth of 2433 m (7,981 ft) at a location 1.1 km southeast of the southern toe of Clifton Hill (Figure 1.3). A review of the geophysical data after drilling the C.H. Stocks 1-A well resulted in the choice of the Bert Winn #1 wellsite as a better location to test the resistivity anomaly. The maximum temperature recorded at the total depth of 7,981 ft, 24 hours after breaking circulation, was 104° C (220° F). Thirty seven hours after breaking circulation, the temperature at 2271 m (7,450 ft) (deepest probe penetration) was 117° C (243° F) and still rising. The Bert Winn #1 well was drilled along the Clifton Hill trend; structurally it was interpreted to have penetrated the horst footwall block (McIntyre and Koenig, 1980). Unfortunately, after the intersection of the fault plane, deepening the well took the hole progressively away from the fault plane thought to carry water to shallower depths. Though the intersected zone found in the well logs was not found to yield high amounts of thermal fluids (McIntyre and Koenig, 1980). McIntyre and Koenig (1980) concluded that neither C.H. Stocks 1-A well or the Bert Winn #1 tested the Preston anomaly satisfactorily. They came to this conclusion because, first, a reservoir of hot saline fluid with minimum temperatures above 149° C (300° F) was predicted from the geochemistry of nearby Battle Creek and Squaw Hot Springs waters. Second, neither well encountered conditions which could account for the low resistivity found in the surface surveys, at the depth penetrated. Third, no major range-bounding fault was intercepted in the deeper section, as indicated by the low temperature gradient, the absence of hydrothermal mineralization or H₂S gas occurrences and the low incidence of CO₂ gas (McIntyre and Koenig, 1980 p. 19). Based on the results of these two deep geothermal test wells McIntyre and Koenig (1980) speculated that it may be necessary to drill to over 3 km to encounter temperatures over 204° C (400° F).

After Sundeco terminated its operations in the NCV, geothermal investigations entered a long hiatus until recently when a local rancher installed a stock watering well at the south end of Clifton Hill and encountered elevated water temperatures at a relatively shallow depth.

In the first ten days of March 2014, Independent Drilling Company used an air rotary drilling rig to install a stock watering well for Mr. David Bosen. The well completion is 15.24 cm (6-inch) diameter steel from land surface to a depth of 60 meters (198 ft) with a nominal 15.25 cm (6-inch) open hole from 60 m (198 ft) to 79 m (260 ft). The well drillers report lists the static depth to water as 40 m (130 ft) below land surface and the rock type is described as predominantly greywacke. Near the drill site, a rock outcrop was observed that appeared to be a greenschist. The rock outcrop is most likely Precambrian age metagraywacke as described by Oriel and Platt, 1980. These rocks form the core of Clifton Hill and are the oldest rocks within the Preston Quadrangle.

The Idaho Department of Water Resources (IDWR) measured the temperature of the Bosen well in March of 2014 using a HOBO U12-015 stainless steel temperature probe (Erickson, 2014). The probe was lowered to the bottom of the well until the temperature began to level off. The measured temperature was 102.9° C (217.2° F).

The fault on the east side of the Clifton Horst trends towards Battle Creek and Wayland Hot Springs. The flow path for thermal waters that are tapped by the Bosen Well appears to be similar to the flow paths supplying water to the Squaw Creek Springs and Wells and similar water may possibly be found in the east Clifton fault, which appears to daylight at Battle Creek hot springs. Alternatively, the flow of thermal water may be associated with the Mink Creek-Bear River lineament, or as suggested by Mitchell it may be associated with the intersection of these two structural trends.

The deep heat source of for the Preston geothermal prospect is not known with certainty. Despite the Cenozoic volcanic activity of the SRP to the north and northeast and the Blackfoot Volcanic field to the north, no evidence has been found for volcanic activity that might be capable of acting as a heat source for geothermal water in the NCV. Typical mechanisms of heat transport in the Basin and Range province involve the deep circulation of ground water along fault planes. In the following section we evaluate the geochemistry of the

area to further characterize the geothermal reservoir waters and deep ground water flow pathways.

GEOCHEMISTRY

The seventeen wells and springs sampled and analyzed by Mitchell (1976), along with selected data from Dion (1969), Young & Mitchell (1963) and Ralston (1981) are summarized in Table 1 (Dion, 1969; Young & Mitchell, 1973; Mitchell, 1976; Ralston, 1981; Table 1). The range of chemical constituents analyzed for included, silica (SiO₂), calcium (Ca), magnesium (Mg), sodium (Na), potassium (K), bicarbonate (HCO₃), sulfate (SO₄), chloride (Cl) and fluoride (F).

As stated earlier, sampling of the Bosen well was completed as part of field work for geothermometry mapping of Southeast Idaho (Cannon et al., 2014). Cannon analyzed the water for boron (B), lithium (Li), beryllium (Be), aluminum (Al), arsenic (As), selenium (Se), rubidium (Rb), strontium (Sr), barium (Ba), bismuth (Bi), carbonate (CO₃), nitrite (NO₂) and bromide (Br⁻) in addition to the range of chemical components listed above for Mitchell's 1976 study. Some of these constituents are required for temperature modeling using RTEst, an inverse multi-component equilibrium geothermometer (MEG) with the capability of evaluating the effects of secondary processes, including boiling, dilution and loss of CO₂. (Palmer, 2013; Neupane et al., 2014).

These data were compared to the data collected by Mitchell (1976), Ralston (1981), Dion (1969), and Young & Mitchell (1973) by Wood et al (2015) (Dion, 1969; Young & Mitchell, 1973; Mitchell, 1976; Ralston, 1981; Wood et al, 2015). Thermal waters of the NCV fall into two main types, the largest group, a Na-Cl water, encompasses all the samples analyzed but one (Figure 1.11) (Wood et al, 2015). The waters of Battle Creek and Squaw hot springs, as well as those from the E. Bingham and Bosen wells are the most extreme of this type. These waters also appear to be only partially equilibrated with the host rock. All other samples were categorized as immature waters, meaning very little equilibration had occurred with the host rock (Figure 1.12) (Wood et al, 2015).

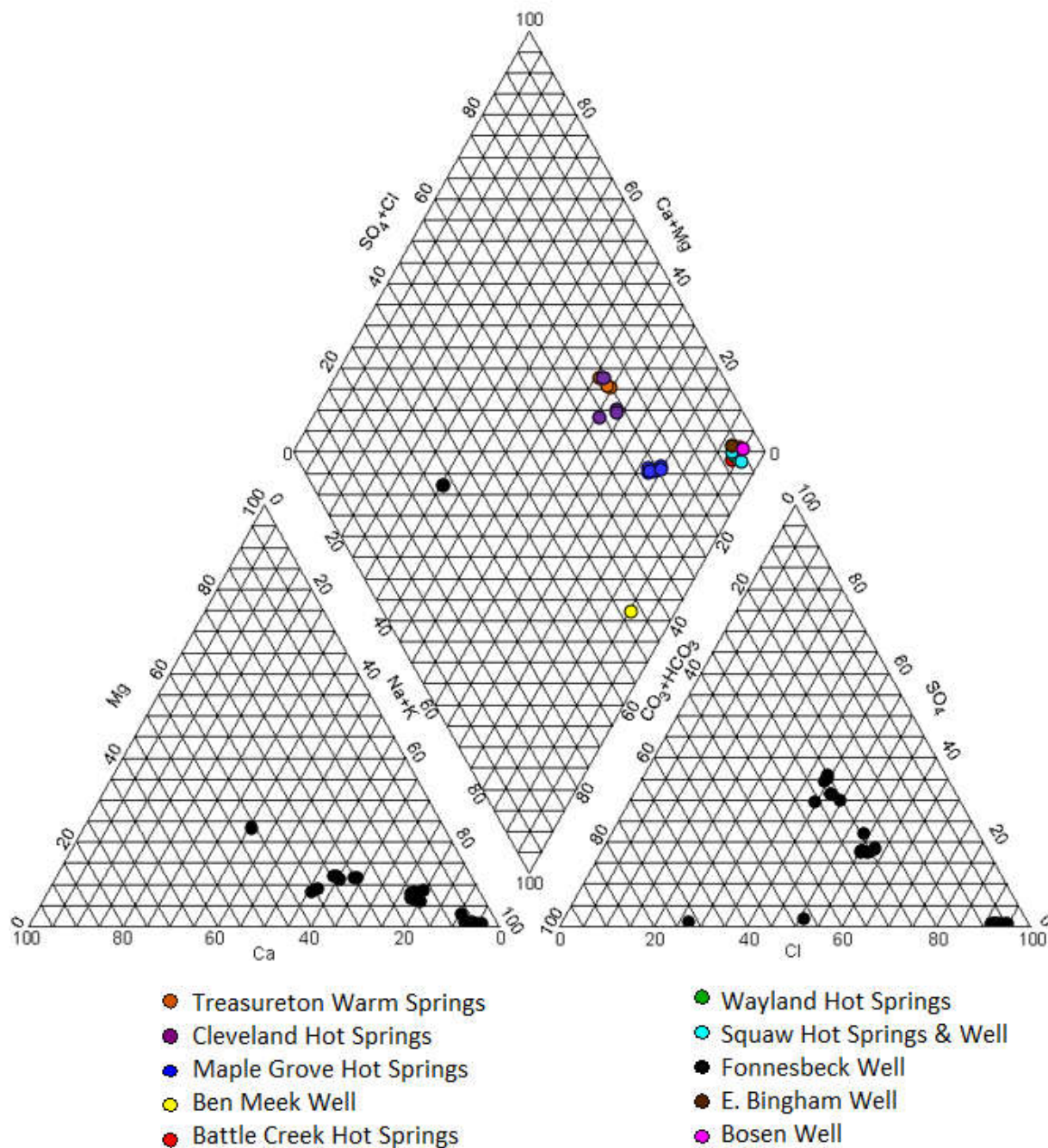


Figure 1.12. Piper diagram mapping the springs and wells of the NCV. Wayland and Battle Creek hot springs are hidden by the cluster of samples plotting on the extreme right hand side of the diagram (Wood et al, 2015).

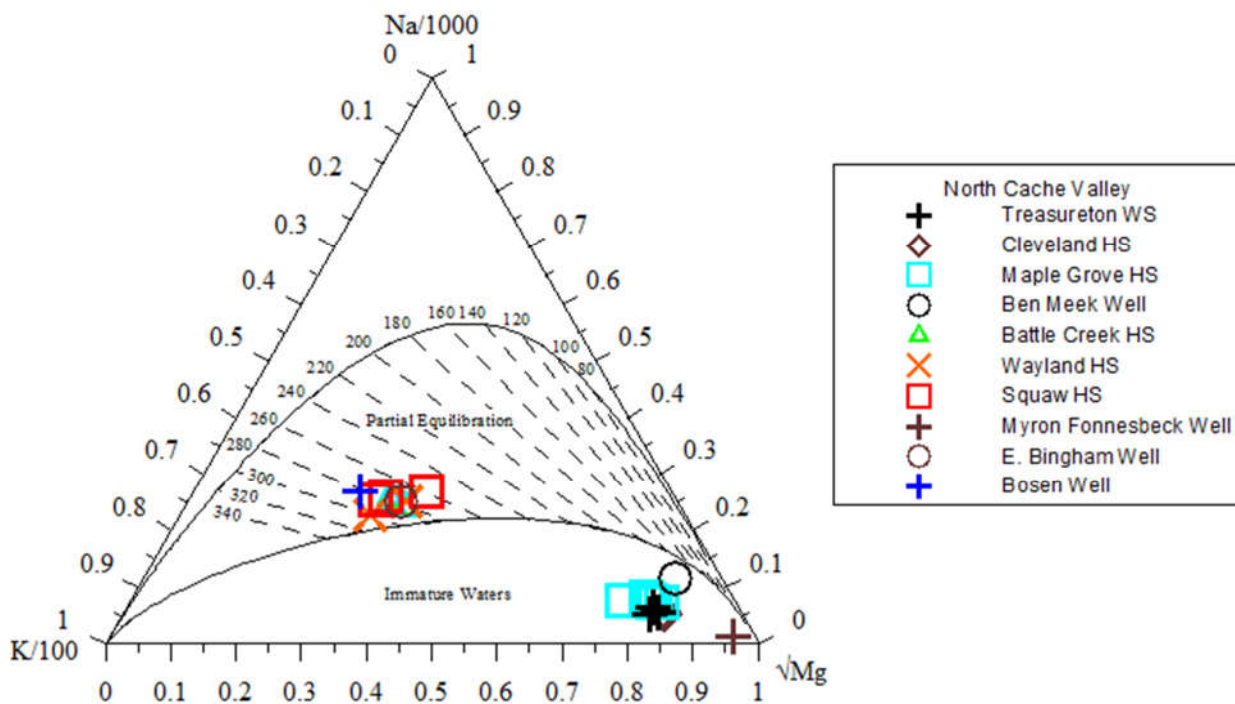


Figure 1.13. Giggenbach diagram depicting spring and well water of the NCV (Wood et al, 2015).

Reservoir temperatures were estimated using four traditional geothermometers, quartz (Fournier, 1977), chalcedony (Fournier, 1977), silica (Arnórsson et al. 1983), and Na-K-Ca (Fournier and Truesdell, 1973) with a Mg correction applied according to Fournier and Potter II (1979), and summarized in Table 1. Calculated temperatures range from 67° C to 227° C, though the highest estimation is unlikely due to high concentrations of Mg. RTest values range from 95±1° C to 179±9° C (Table 1.1) (Wood et al, 2015).

CHAPTER 2 : NEW RESEARCH

Attention returned to the NCV after the drilling of the Bosen well, and discovery of boiling water at 250 ft below ground surface. Recommendations from legacy reports suggest additional geophysical surveys to better define the fault system in the study area. Magnetics and gravity investigations are chosen. To explore the relationship of the local shallow aquifer, a survey of ground water level and temperature in the area is planned.

NEW SURVEYS

With renewed interest in the Clifton Hill prospect spurred by the reservoir temperature estimation of the Bosen well and re-examination of legacy thermal data in the vicinity, it was decided that further research was warranted in the area. The structure of the system of faults surrounding Clifton Hill has long been only partially understood, and thus new investigations into this structure would be a prudent next step in a re-characterization of the area. McIntyre and Koenig (1980) concluded, that the Clifton Hill area was not adequately tested, and that in particular, permeable sections of the Clifton Hill range front faults were not intersected by either Stocks 1-A or Bert Winn #1 (McIntyre & Koenig, 1980). It was suggested by the authors that gravity surveys, would be helpful in determining more precise locations of the Clifton Hill range front faults (McIntyre & Koenig, 1980). Geophysically based interpretation of the structure of Clifton Hill's bounding faults were drawn primarily from gravity data from Peterson and Oriel (1970) and were limited. Peterson and Oriel (1970) concluded that the Clifton Hill east-bounding fault likely dips steeply to the east, and that a steeply dipping fault probably exists on the western side, but whether it dips to the east or west was not determinable from the data (Peterson & Oriel, 1970). The recommendation for a gravity survey to better understand the local fault system was still valid in 2015, therefore, a gravity and supplemental magnetics survey were undertaken as part of this investigation. Magnetics and gravity data are examples of potential field measurements. Potential fields are forces that act at a distance, and measurements of these are inexpensive, quick and simple to collect over large areas, making them ideal methods of early investigation (Mariita, 2007 (1 & 2)).

During the program development stage, it was hoped that magnetically and gravimetrically mapping the fault structure of the prospect, would serve to better define the deep plumbing of the geothermal system. This plumbing system, which is likely a network of permeable faults and fractures, facilitates the circulation of cold water to depth and the upward movement of hot water where it is expressed in numerous hot springs along the Bear River. Improved definition of the fault system in the area only represents part of the geothermal system. The faults must have sufficient permeability to transmit water, possibly via a fracture network so that water can travel downward, absorb heat and return to the shallow subsurface. In many Basin and Range geothermal systems this is accomplished when cold meteoric water travels downward along extensional range bounding faults, is heated at depth and travels back to the surface where it is expressed in hot springs and warm wells (Figure 2.1).

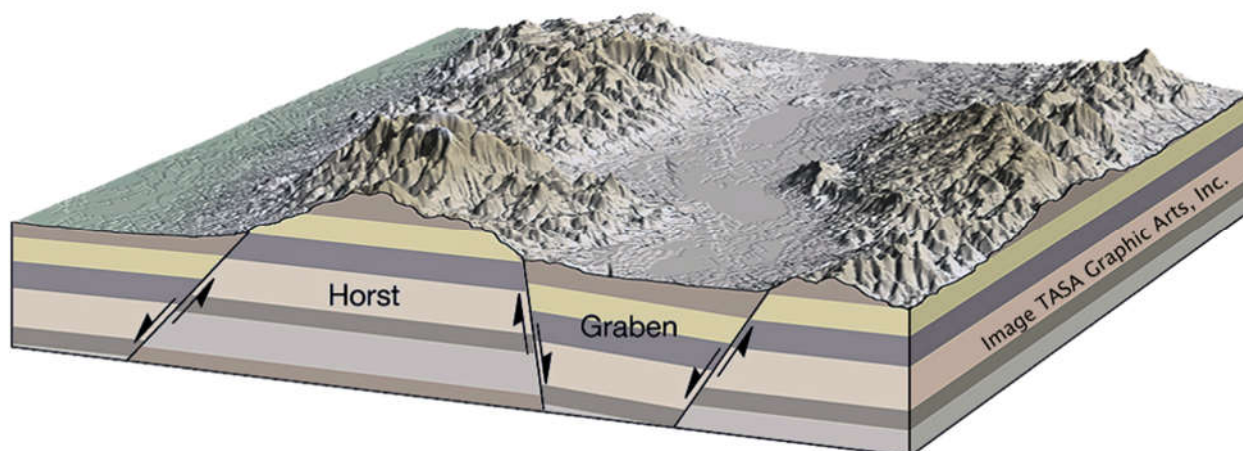


Figure 2.1. Cross-sectional diagram depicting horst and graben structure and behavior typical of the Basin and Range province. Source: http://geology.isu.edu/Alamo/devonian/basin_range.php

Once the fault system was better characterized, the fluid circulation system of recharge, heating and discharge could be conceptually modeled. The second piece of the conceptual model is the hydrogeology, specifically, water temperature and aquifer head field, which will be described in a subsequent section.

MAGNETICS

Magnetics measurements are values of the intensity of the earth's magnetic field at a specific location (Mariita, 2007 (1)). Variations between measurements at different locations are anomalies caused by differences in the magnetization of the subsurface material, and may be

the result of either induced or remanent magnetism. Induced magnetism is a secondary form of magnetization of a ferrous body that exists only in the presence of another field, such as the earth's magnetic field (Mariita, 2007 (1)). The magnetic signal can be recorded in a rock body at the time of the formation of that same rock body and as such the unit will remain magnetized in the absence of an external field. Magnetic anomalies are commonly caused by the presence of basalt layers, faults and dikes. Areas of high magnetic susceptibility (the latent magnetism of a rock) correspond to locally strong magnetic fields (USGS, 1997). Measurements of magnetism measure magnetic flux density, and carry the unit Tesla (T), named for Nicolai Tesla. One Tesla is equivalent to one kilogram per second squared per ampere. In the magnetics survey described here, the nanotesla (nT) is most commonly used.

In a magnetics survey, such as the one planned, both remanent and induced magnetism are recorded. The local Bannock Volcanic and the metadiabase units are likely to feature remanent magnetization, due in large part to their igneous origins. Both are also slightly metamorphosed, which can affect the remanent magnetization of the unit if, during the metamorphic process, the temperature of the rock approaches or exceeds the Curie temperature for that rock type. The signature recorded from these two units therefore, will likely be primarily due to remanent magnetization. The other prominent geologic unit in Clifton Hill is the metasedimentary Scout Mountain member of the Pocatello formation. A magnetic signature from this unit will likely be smaller than the other two meta-igneous units and will be produced by the induced magnetization of sedimentary rock and the changes it has undergone from the metamorphic process. The largest anomalies recorded are that of the meta-diabase intrusion.

In designing the survey, conclusions made by Peterson and Oriel (1970) were included in consideration of the initial locations of the faults. They conclude the existence of a steeply eastward dipping fault on Clifton Hill's east side and the likely existence of west bounding fault(s) located on the base of Clifton Hill's west side (Figures 1.3, 1.4). Given the regional extension of this Basin and Range setting we hypothesized that the westward bounding fault is steeply dipping to the west. The surface expression of additional faults were based on field mapping by Dr. Ismail Kuscu, of Blackrock Geosciences and field mapping by Dr. Paul Link

of Idaho State University (ISU) (Figures 1.3, 1.4) (Peterson & Oriel, 1970; Dr. Ismail Kuscu, personal correspondence, 2014; Link & LeFebre, 1983).

It was anticipated that the most important faults and therefore the primary targets were near the base of Clifton Hill because the structural trends and natural lineaments of the area were in line with hot springs exposed near the Bear River. Therefore, survey lines were planned wherever possible to cut perpendicularly across these trends and Clifton Hill. Nine magnetics lines were planned along roads and, where permitted, on private lands. The survey was conducted between August 18th and 24th, 2015. For the study, two magnetometers were employed, a pack-mounted G-859AP Cesium Vapor Magnetometer to be worn while walking the lines, and a G-857 Proton Precession Magnetometer for use as a continually recording magnetic base station. The base station magnetometer was placed each day of the survey at the same location (Figure 2.2) and set to record on a 30 second interval.

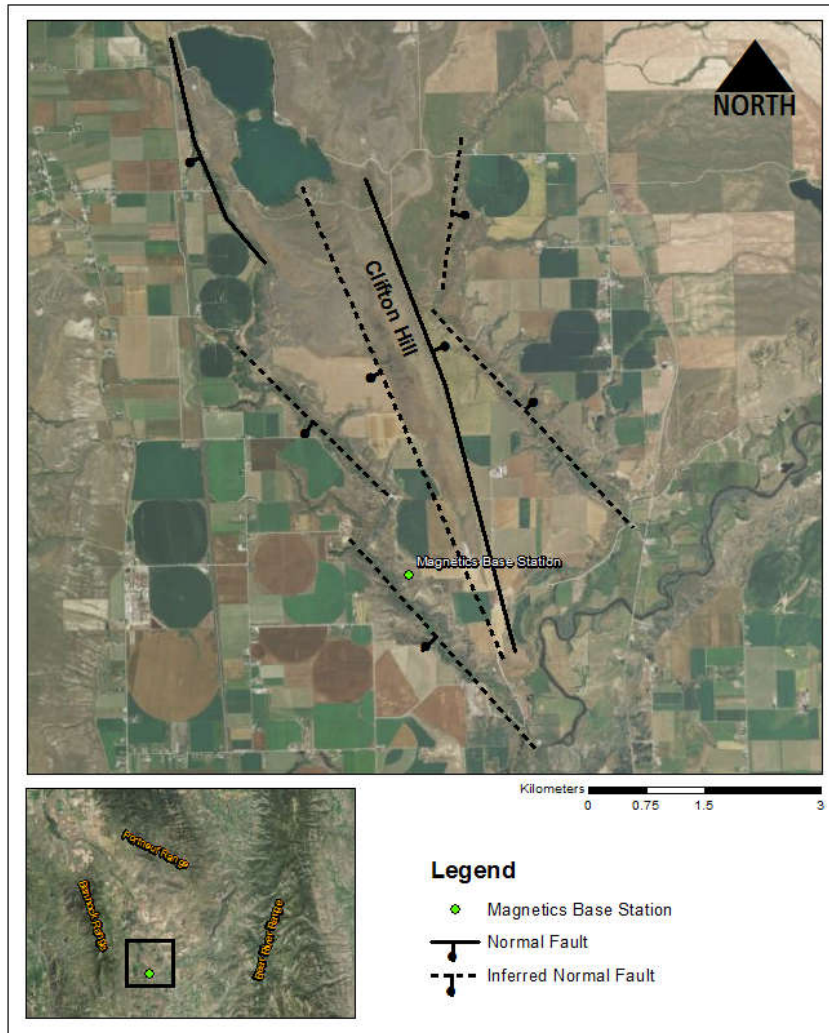


Figure 2.2. Location of the magnetics base station used for the duration of the magnetics survey.

During the survey, one researcher, wearing the pack mounted magnetometer, would record while another walked at least 50 meters ahead. This separation distance ensured magnetic interference was not generated by the second researcher. The researcher wearing the magnetometer took care to ensure that he was free of any articles of clothing which may influence the magnetic reading, and noted in the magnetometer control console any nearby objects in the surrounding area which may influence the recorded signal. The second researcher walking ahead of the magnetometer communicated with the first and kept a physical record of any of these ‘marks’ and what they corresponded to. Two vehicles were utilized, one left at the end of the line and the other used to transport both researchers and their equipment to the starting point. When the line was finished the researchers would use

the vehicle at the end point to travel back to the vehicle at the starting point. From there the researchers would move on to the next line. After each day of recording, the data from both magnetometers, base station and wandering unit, were downloaded and checked for quality control.

Data along six lines was collected for analysis (Figure 2.3). With recording finished, a diurnal correction was applied to the data from each line using Geometrics' MagMap2000 software. Daily variations in the magnetic field are calculated from the base station data. These daily variations are then removed from the data, this is referred to as a diurnal correction.

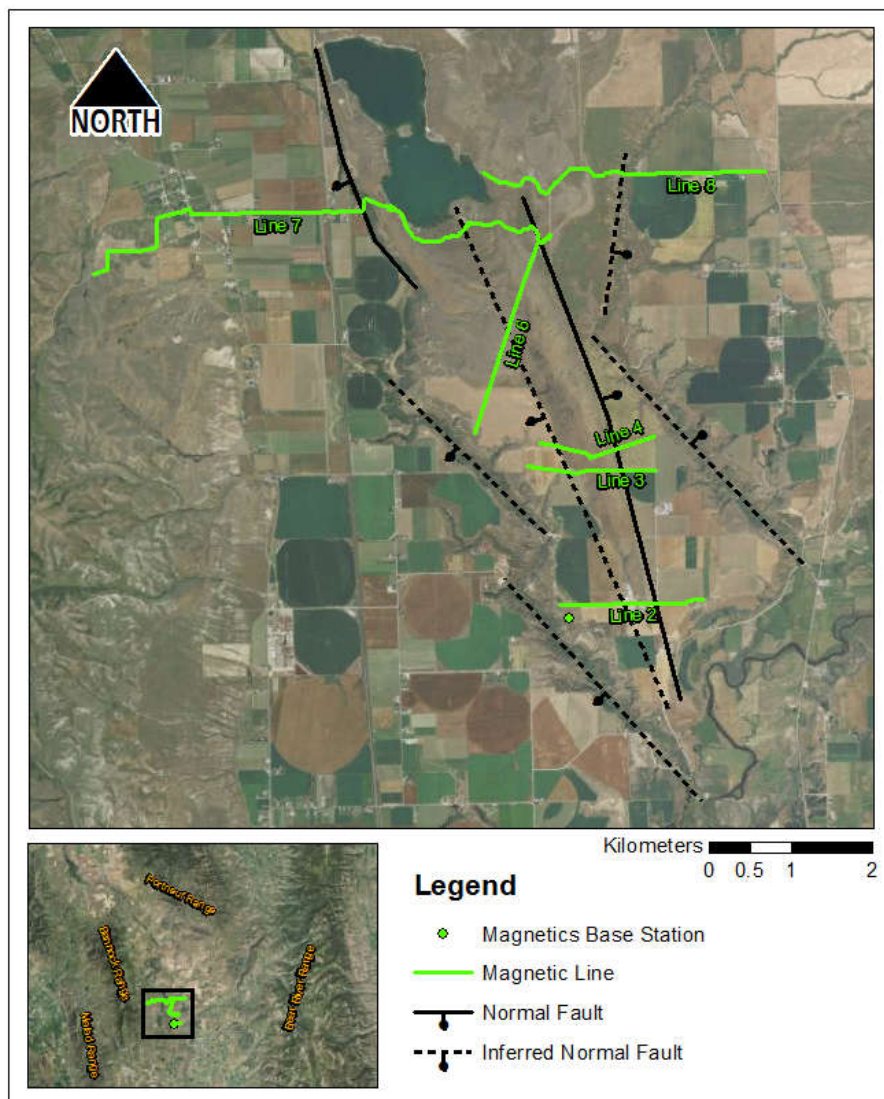


Figure 2.3. Locations and extent of magnetics lines collected for analysis.

GRAVITY

After the magnetic data had been collected, gravity lines were planned to coincide with the magnetic data lines. Gravity is an attractive force exerted by an object on its surroundings. The size of this force is a function of the mass of the objects and the distances between the objects involved (Mariita, 2007 (2); USGS, 1997). Gravity surveys measure the acceleration due to gravity, or strength of the gravitational field at discrete points on the surface of the earth, a higher value is induced by higher density materials and a lower value by a lower density materials. Gravity is measured in Gals, named for Galileo, with 1 Gal equaling 1 cm/sec^2 . When values are compared to adjacent readings, inferences in the changes of the subsurface density can be made. Using this method, given appropriate densities of various rock types and sufficient proximity to features of interest, contrasts in rock types across faults are identifiable. Many factors besides density and distance from the measurement point affect the gravitational field. For instance, variations in tidal cycles and the earth's rotation both influence the reading (Mariita, 2007 (2)).

A gravimeter is used to measure gravity, and there are two types. Absolute gravimeters are able to discern an actual value of acceleration due to gravity. These are very precise, but are also very expensive, heavy and cumbersome. The second type is a relative gravimeter. These measure the change in gravity between two positions, or the relative value of gravity between them. Though not as precise as absolute meters, relative meters can attain a precision of 0.005 mGals, are cheaper than an absolute meter and far easier to transport (Mariita, 2007 (2)). Relative gravimeters must be "tied" to a nearby base station. This entails taking a measurement at a known and established gravity station at regular intervals throughout the day. This is done so that the subsequent relative measurements are "tied" to a fixed station for which an absolute value is known.

A LaCoste and Romberg relative gravimeter, model 264, was borrowed from the University of Utah. This instrument is precise to 0.1 mGal (Cook & Carter, 1978). This model is a relative gravimeter and thus requires a base station for data tie-ins. The nearest existing base station for which access could be easily obtained, was Salt Lake City BM8, located in President's Circle at the University of Utah, Salt Lake City, UT (Winester, 1998). However, the station is located 120 miles from the area of study, and so it was not feasible to use this

existing base station on a daily basis. Therefore, a new base station was established closer to the Clifton Hill area. A base station is established by making consecutive gravity measurements alternating between an established base station, such as Salt Lake City BM8 and a second location of one's choosing. The Preston, ID Federal Post Office was chosen for the site of the new base station, and establishment was carried out on September 11th and 12th, 2015; see Appendix A for more details.

Other important aspects of a gravity survey are accurate and precise positioning of each gravity measurement and making accurate in-field terrain and tidal corrections. Positioning is crucial, as the strength of the gravitational field changes with elevation. The precision of the LaCoste & Romberg G-264 gravimeter used in this survey is 0.1 mGal (Cook & Carter, 1978). An isostatic gravity anomaly will be produced from measured gravity data, and if assuming a change in signal of 0.1 mGal per meter for the Isostatic gravity anomaly, a required vertical precision of under 1 meter can be calculated. For this survey a Trimble Geo 7x GPS unit equipped with an external antenna was used, capable of a vertical positioning accuracy of 1.5 cm, well below the sub 1 m requirement. Tidal corrections compensate for the gravitational effects of the tidal cycle at a particular date and time, while terrain corrections remove the unwanted effects of any topographic features which diverge from an ideal geoidal model. The terrain corrections made to the data are best made while in the field, at the time the measurement is taken, where the correction values can be calculated while still observing the physical terrain they represent. In calculating these corrections differences in elevation and angles of slope to these differences were estimated, and tables were consulted. Tidal corrections do not have to be made in the field, though in this case they were made at the time of measurement. Tables of tidal corrections were obtained from the United States Geologic Survey (USGS) Geophysics Unit of Menlo Park, CA (GUMP), and terrain corrections were calculated by observing localized distances to any nearby topographical features and consulting tables also provided by GUMP.

Gravity data from 300 stations were collected in September, 2015 (Figure 2.4). Typical spacing of gravity stations was 50 meters when in close proximity to structures of interest, such as the Clifton Hill bounding faults, otherwise spacing became further apart for the purpose of constraining the regional field. An average of 30 gravity stations were occupied

per day. The newly established Preston base station was the first and last station to be occupied every day.

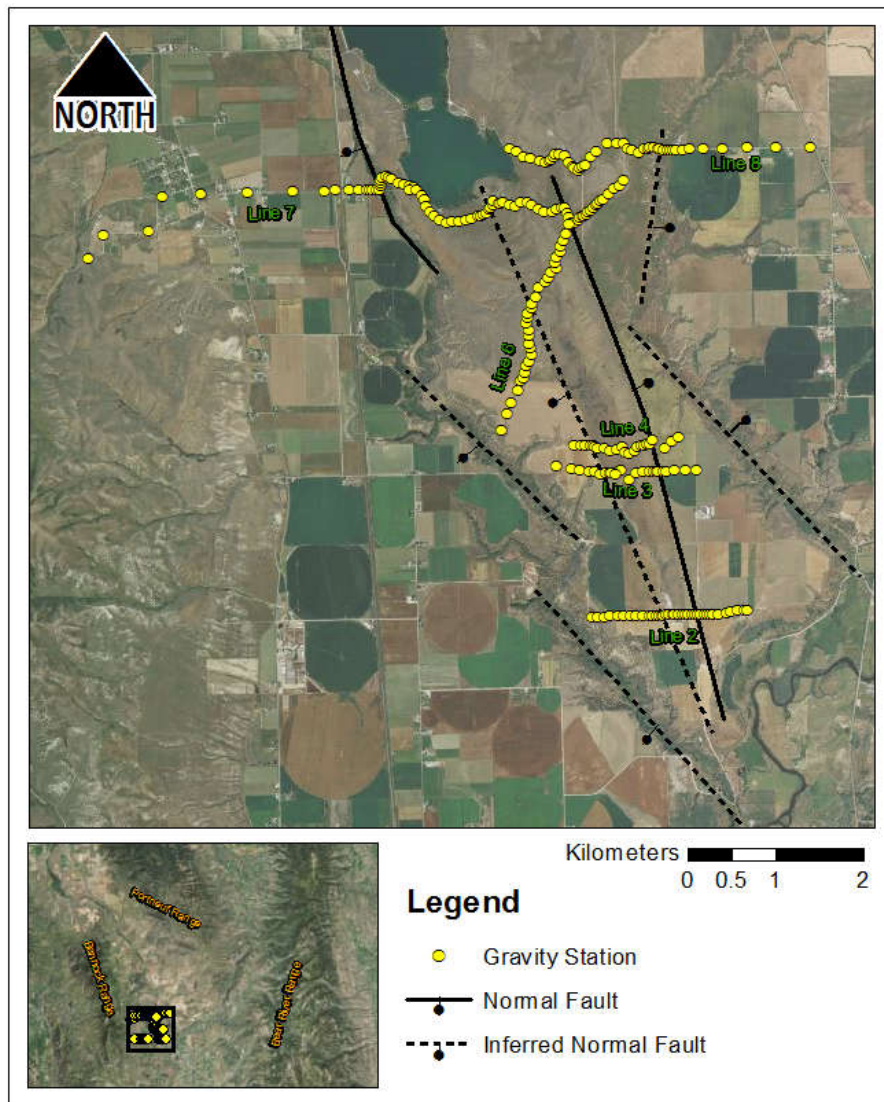


Figure 2.4. Locations of gravity stations occupied during the gravity survey.

The differences between these readings is called the closure. The daily closure is one of the most important aspects of the survey, as it serves as an “anchor point” for the data, and reveals any errors which may have occurred during the course of the day. A daily closure of 20 mGal or less is considered good, between 20 and 50 mGals is troubling and above 50 mGals may indicate that a tare occurred during the day’s measurements. A tare is essentially a step function that is introduced into the data, often via a physical jolt to the measuring gravimeter during transport. These should be avoided at all costs, as they often render most

or all of the day's work useless. LaCoste and Romberg gravimeters, such as the one used during the survey, are equipped with a clamp that protects sensitive mechanisms against tares which should be engaged at all times when the gravimeter is not making a measurement.

GPS data were reduced at the USGS Menlo Park, CA office by correcting the data using nearby regional GPS stations with a high percentage of data coherence, or agreement on the overall trend in the data. For processing these data, the Hyrum, UT station was used. After correction, the data were combined with gravity and magnetic data and exported to a text format and run through further custom scripts and in-house software developed by GUMP.

SHALLOW AQUIFER SURVEY

The local groundwater survey was designed to determine if there exists a trend of increasing temperature and decreasing depth to water (increasing head) as the distance to the Clifton Hill bounding faults (system of faults acting as the plumbing) decreases. Such a trend would suggest upwelling thermal waters near the faults of interest.

Wells were selected for measurement based on proximity to Clifton Hill, and other hypothesized faults of the study area (Figure 2.5). Previously collected temperature and water level data from the area were documented by McGreevey and Bjorklund (1970). These data, plotted on a map of the area, reveal a gap in areal coverage in the study area, namely the areas adjacent and to, north of and south of the Clifton Hill bounding faults (McGreevey & Bjorklund, 1970; Figure 2.6).

During the survey, water levels were measured using either a Solinst Model 101 Water Level meter (also known as an E-line), equipped with a P2 probe or an Eno Scientific WS2010 Well Sounder. In cases where installation and extraction did not endanger the well or pump or there was minimal risk to the measuring equipment, temperature was measured using a HOBO temperature and data logger probe, and water level measured using the Solinst E-line. In all other cases, temperature of well water was measured from a spigot drawing from the well using an Omega HH806AU thermistor, and depth to water measured using the well sounder. Measurements were made on March 19th and 21st, 2016, eleven wells were measured.

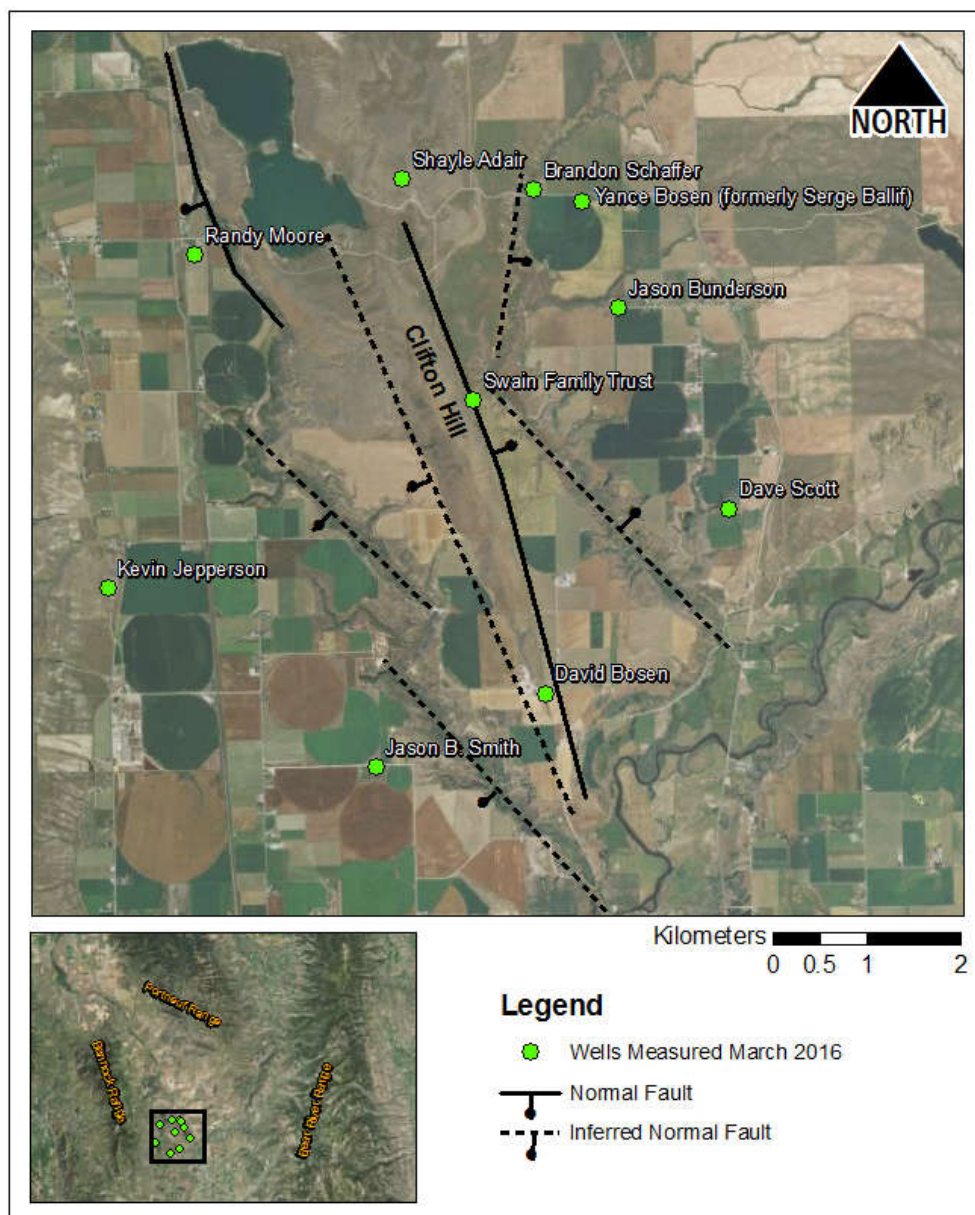


Figure 2.5. Wells chosen for new water level and temperature survey.

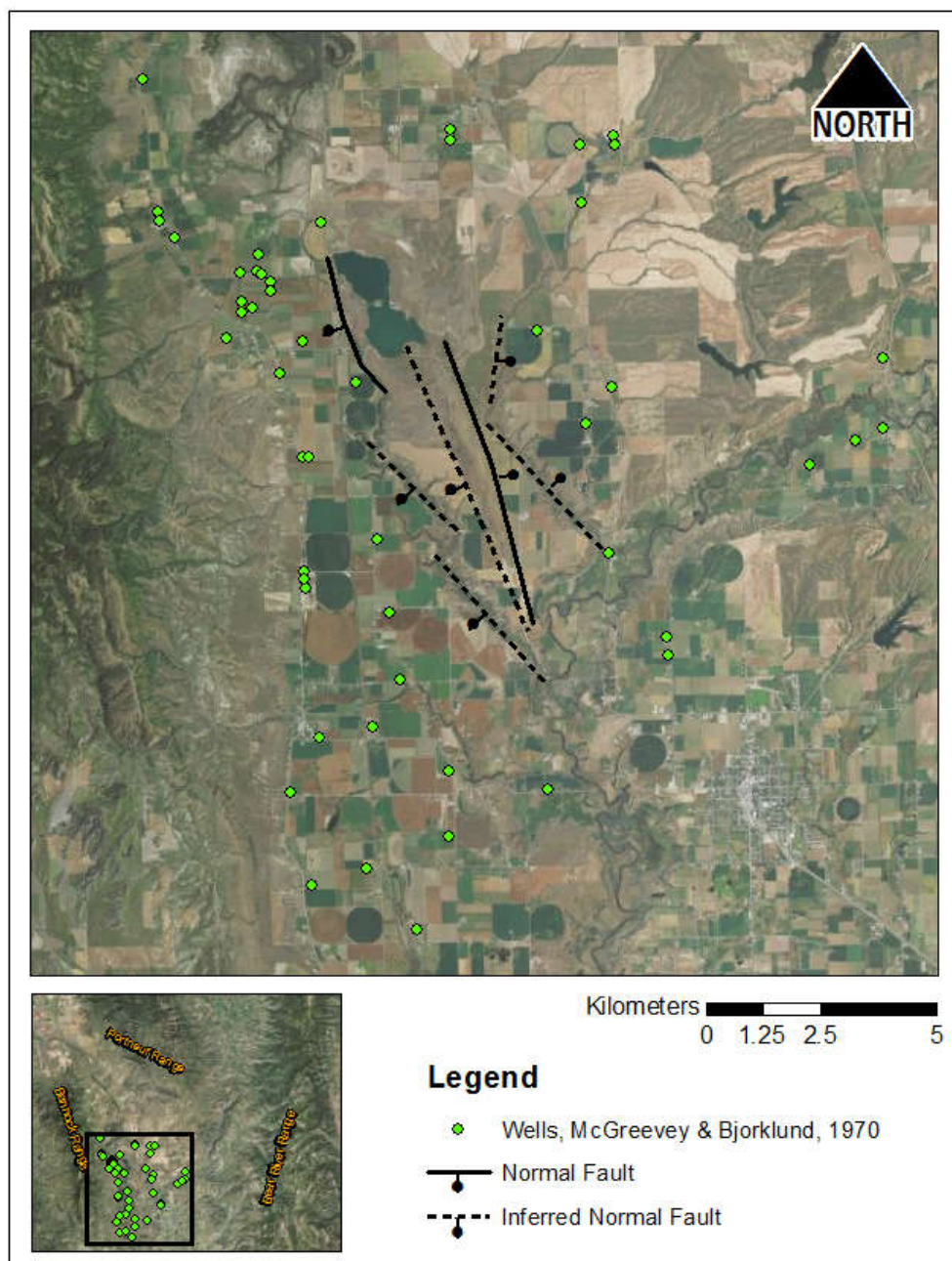


Figure 2.6. Wells previously measured for temperature and water level, McGreevey & Bjorklund, 1970.

CHAPTER 3 DATA AND DISCUSSION

Gravity, magnetic and GPS data were reduced (put through preprocessing steps) to the isostatic anomaly using software developed by Donald Plouff of the USGS, at the USGS Menlo Park, CA office (Ponce et al, 2009). Analyzing the data, entails a forward modeling approach where geologic models are created at appropriate depths and geometries and the predicted geophysical responses to the geologic model are matched to the field data. By iterations, the geologic models are modified until a satisfactory match to the field data is achieved. Modeling was completed using the Oasis Montaj software suite. The size and shape of the subsurface geologic structure may be manipulated to better match the field data. Values of error are calculated via a root mean square (RMS) method by the software and presented in units of nT and mGal for magnetics and gravity, respectively.

The physical properties of the geologic media (magnetic susceptibility and density) can also be manipulated within a representative range for the geologic media. These representative ranges for density and susceptibility were determined from field measurements and laboratory testing (Table 3.1; Appendices B, C). However, it is common for magnetic susceptibility values to range over two orders of magnitude (Mariita, 2007 (2)). Density values are measured in Kg/m^3 and do not vary nearly as much. Acceptable deviations of density from the experimentally determined high and low bounds is less than 200 Kg/m^3 .

Table 3.1. Magnetic susceptibility ranges from measurements collected in the field, and density ranges from values measured in the laboratory. Density units are Kg/m^3 and susceptibility units are $\times 10^{-3}$ SI. See Appendix B and C for more information.

Group	Density Range	Susceptibility Range
Scout Mtn Mem	2.56-2.79	0.02-0.49
Bannock Volcanic	2.57-3.07	0.43-0.69
Miocene Diabase	2.80-3.07	0.76-0.90

Groundwater levels and temperature data were analyzed via graphical plotting with a geographical information system (GIS) and contouring. The interplay between the temperature and groundwater data and the geologic framework (as defined by the forward modeling) provides insights into the nature of the geothermal resource.

MAGNETIC DATA

As stated previously, magnetics data were collected along six lines, totaling over 20 km. Noisy data caused by interference from cultural artifacts (nearby objects such as telephone poles, fences, metal structures, cars, underground culverts, cattle guards and railroad tracks) were removed during processing, prior to modeling. The remaining magnetic signature represents what is believed to be “real” magnetic signals or anomalies, caused by changes in the magnetic susceptibilities and/or geometry of subsurface bodies. For this discussion, the term “anomalies” is used to describe signal which deviates from what would be produced by an ideal subsurface body of uniform magnetic susceptibility.

Trends in the magnetics data can be easily identified when the processed magnetics signal is overlaid on a map of the study area (Figure 3.1).

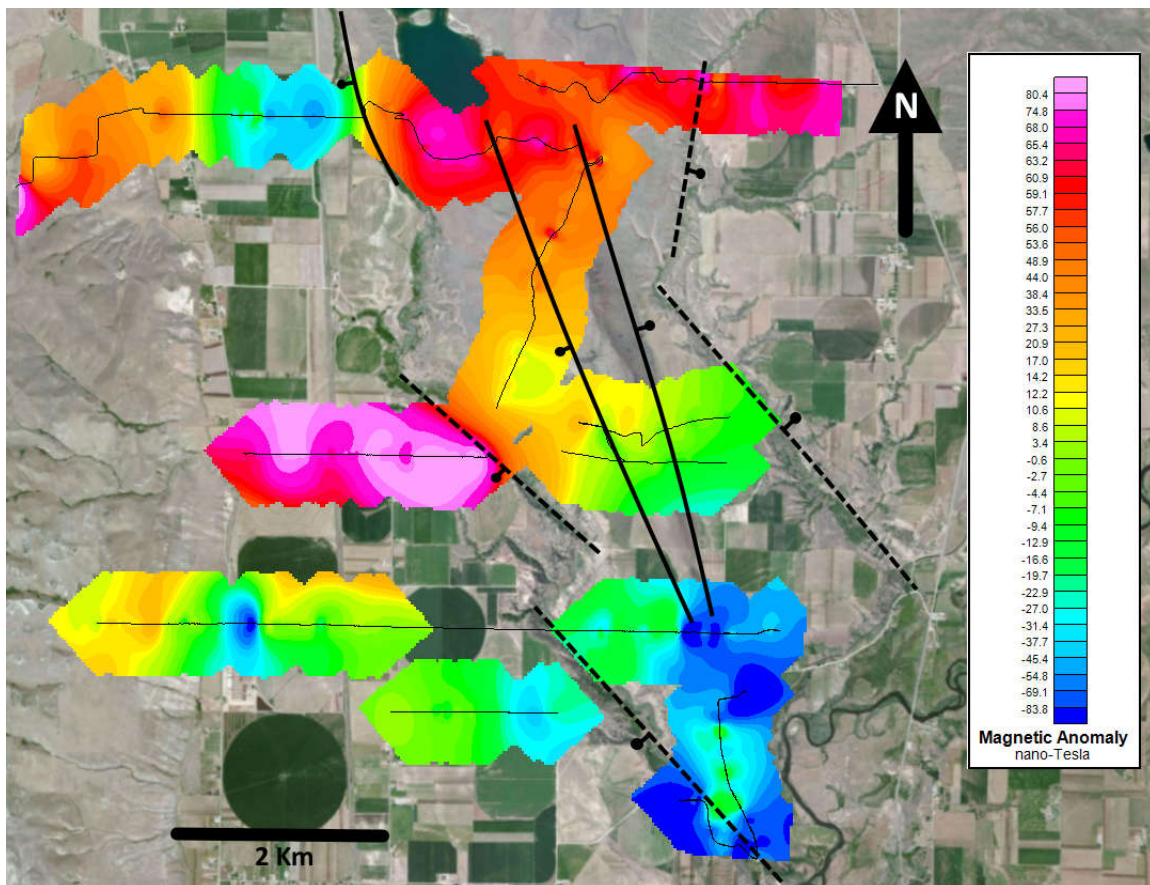


Figure 3.1. Gridded magnetic data collected across the survey area. Additional lines are included in the southwestern portion of the study area which were did not cross any structures of interest and so were analyzed for the purposes of this thesis.

It is important to keep in mind the scale of the line while interpreting geophysical data. Magnetic signal from lines spanning larger distances, like line 7 better correlates to topographic changes than smaller lines like lines 3 and 4 (Figure 3.1). Lines 3 and 4, which roughly parallel each other as they approach, cross the crest and descend Clifton Hill, exhibit magnetic signals that decrease from west to east. Line 7 begins in the foothills of the Bannock Mountains, descends to the basin 100 m below and then rises again 30 m to cross southern extent of the Twin Lakes Reservoir, which lies just northeast of Clifton Hill. Similarly, the magnetics data is high at both ends, and low in the middle; this is likely due to the large line being underlain by more magnetically susceptible materials on either end, allowing large scale trends to be correlated with trends in the topography. One possible cause for this is, assuming similar susceptibility values across the line, is a thickening of the quaternary sediment in the basin and a subsequent thinning as the elevation increases again near the reservoir. This is explored later in discussion of the line 7 model.

GRAVITY DATA

Gravity highs in the data tend to correspond to topographical highs (i.e. mountain peaks and hill tops) while lows tend to correspond to topographical lows (i.e. valleys). This is primarily due to less dense materials underlying valleys in the field of study, and denser rock units forming mountains, hills and other topographic highs. Trends to this effect are easily identifiable in the study area (Figure 3.2).

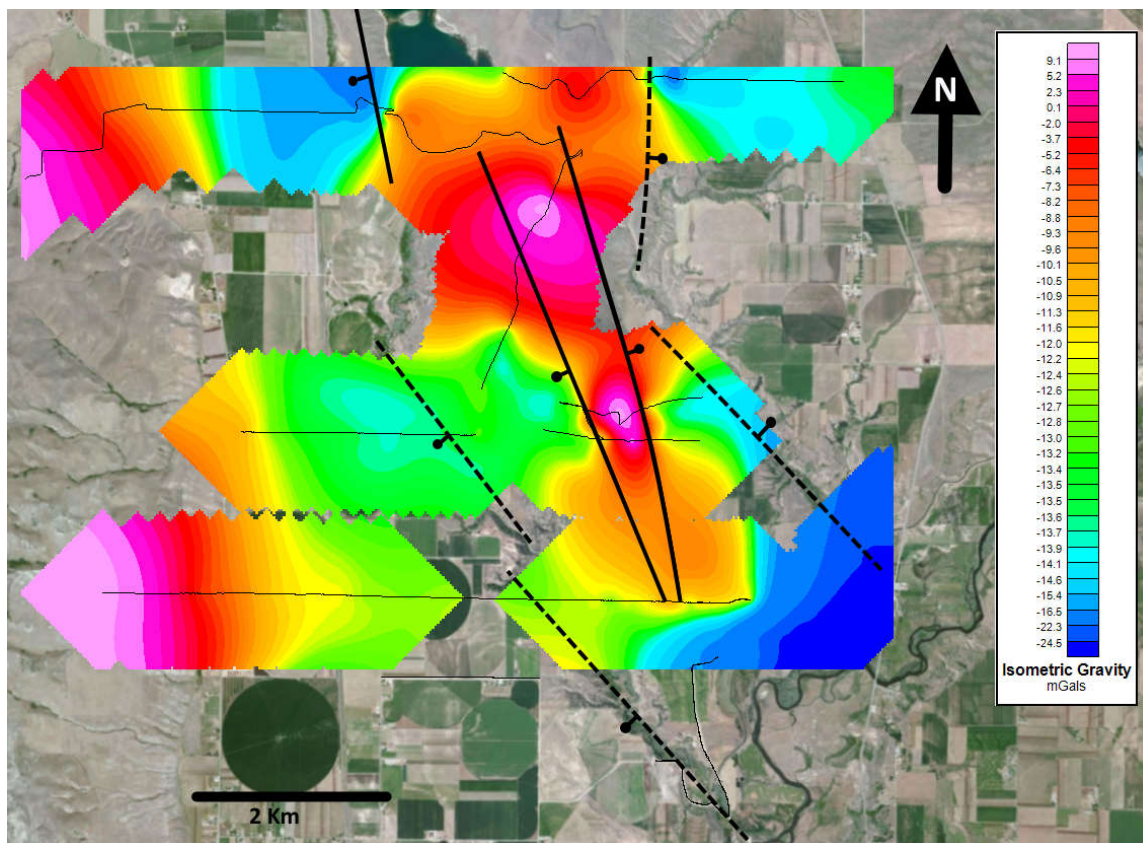


Figure 3.2. Gridded isostatic gravity data collected over the survey area. Additional lines are included in the southwestern portion of the study area which were did not cross any structures of interest and so were analyzed for the purposes of this thesis.

Gravity highs can be seen in the mountain foothills and the main body of Clifton Hill and its northern extension near the Twin Lakes Reservoir. The valleys separating Clifton Hill from the Bannock foothills and east of Clifton Hill have a lower gravity field. Most likely because the basin is filled with low density sediments, while the foothills and Clifton Hill produce higher signals due to denser older rock in the shallow subsurface (Figure 3.2). This is examined in more detail during discussion of specific survey lines.

SHALLOW AQUIFER DATA

Water levels ranged from just over 5 meters to 68.5 meters below ground level. When water levels are converted to elevation, a general trend exists of decreasing head (elevation of water level) to the southeast (Figure 3.3). Temperatures measured varied from a high of 108.2°C to a low of 2°C. The highest temperatures were clustered in the south near the southwestern toe of Clifton Hill and in southwestern portion of the study area (Figures 3.4 and 3.5). Of the

newly collected data, the mean temperature is 25.5°C, and half of the temperatures measured were greater than 15°C.

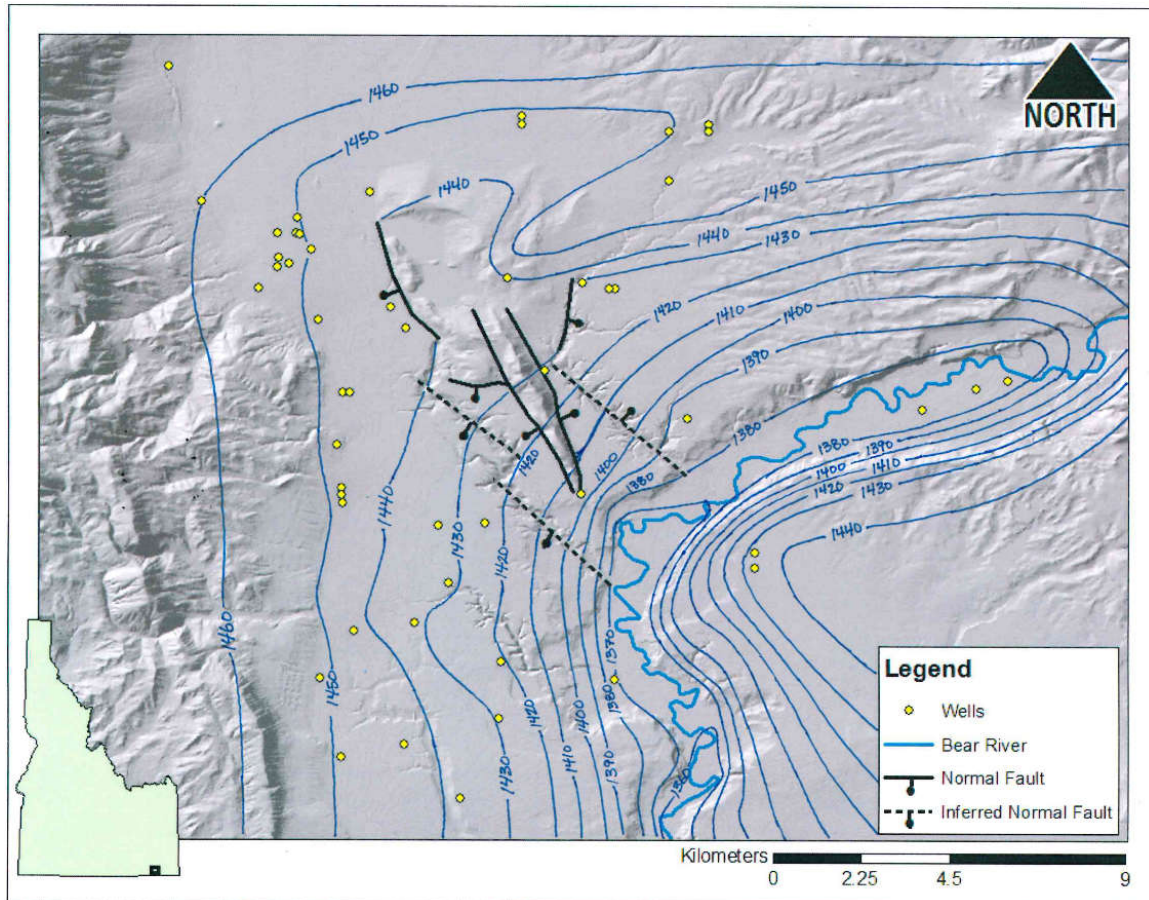


Figure 3.3. Contoured water level map of the study area. Water level values are in meters above mean sea level (AMSL). Ground water flow in the valley is towards the Bear River. Fault system layout has been updated based on interpretation of geophysical models.

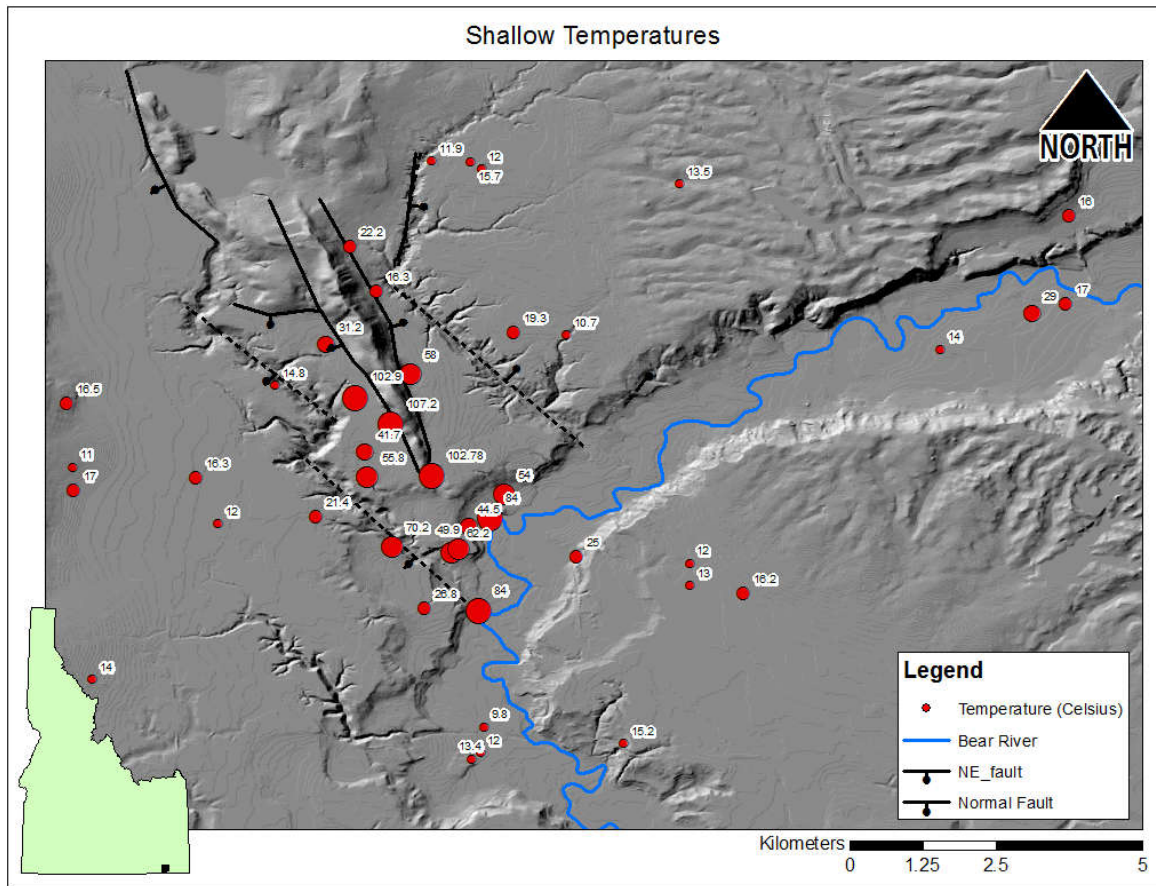


Figure 3.4. Well temperatures from the shallow depth range (1,439 to 1,354 m). Red dots indicate temperatures measured in wells (with the exception of two hot springs temperatures included along the Bear River) and are graduated based on the temperature value, i.e. higher temperatures corresponds to a larger circle. Fault system layout has been updated based on interpretation of geophysical models.

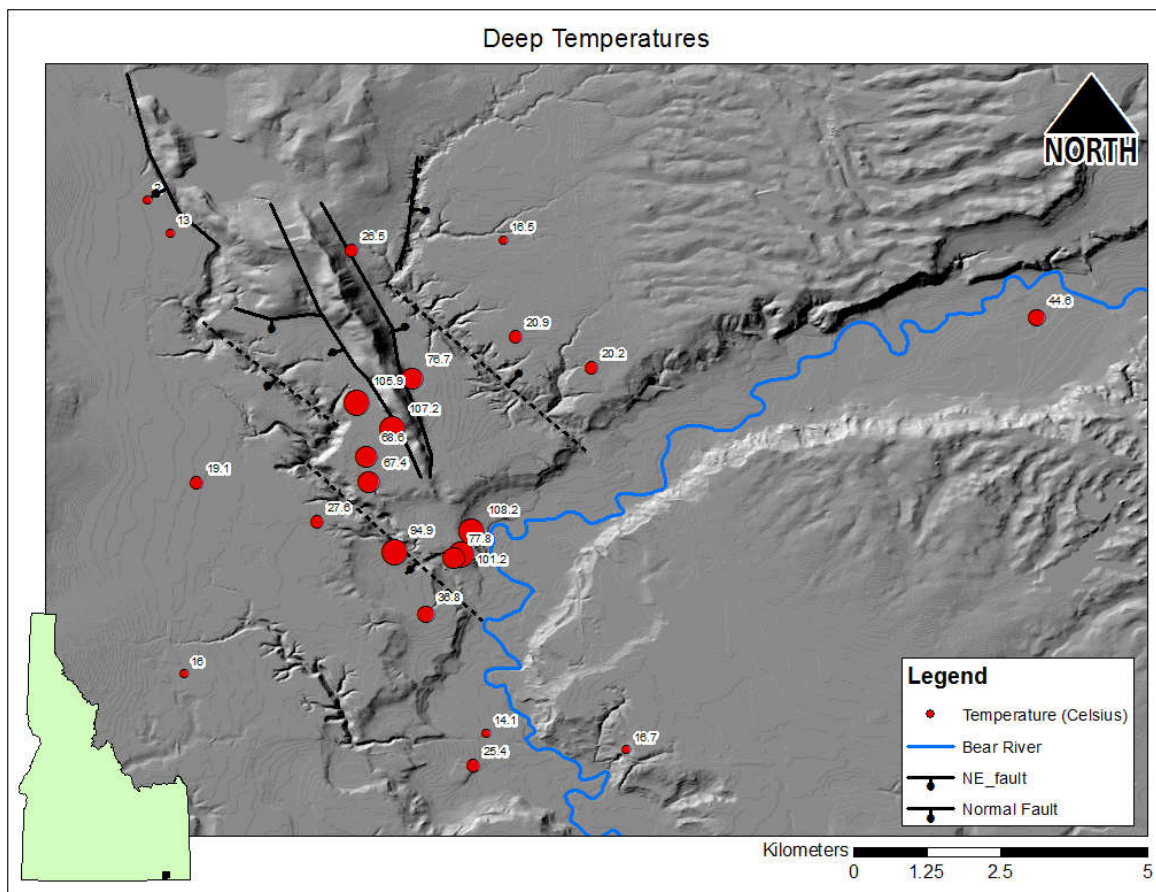


Figure 3.5. Well temperatures from the shallow depth range (1,439 to 1,354 m). Red dots indicate temperatures measured in wells (with the exception of two hot springs temperatures included along the Bear River) and are graduated based on the temperature value, i.e. higher temperatures corresponds to a larger circle. Fault system layout has been updated based on interpretation of geophysical models.

MAGNETIC AND GRAVITY MODELS

The primary aims of the geophysical surveys are to better characterize the faults bounding Clifton Hill and to improve the conceptual model of the geothermal system. The datasets were analyzed graphically by varying the geophysical models and improving the match to gravity and magnetic signals. The resulting geophysical models provide insight into the location and orientation of the local fault system.

The utility of geophysical data, especially magnetic data, is often enhanced when it complements another form of geophysical data, such as gravity. Thus, the magnetic and gravity data are analyzed concurrently. Isolated magnetic anomalies when not accompanied by a gravimetric anomaly tell the geophysicist only that the magnetic susceptibility of the underlying rock unit has changed. This change does not mean that the rock type changed,

only that the magnetic properties and or depth of the unit are different from one point to another. When a magnetic anomaly is accompanied by a gravity anomaly, it indicates that the rock type and thus the density (causing a change in the gravitational field) and magnetic susceptibility (causing a change in the magnetic field) are different, which relates to different rock types and/or depths. The coincidence of magnetic and gravity anomalies can be observed in all the lines analyzed and modeled (Figures 3.6-3.11).

The geometries presented in the following geophysical models are not unique solutions, meaning that there is more than one way to interpret the gravity and magnetics signals measured. The following interpretations fit the measured data within the bounds of the representative density and susceptibility values assigned to the units. In many instances the modeled signal may not fit the measured data exactly. This does not mean that the model is invalid, but that in simulating the properties of subsurface units and conditions, the model is not perfect, and has room for improvement. In a majority of the models the magnetic susceptibility was varied substantially even within units of the same rock type, sometimes as much as an order of magnitude to match the field data.

Magnetic and gravity signatures and the corresponding geophysical models for lines 2, 3, 4, 6, 7 and 8 are presented in Figures 3.6-3.11, respectively. In these figures, the upper window displays the magnetics signature, the center window displays the gravity signal and the lower window displays the geophysical model. Color of the units is assigned by the modeling software and based on density of the unit. The colors may vary depending on the ranges of densities used in each line, as such units of the same type and density but in different lines may have different colors.

Lines 3, 4 and 6, were modeling using 2³/₄ dimension (D) applications available in the Oasis Montaj software suite. These applications allow the geometry of the geologic units to be projected specified distances away from the survey line. This was done to account for the trend of the survey line coming into close proximity of faults and changing rock units. Using these applications, the software is able to calculate the effect a different geologic unit located north or south of the line will have on the magnetics and gravity signal. In modeling line 2, remanent magnetization, magnetic inclination and magnetic declination were included in the models of the Scout Mountain and Meta-dabase units. These characteristics were only

included in line 2 and was done to assist modeling the magnetics data across the large gap (Figure 3.6).

Line 2 trends west-east directly south of the toe of Clifton Hill, and though the relief does not express the presence of a subsurface density contrast, there is a local gravity high which suggests one. The magnetic signal is unable to support or discredit this assertion, as the signal across the same interval was removed due to the data being influenced by nearby farming equipment and infrastructure (metal silos, houses, buildings and machinery). There is, however a marked decrease in the magnetic signature which coincides with a dip in the gravity signature following the gravity high over the subsurface extension of Clifton Hill (Figure 18). This may be due to a low density and magnetically neutral sediment filled “trough” or “hole” adjacent to the buried horst block. This interpretation agrees with existing published literature on the area, asserting that the body of Clifton hill is tilted to the south, and extends at an angle beneath the ground surface south of where it terminates (Link & LeFebre, 1983; Figure 3.6).

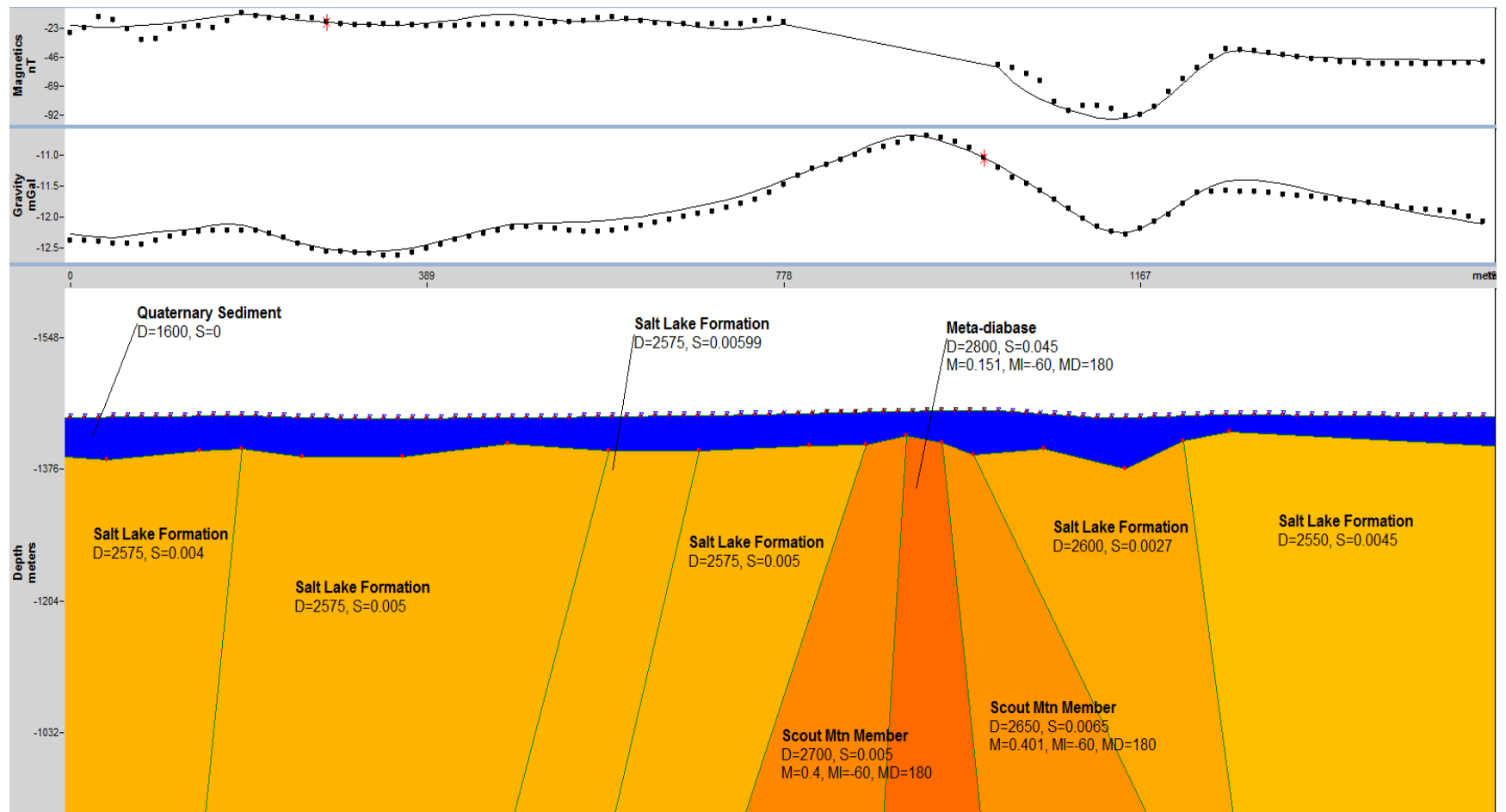


Figure 3.6. Geophysical model fitted to the magnetic and gravity data for line 2. M refers to remanent magnetism in ampere per meter, MI refers to magnetic inclination, MD refers to magnetic declination. Magnetic error: 4.74 nT; Gravity error: 0.091 mGal. Vertical Exaggeration = 0.75.

Line 3, which crosses Clifton Hill and its bounding faults, demonstrates how a regular trend in the magnetic field can correspond to a large perturbation in the gravitational field (Figure 3.7). The magnetics signal across line 3 shows a declining trend, beginning at a value of 43 nT on the west, and ending with -17 nT on the east. The portion of the magnetics signal surrounding Clifton Hill (960-2015 m) displays the most localized variation, with fluctuations on the order of 2-3 nT, superimposed on the overall decreasing trend in the data. It is the continuation of this overall trend across Clifton Hill that suggests the larger signal behavior may be a regional expression of magnetic field from a regional structure. One such structure large enough to cause large wavelength trends in the magnetics signal is the East Oxford-Dayton fault, a high angle normal fault system located on the western margin of the NCV (Figure 1.2). The modeled data can be fit to this long wavelength trend with the addition of a magnetic, wedge-shaped geologic block seated underneath the existing model, meant to simulate the footwall of the regional fault. The exact value of susceptibility assigned to the block can vary according to the shape and size of the block, as both can be manipulated to fit the wave form. Such regional behavior in the magnetics signal can also be observed in lines 4, 6 and 8 (Figures 3.8, 3.9 and 3.11).

The smaller, localized variation in the magnetic field of line 3 correlates approximately to the increase in the gravity signal. This gravity high in turn correlates closely to the topography as the line nears, crosses and moves away from Clifton Hill. The magnetic signal however, increases only slightly, by approximately 2 nT, before continuing a slow and steady decrease towards the termination of the line. This relatively small deviation from the overall magnetic trend indicates that only a slight change in the magnetic susceptibilities of the underlying rock units occurs, while the gravity high suggests that there is a marked change in rock density for Clifton Hill (Figure 3.7). This marked change in rock density indicates a fault on either side of Clifton Hill.

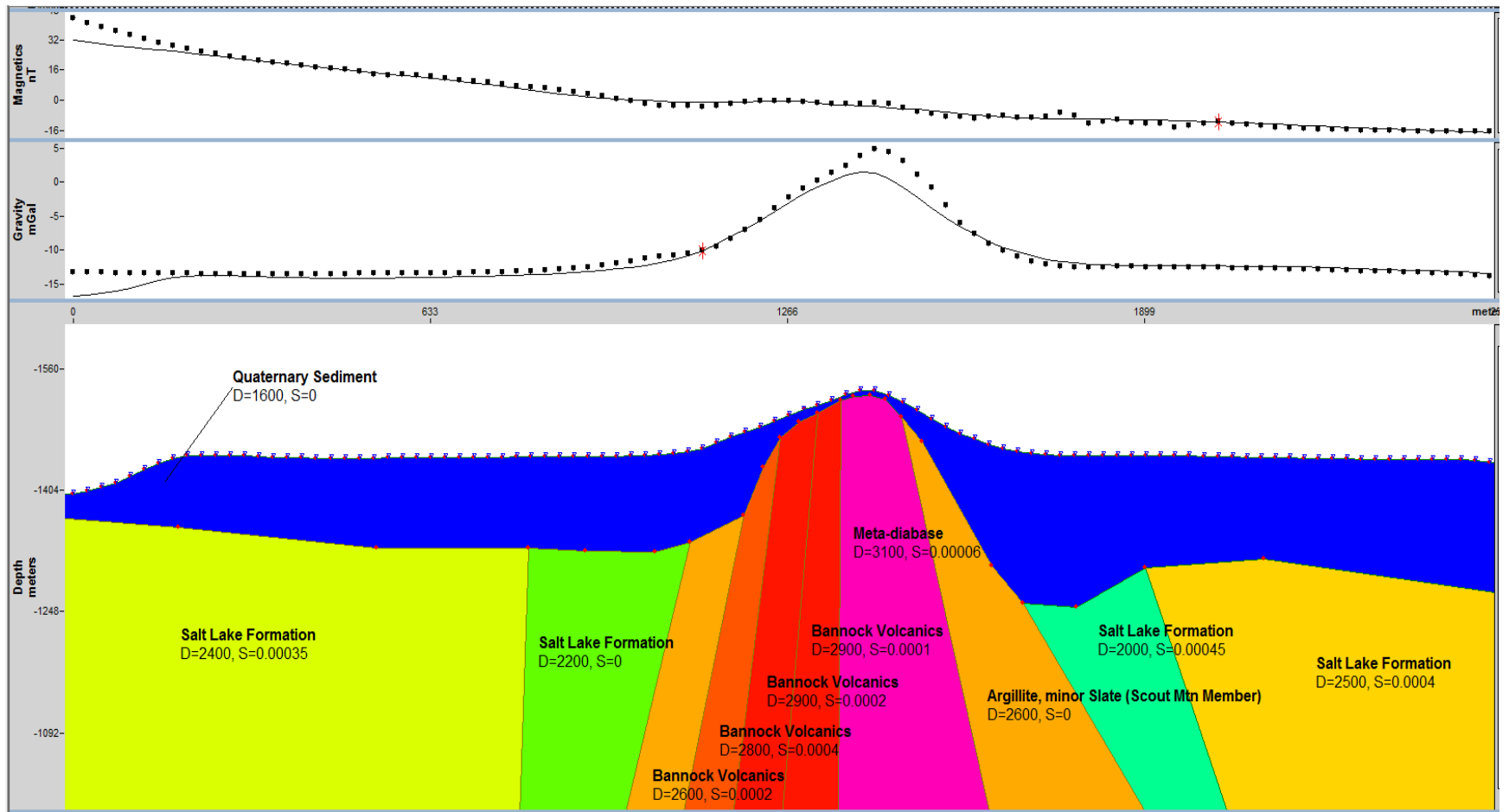


Figure 3.7. Geophysical model fitted to the magnetic and gravity data for line 3. Magnetic error: 2.395 nT; Gravity error: 1.045 mGal. Vertical Exaggeration = 1.25.

It is possible that the faults bounding either side of Clifton Hill are vertical or reverse, though this is unlikely, due to multiple factors. The first being that Clifton Hill is located in a Basin and Range graben structure, where the regional stress is extensional. So, a reverse fault, which is most commonly found in the presence of a compressional stress field, would be unlikely. Secondly, the Stock 1 and Stocks 1-A wells, penetrated an unconformity to the west of Clifton Hill (McGreevey & Bjorklund, 1978); above these unconformities the stratigraphic units described consisted of unconsolidated sediment and partially consolidated gravel, sand, silt and clay and below the unconformities were units of the Precambrian Pocatello formation. If these unconformities encountered by the Stock 1 and Stocks 1-A wells represent two points on the fault plane of Clifton Hill's western bounding fault, then the fault dips to the west and an approximate angles of dip can be calculated using principles of geometry. Using the measured depth to the unconformity and the distance between the wells and the western flank of Clifton Hill, the estimated angle of the fault at the position of Stock 1 is 35° , and the estimated angle of the fault where Stocks 1-A intersected it is 47° . These estimates of the dip of the fault is supportive of the assertion that the western bounding fault is a westerly dipping normal fault, and so the Clifton hill bounding faults in the geophysical are modeled as such. There is no well log data available to estimate the dip of the east bounding fault.

Line 4 displays both low and high amplitude anomalies in the gravitational and magnetic fields. The variations in the magnetic field along line 4 are smaller in magnitude than those measured on line 3, and moderate in comparison to other lines. A pronounced low in the magnetic signal coincides with the western extent of a broad gravity high over Clifton Hill, reflecting a clear change in lithology (Figure 3.8). Smaller variations in the magnetic field over Clifton Hill likely correspond to changes in lithology between the Bannock and Meta-diabase units, which are not reflected in the gravity anomaly because these units have similar densities. (Figure 3.8).

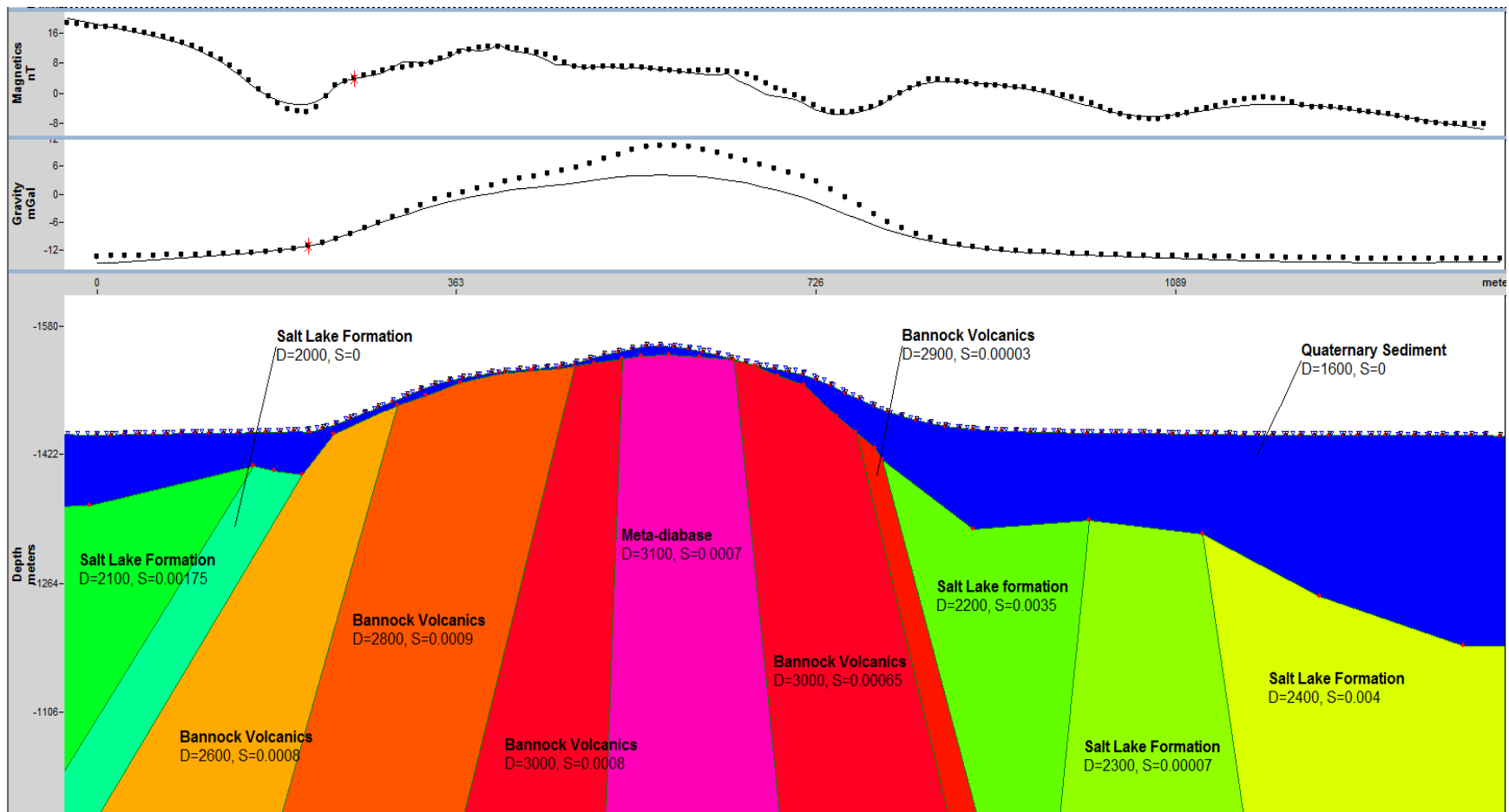


Figure 3.8. Geophysical model fitted to the magnetic and gravity data for line 4. Magnetic error: 0.855 nT; Gravity error: 2.388 mGal. Vertical Exaggeration = 0.75.

The gravity signal seen in line 6 increases gradually to the northeast and is accompanied by small wavelength highs in the magnetic anomaly. Faults are identifiable at 400 and 1,250 m by sharp changes in the slope of the gravity high over Clifton Hill. Overall, the gravity trend can be explained by the presence of material(s) of similar densities, the positions of which rise with the topography. The magnetic data also increases slowly throughout the line at a rate of approximately 0.0022 nT per meter, with the exception of four instances where “spikes” can be found. In this case however, the very low values seen in the magnetic data, between 0.93 and 5.7 nT, and the very slow rate of change over the course of the line, mean that very subtle changes in the orientation and thickness of subsurface bodies makes a very noticeable change in the magnetic signature. Thus, the magnetic spikes in line 6 can be modeled by thinning the top layer of magnetically neutral Quaternary sediment (Figure 3.9). This decreases the distance from measurement to source, and models the change in distance as an increase in the magnetic signal. This isn't the only way to model this data, given the values of susceptibility used; it proved to be effective and matched the conceptual understanding of the geology.

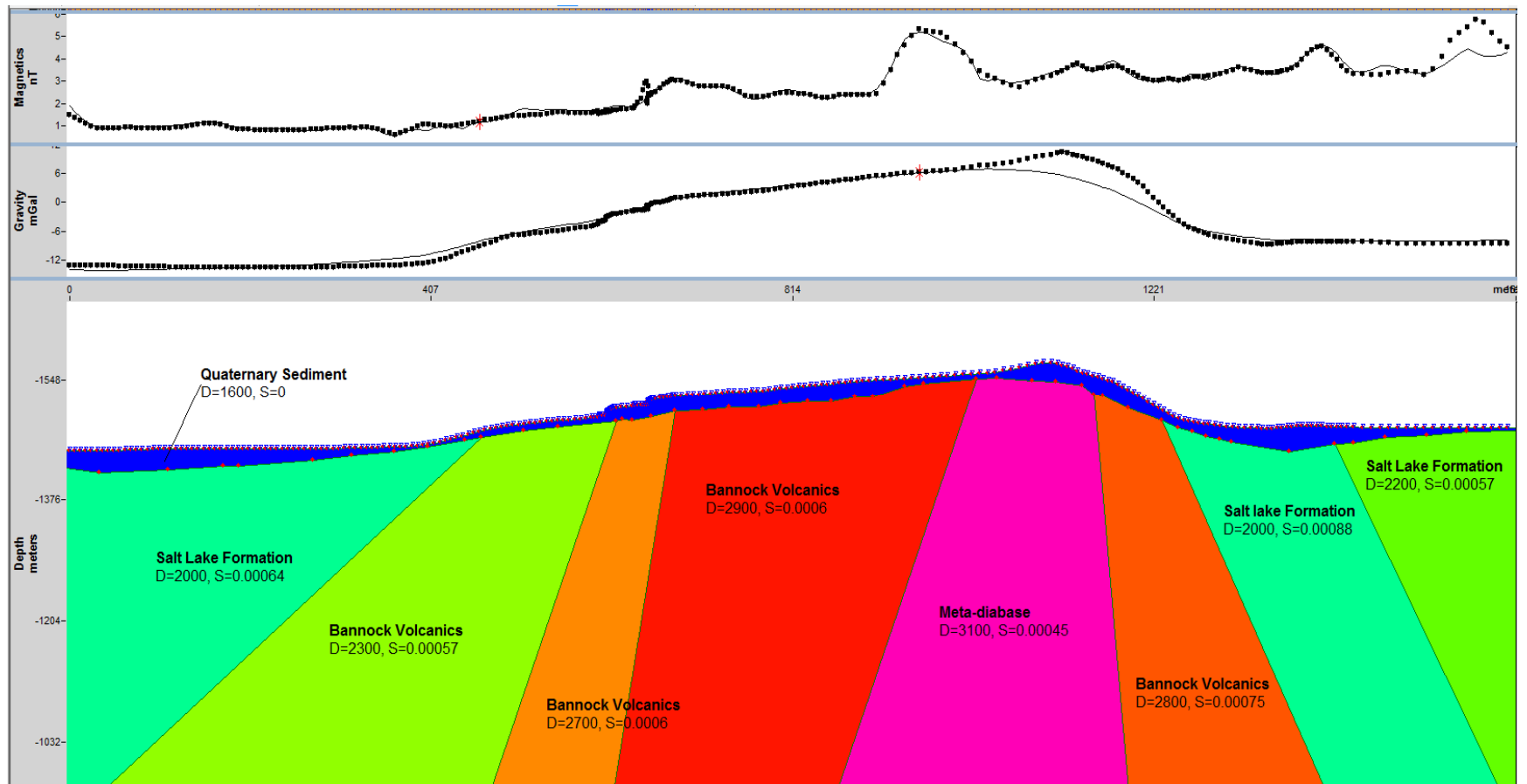


Figure 3.9. Geophysical model fitted to the magnetic and gravity data for line 6. Magnetic error: 0.229 nT; Gravity error: 1.48 mGal. Vertical Exaggeration = 0.75.

Line 7 is the longest line in the survey (7 km), and covers the entire basin between Clifton Hill and the foothills of the Bannock Mountain Range (Figure 3.10). The line is dominated by broad gravity and magnetic lows that correspond to the thick basin fill (Salt Lake Formation and the Quaternary sediment). The higher gravity signal on the west side of the line may be due to the thickness of the Quaternary sediment covering the Bannock Volcanic unit on the west is thinner than on the east. It may also be due to the Bannock Volcanics on the west being denser than those on the east (Figure 3.10). Topographically there is a local high positioned at 3845 m along the line, which has proven difficult to model (Figure 3.10). It may be formed by a cap of low density material (perhaps through weathering) and low values of magnetic susceptibility. Or it could be an anthropogenic artifact caused by quaternary fill materials associated with the canal infrastructure in this area. Near this position are earthworks and a pumping station which pulls water from the Twin Lakes Reservoir into a large water pipe which travels down the steep gradient and across the basin to the west.

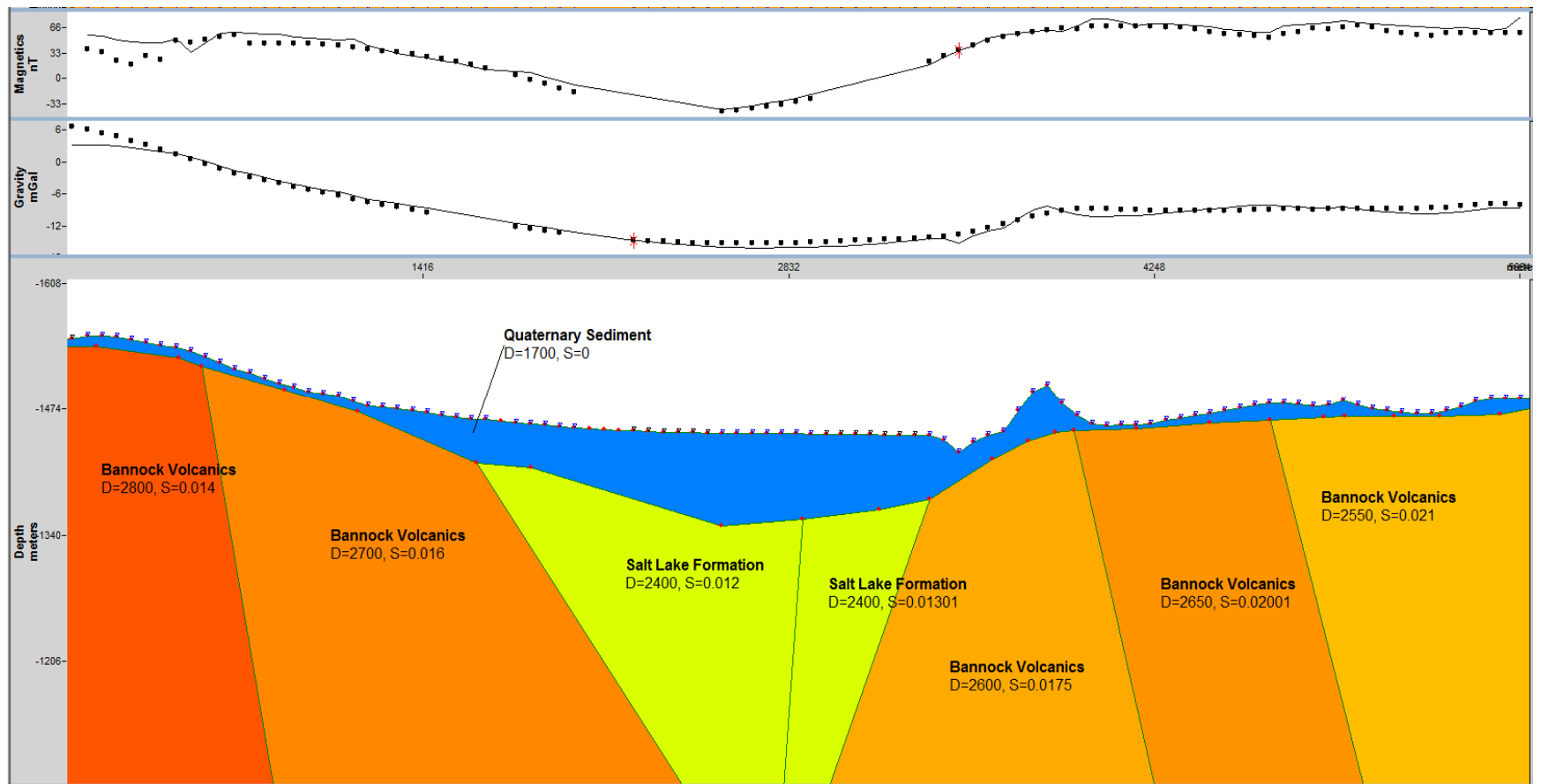


Figure 3.10. Geophysical model fitted to the magnetic and gravity data for line 7. Magnetic error: 9.189 nT; Gravity error: 0.894 mGal. Vertical Exaggeration = 3.5.

Line 8 (Figure 3.11) begins on the east side of the Twin Lakes Reservoir and trends east across the elevated terrain north of Clifton Hill, before crossing Battle Creek and an inferred fault (Figures 2.3, 2.4, 3.1 and 3.2). There is a broad, positive gravity signal over the elevated topography decreasing to a low where the line crossed the Deep Creek drainage. East of the Deep Creek drainage, the gravity signal increases slowly from -14.5 to -13.25 mGal over a distance of ~1360 meters. The magnetics signal behaves very differently (Figure 3.11). Between the beginning of the line and 715 m, the magnetic signal displays low amplitude deviations, on the order of 2-3 nT, with a localized minimum value of 51 nT at 455 m. Between 455 and 2,400 m, the short wavelength changes become greater, on the order of 6-7 nT, with a local high of 69.9 nT at 1,796. Between 2,415 and 2,797 m deviations of the signal strength lessen and are similar to the first portion of the line (0-715 m), but still slowly increasing at approximately 1 nT/100 m. From 2800 m to the end of the line the signal increases sharply by 9 nT and then begins to decrease (Figure 3.11). With the exception of instances at 1,312 m and 1,670 m, the magnetic anomalies do not correlate to a gravity anomaly. These magnetic anomalies could be caused by unseen cultural artifacts such as buried utilities or infrastructure, or by lateral heterogeneities in magnetic susceptibility along the eastern half of the line. At 1,312 and 1,670 m, the magnetic anomalies correlate to gravity anomalies, a slight change in the slope at 1,312 m and a low at 1,670m (Figure 3.11). The anomalies at 1,312 m are approximated by deeper Bannock Volcanic and thickening of the quaternary sediment. This is adjacent to a sequence of magnetic anomalies which can be modeled with a change in geologic units, separated from one another by a normal fault dipping to the east (Figure 3.11). It is important to note that the high occurrence of short wavelength magnetic anomalies make it difficult for the magnetic signal to be modeled with great accuracy. The presented geophysical model is a best fit of the simulated magnetic signal to the measured data.

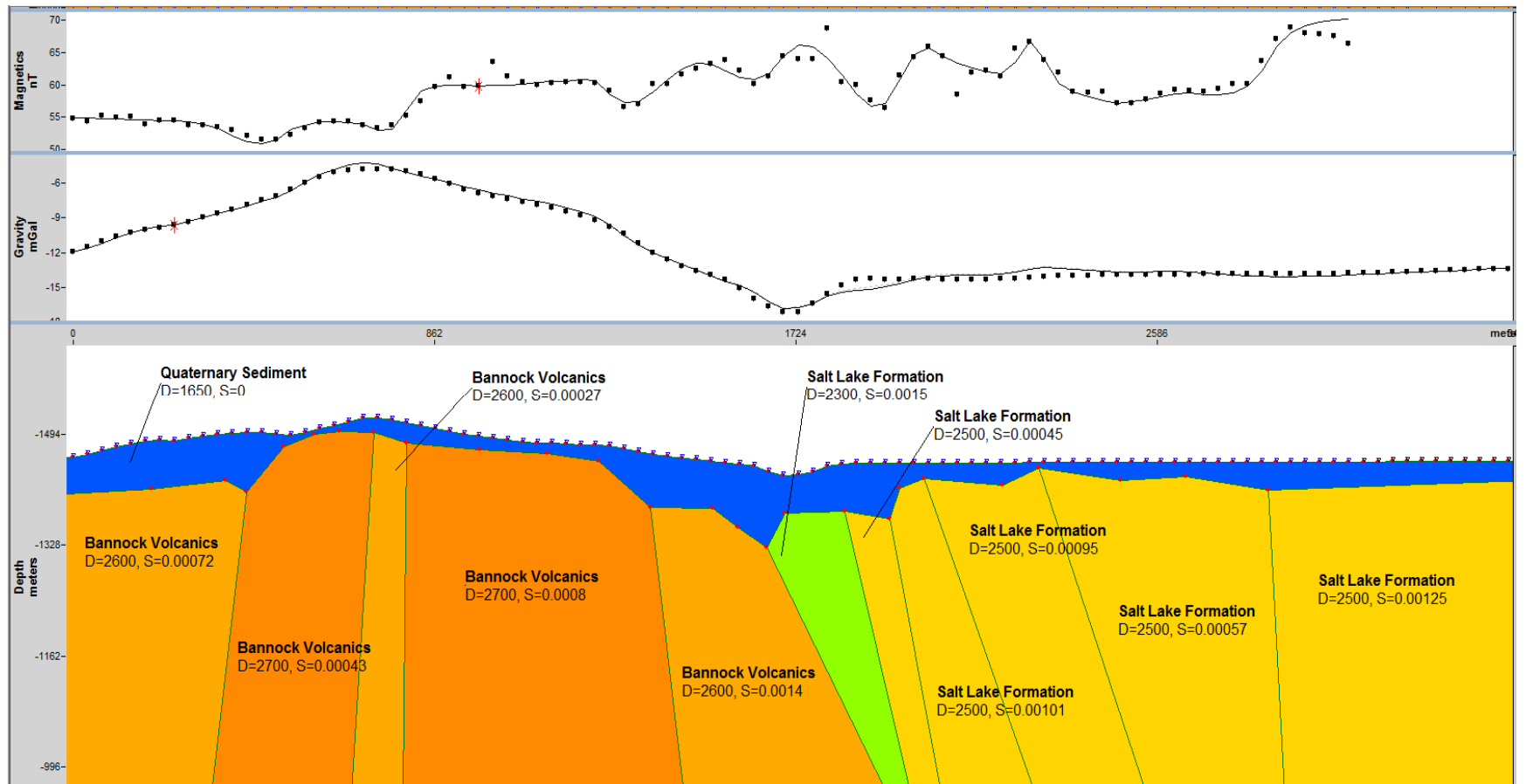


Figure 3.11. Geophysical model fitted to the magnetic and gravity data for line 8. Magnetic error: 1.245 nT; Gravity error: 0.313 mGal. Vertical Exaggeration = 1.5.

From the geophysical models a plan-view of the fault structure can be developed for Clifton Hill (Figure 3.12). Modeling of the potential field data revealed the faults trend very tightly to the base of Clifton hill and there exists another fault unaccounted for in the previous fault map crossed by line 6 (Figures 3.12 and 3.9). This third fault appears to branch off from the western bounding normal fault approximately half way up its length, and appears to be a normal fault dipping to the south (Figures 3.9, 3.12).

A comparison can be drawn between the previous interpretation of the Clifton Hill bounding faults and this new interpretation by constructing a geophysical model of the previous interpretation and comparing the magnetic and gravity error values. In this way, the improved interpretation based on new data reduces the magnetic error by approximately 80% and reduces the gravity error by approximately 28%.

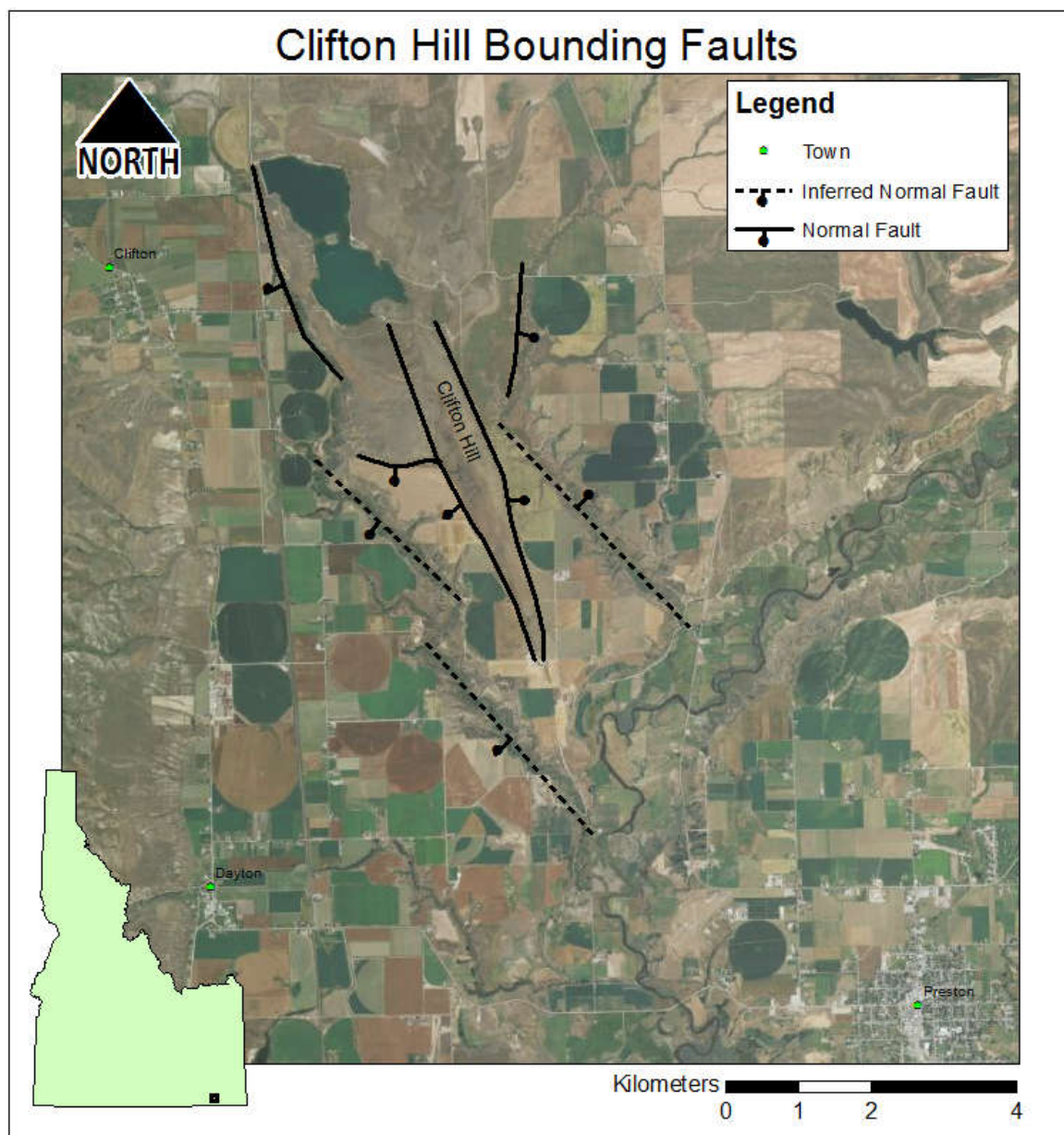


Figure 3.12. Updated fault layout for the Clifton Hill bounding faults based on interpretation and modeling of potential field measurements taken from the area.

STRUCTURAL ANALYSIS

The resolution of the geophysical methods is insufficient to assess the absolute dip of Clifton Hill faults. From the well log data discussed previously though, estimations of the dip of the western bounding fault can be made. These estimations indicate that the angle of dip below horizontal between Clifton hill and Stock 1 well is 35° and for Stocks 1-A the angle is 47° (Figure 3.13).

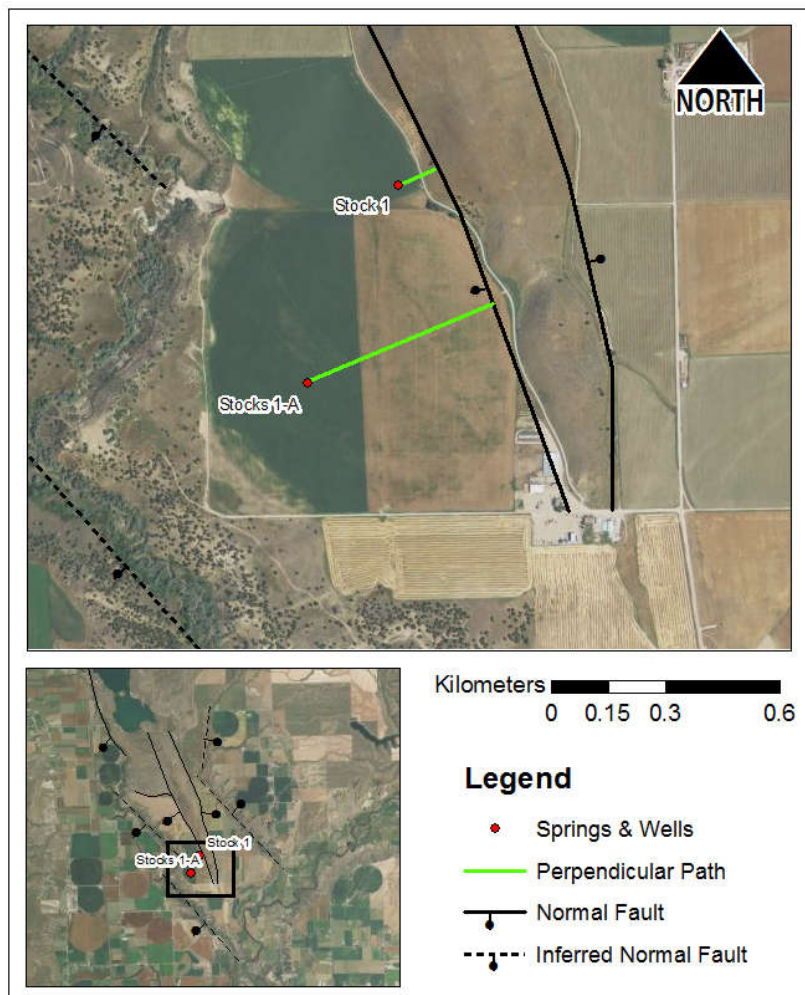


Figure 3.13. Position of the Stock 1 and Stocks 1-A wells and the distances separating them perpendicularly from the Clifton Hill bounding faults.

Although these types of fault boundaries can carry thermal fluids (Faulds et al, 2011), a significant increased permeability was not detected at the contacts in either well. However, portions of the same fault can act as either barriers or conduits to groundwater flow depending on the compressional or extensional status of the fault segment (Fairley and Hinds, 2004). Another explanation may be the fault planes are uneven and disjointed small blocks can create an uneven and discontinuous fault plane or series of fault planes along which permeable pathways can be separated by less permeable zones. In this case, the wells drilled into a portion of the fault between vertical permeable zones and thus, did not penetrate a conductive zone carrying thermal fluids from depths. We have no direct evidence of the vertical permeable zones other than the presence of hot water in the vicinity of the Clifton Hill Faults.

AQUIFER TEMPERATURE AND WATER LEVEL DATA

The local shallow aquifer of the NCV is hosted predominantly in Quaternary valley fill and the Salt Lake formation. The older volcanics and metamorphic units have much lower hydraulic conductivity and are thought to act mostly as confining layers (except where fractured or faulted). The quaternary sediments that cover the valley floor are comprised of unconsolidated lacustrine sand, gravel, clay and silt deposited in Pleistocene lake Bonneville and its predecessors. The Neogene Salt Lake formation is semi-consolidated lacustrine and tuffaceous sediments. From the Mid-Miocene to early Pliocene areas of the Basin and Range were isolated, flooded and drained, filled with ash from the caldera eruptions in the Snake River Plain (Janecke and Evans, 1999). This created heterogeneous sequences of silts, clays, sands, gravels and smaller amounts of fresh water limestone. During low lake stages gravel bars and sand stringers were deposited. Ultimately an aquifer comprised of interconnected saturated lenses, permeable interconnected strands of sand and gravel, and other irregularly shaped units was created. Wells in this aquifer, including those measured, serve agricultural or domestic purposes with flows ranging from 10 gpm to a few 100 gpm. The relatively shallow domestic and agricultural wells provide important data for this study, including water temperature and depth to water.

Additional temperature and water level data were taken from older studies including: McGreevey and Bjorklund (1970), Ralston (1981) and Mitchell (1973). Data from exploration efforts in the late 70's by Sunedco and Chevron, fill gaps in the existing coverage (Figures 1.4 and 1.5; McIntyre and Koenig, 1978 & 1980; Munoa, 2016). Thermal gradient holes drilled by Sunedco and Chevron range in depth from 86 to 1492 ft and provide important hydrogeologic information over a large area. Unfortunately, these wells were abandoned and are no longer available for monitoring. Thermal gradients in these wells were measured in the spring and summer of 1978. Since that time, long term and seasonal trends have undoubtedly impacted aquifer water levels. Typically, a correction might be applied to an old data set to account for long term trends in water levels, however, a long term aquifer level record could not be found for the aquifer anywhere near the site. USGS monitoring data for the area has gaps in the record and monitoring was terminated in 1993. Thus, data presented here are used without correction or modification. The level of uncertainty in the

resulting interpretations, such as ground water flow direction is not known. It is assumed that the direction of flow and water levels are reasonably correct, but the data are insufficient to quantify uncertainty.

Water level data was utilized from McGreevey and Bjorklund (1970) and the new survey data collected specifically for the purposes of this research. Sunedco and Chevron data was excluded due to that data being exclusively temperature data. The Sunedco and Chevron thermal wells were logged for resistivity, but a definite water level in the temperature boreholes was not determinable (Munoa, 2016). As expected, the contoured water levels show that the flow of groundwater is towards the Bear River (Figure 3.3). Groundwater discharges to the Bear River or flows in the subsurface down the axis of the Bear River drainage and out of the basin. Based on the data, a definite difference in the head values can be found on either side of the Clifton Hill faults. This may indicate an actual head differential across these faults, or this may be due to the spatial or temporal sampling of the data. This could be resolved with higher resolution data on either side of the hypothesized faults.

All of the industry thermal gradient wells have temperature logs. Because of the variation in well depths, temperature data were separated into two depth categories. This allowed for temperatures from shallower wells that did not penetrate to depths sufficient to reach maximum temperature to be compared with temperatures in deeper wells measured at shallower depths. The division of the wells was based on elevations; elevations above mean sea level (AMSL) from 1,439 to 1,354 meters were designated “shallow” measurements, while those made at 1,353 to 1,256 meters AMSL were designated “deep” measurements.

Temperatures of the shallow and deep wells as shown on the maps are hottest near the western margin of Clifton Hill and its southern toe (Figures 3.4 and 3.5). The highest temperature of the deep groups was in Sunedco’s Stock 1 well (107.2°C) near the western bounding fault (Figures 1.3, 3.4 and 3.5). Generally, as distance from the southern portion of Clifton hill increases, water temperature decreases. From both depth ranges, it can be seen that there is a predominance of high temperatures clustered near the Bear River to the southeast of the southern toe of Clifton Hill. This may be due to the Clifton Hill bounding faults on the east and west sides interacting with each other to the south of the end of Clifton

Hill. Or it may be due to interaction with the Mink Creek-Bear River lineament which cuts through the area south of Clifton Hill (Figure 1.6).

A pattern of elevated temperatures is observed on trend in a southeasterly direction along the axis of Clifton Hill terminating at hot springs along the Bear River. Opposite the Bear River, the well data are very sparse, but existing data suggests that the thermal trend ends at the Bear River in the vicinity of two major hot springs (Battle Creek and Squaw). Flow from Battle Creek hot springs can reach 2,160 liters/minute with temperatures as high as 84°C, while flow at Squaw hot springs is less, 450 liters/minute at 73°C (Mitchell, 1973).

Contoured temperature values show the effect the directional flow of ground water has on the thermal plume(s) emanating from the aquifer somewhere near the southwest end of Clifton Hill (Figures 3.14 and 3.15, Tables 3.2 and 3.3). Figure 3.14 is the thermal plume in the shallow interval and Figure 3.15 is the thermal plume in the deep interval. The central axes of the plume trend northwest to southeast. In the shallow plume, the southeast toe deflects slightly to the southwest, this may be due to the southwest-ward flux of groundwater down the axis of the Bear River. Deeper temperatures depict less deflection in this direction, but the plume contours are drawn deflected in this manner because of an elevated temperature measured in well 2-78-7 and the Squaw Hot Spring well (Figures 1.3, 1.4 and 3.15). This temperature may be influenced by the possible fault indicated by the dashed line.

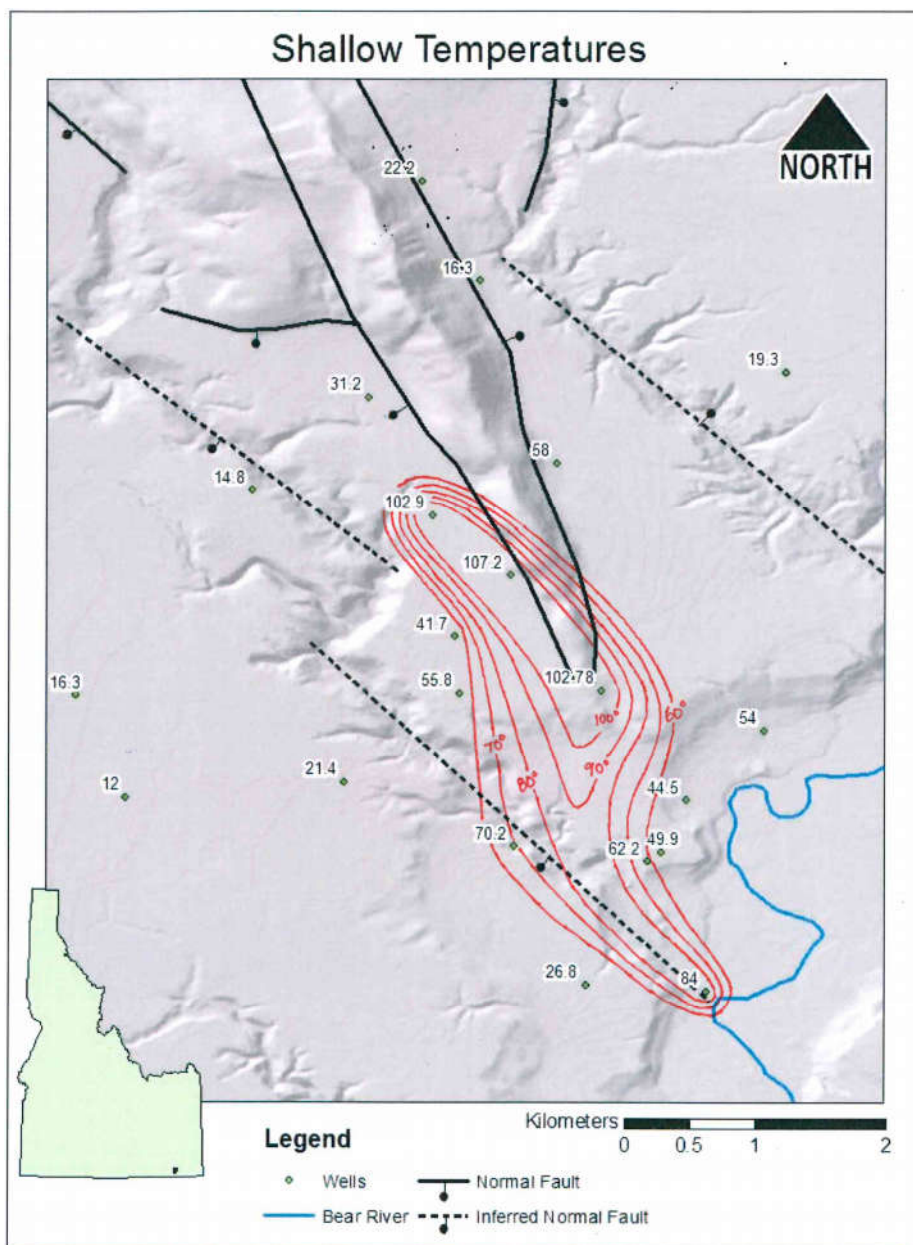


Figure 3.14. Temperature (Celsius) contours in the Shallow depth range of the Clifton Hill geothermal prospect. Deflection of the toe of the plume to the sw may be caused by the flux of ground water down the axis of the Bear River Valley.

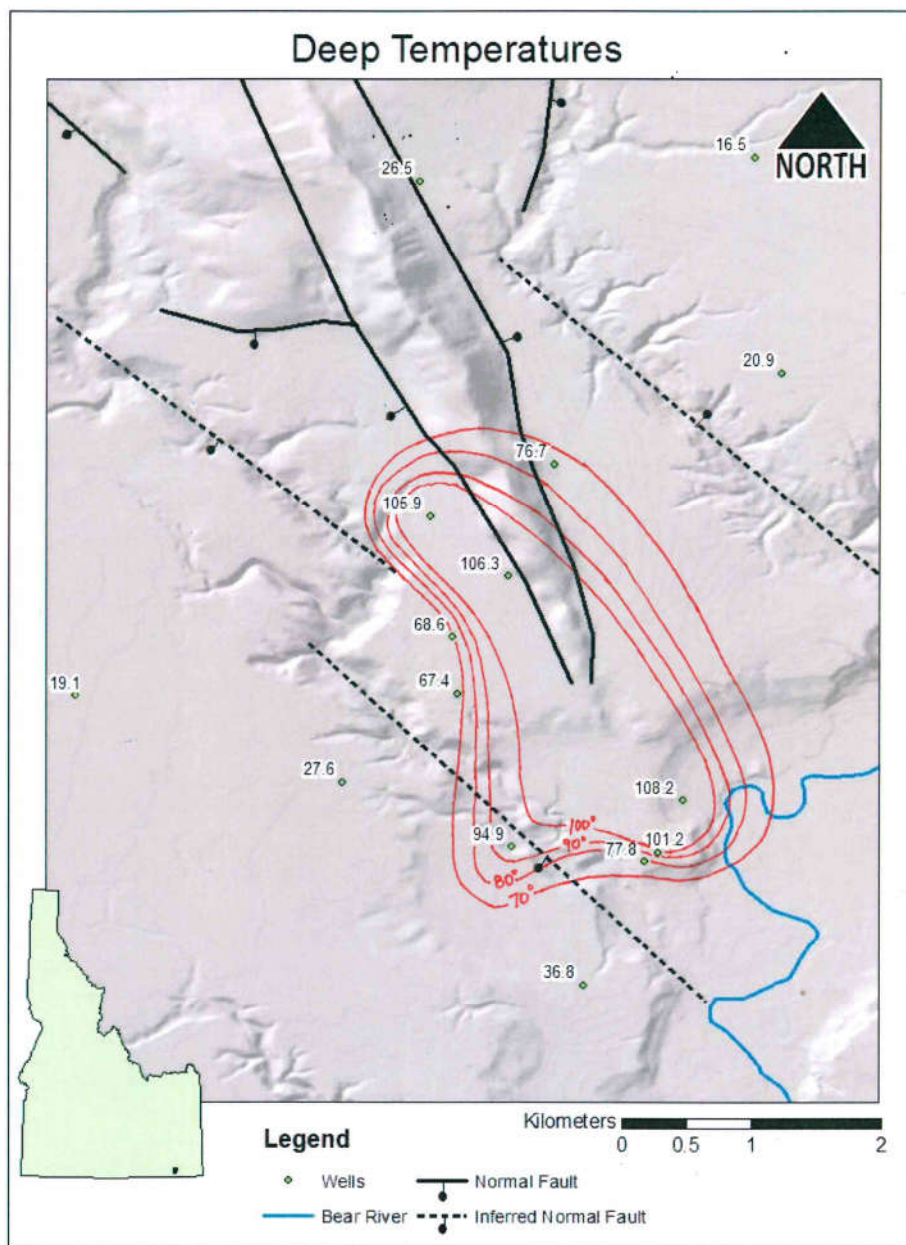


Figure 3.15. Temperature contours in the deep depth range of the Clifton Hill geothermal prospect. Deflection of the toe of the plume to the sw may be caused by the flux of ground water down the axis of the Bear River Valley.

Temperatures from the deep subsystem are highest near Clifton Hill (Figures 3.5, 3.15). As a comparison, the thermal well 2-78-3 on the west side of the hill measured 105.9°C while the measured temperature from Chevron well BR-78-21 on the east side of Clifton Hill was 76.7°C. Well 2-78-8 (108.2°C) has the highest temperature of the deep range, this well is located to the southeast of the toe of Clifton Hill, along the Bear River (Figures 1.4, 3.4, 3.5, 3.14 and 3.15). Also, well 2-78-7 (94.9°C), near the southern end of the hypothesized fault

(dashed line), yields a hotter temperature than would be expected given its position relative to other temperatures nearby. Unfortunately, no potential field data was collected across this inferred fault that would have helped to confirm or deny its presence. The elevated temperature and the position of the Squaw Creek hot springs at its' southeastern end suggest that the inferred fault may be real and that it may act as a permeable conduit carrying thermal fluids upward from depth to discharge into the shallow aquifer (Figures 1.4 and 3.14).

There is an increase in the contoured area of elevated temperatures between the shallow and deep elevation ranges. One possible explanation for this is that as thermal fluids rise along the Clifton hill faults (specifically the western fault), they spread outward into the aquifer preferentially along zones of increased horizontal permeability. This suggests that there is a section of the deeper depth range which is more permeable than the shallow depth range. The rate of the spreading of the thermal plume (pattern of flow) is a function of the hydraulic conductivity and head gradient of the layers encountered. Variations in the horizontal hydraulic conductivity are expected, due to the heterogeneous and anisotropic nature of the aquifer. Another explanation is that the area of the thermal plumes is influenced by local groundwater flow where temperatures are pushed and cooled to the southwest by the flux of ground water down the axis of the Bear River Valley (Figures 3.3, 28-29). Additional wells are needed to fully evaluate the areal extent of the thermal plumes with depth.

Well temperatures suggest that the southwestern most hypothesized fault may be transporting thermal fluids (Figure 3.14). Temperatures produced by Sunedco Well 2-78-7 were 70.2°C in the shallow depth range and 94.9°C in the deep range (Figures 3.14 and 3.15). This fault is also on trend with Squaw hot springs (Figure 1.3). If the fault is a permeable pathway for thermal fluids it may be providing a conduit of flow to Squaw hot springs. Temperature logging of Well 2-78-7 depicts a profile of increasing temperature from approximately 140 F to 204 F at a depth of about 300 ft (Figure 3.16). This temperature remains constant to a depth of approximately 340 ft, below which the temperature decreases to 185 F at the bottom of the well, 480 ft. This profile follows a pattern reminiscent of a thermal outflow plume, a specific type of thermal flow pattern found in many geothermal areas (Goff et al, 1988).

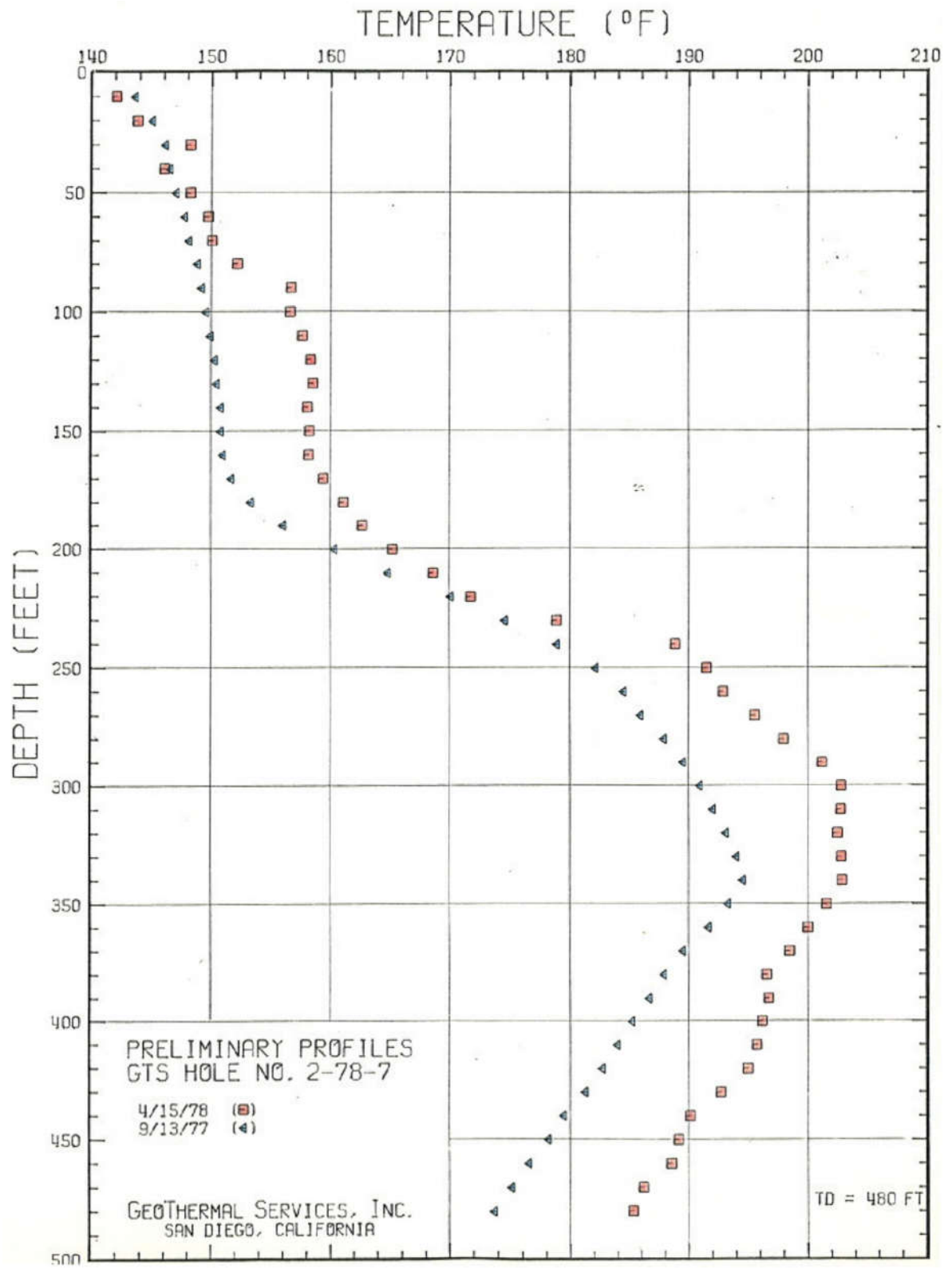


Figure 3.16. Temperature gradient profile for Sunedco test well 2-78-7.

An outflow plume from a geothermal source is a pattern of subsurface hydrothermal flow which convectively travels upwards into a lateral conduit of flow, such as a fault or permeable unit of an aquifer where it travels horizontally (Goff et al, 1988). These plumes travel down gradient and their distinctive temperature profile can be found along this trace. Though not always, hot springs have been associated with outflow plumes and are often located down gradient near the end of the plume. Temperatures measured in outflow plumes increase relatively quickly then level off or decrease with depth. It is common for temperatures to decline with depth, known as a temperature reversal; though this is not always present, it can be used to identify zones of lateral flow (Goff et al, 1988; Shevenell et al, 2012; Figure 3.17). In the Clifton Hill area several other temperature gradient profiles in wells such as Stock 1, 2-78-9, 2-78-1002 and 2-78-8 also display temperature reversal patterns (Figures 1.3, 1.4 and 3.18-3.21).

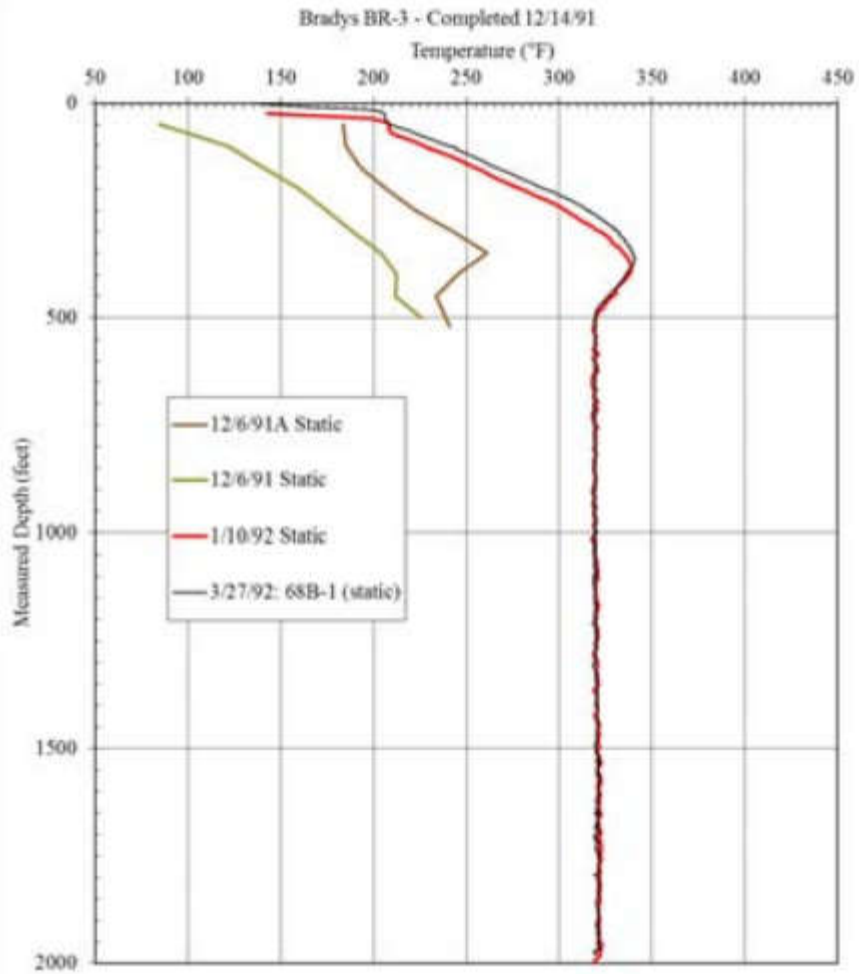


Figure 3.17. Temperature gradient exemplifying an outflow plume pattern and temperature reversal at approximately 350 ft. The inflection point at which the temperature reaches a maximum is indicative of the depth at which a permeable lateral flow layer exists. After Shevenell et al, 2012.

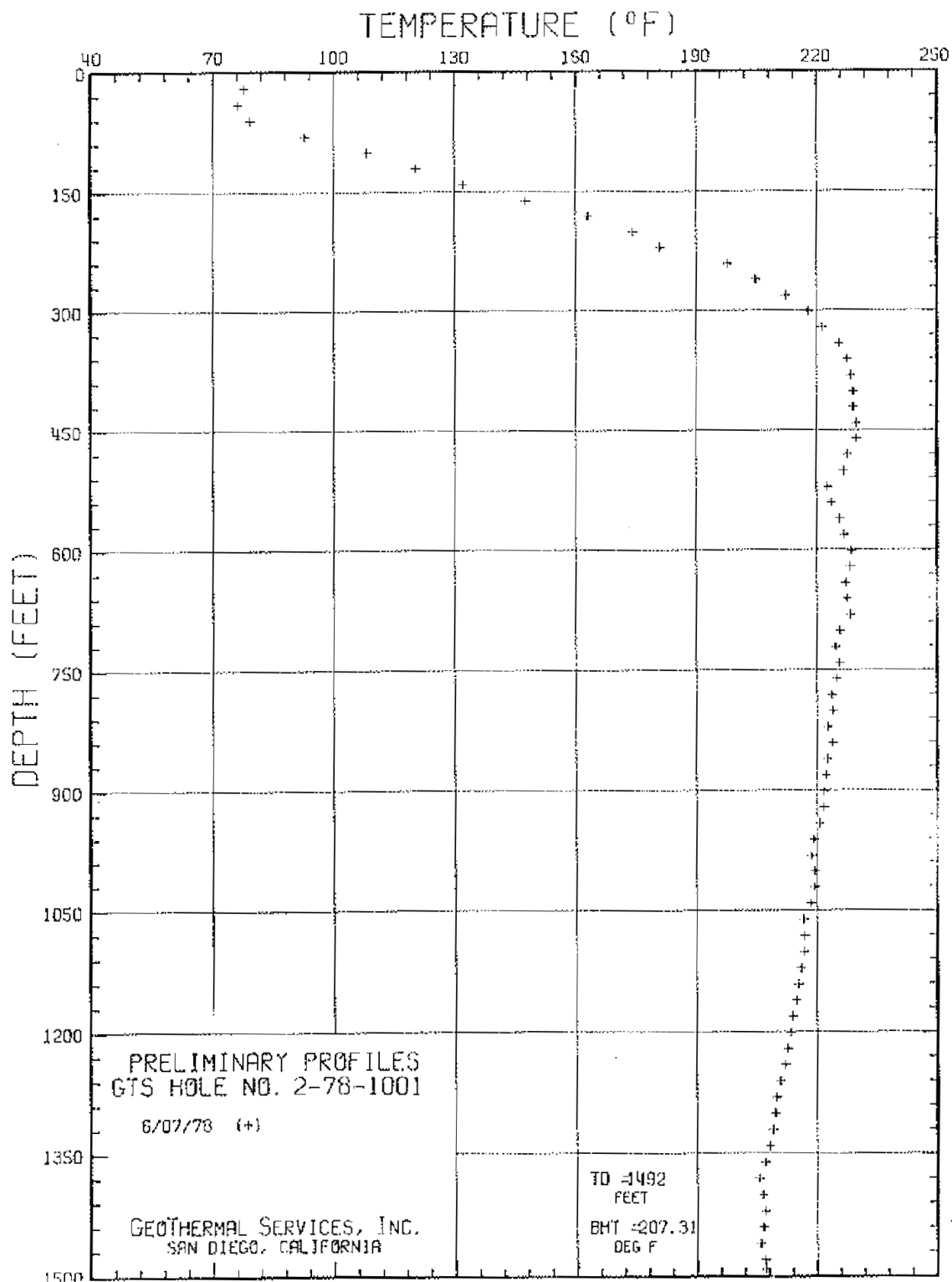


Figure 3.18. Temperature gradient profile for the Stock 1 well (2-78-1001).

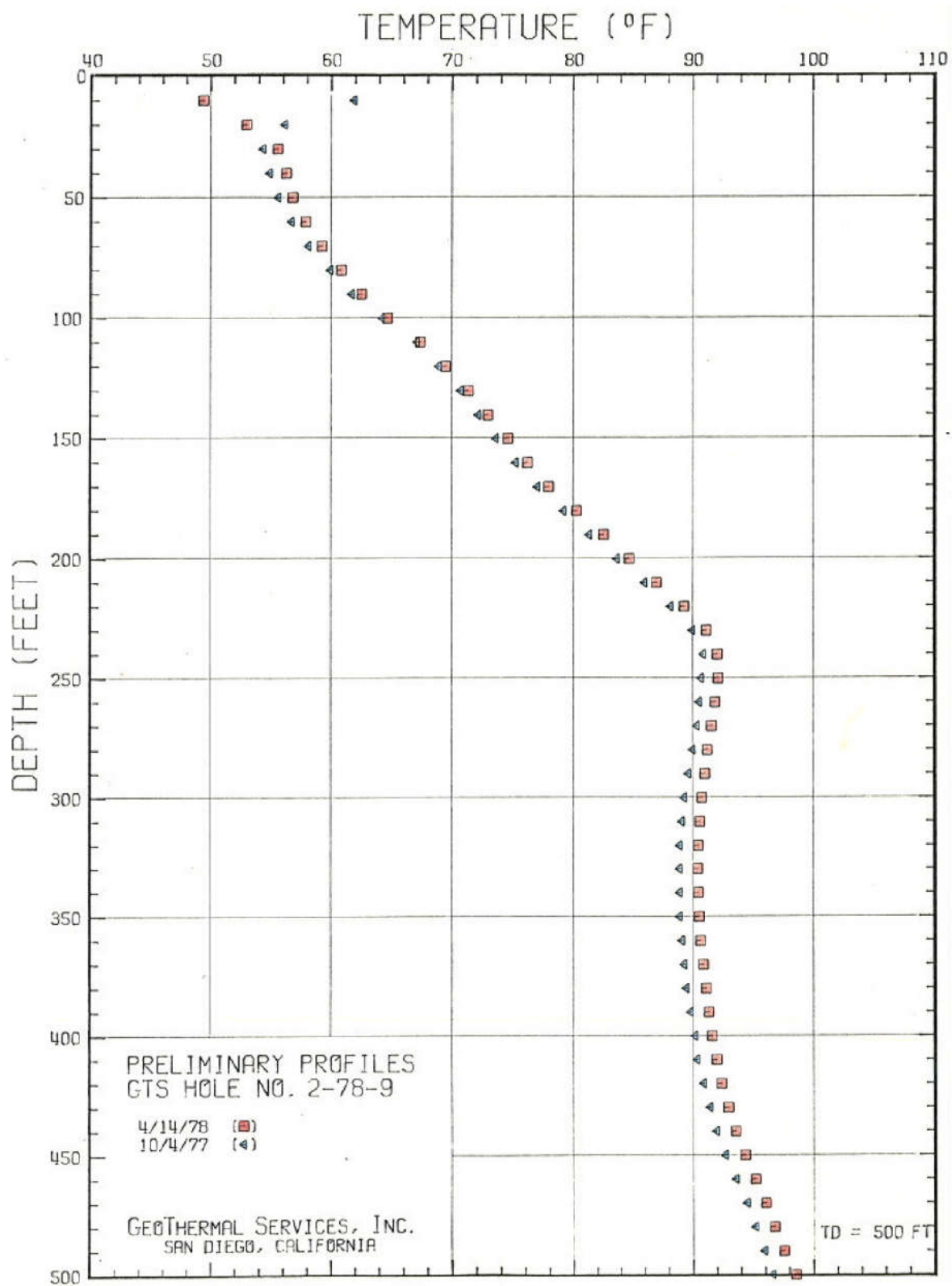


Figure 3.19. Temperature gradient profile for Sunedco test well 2-78-9.

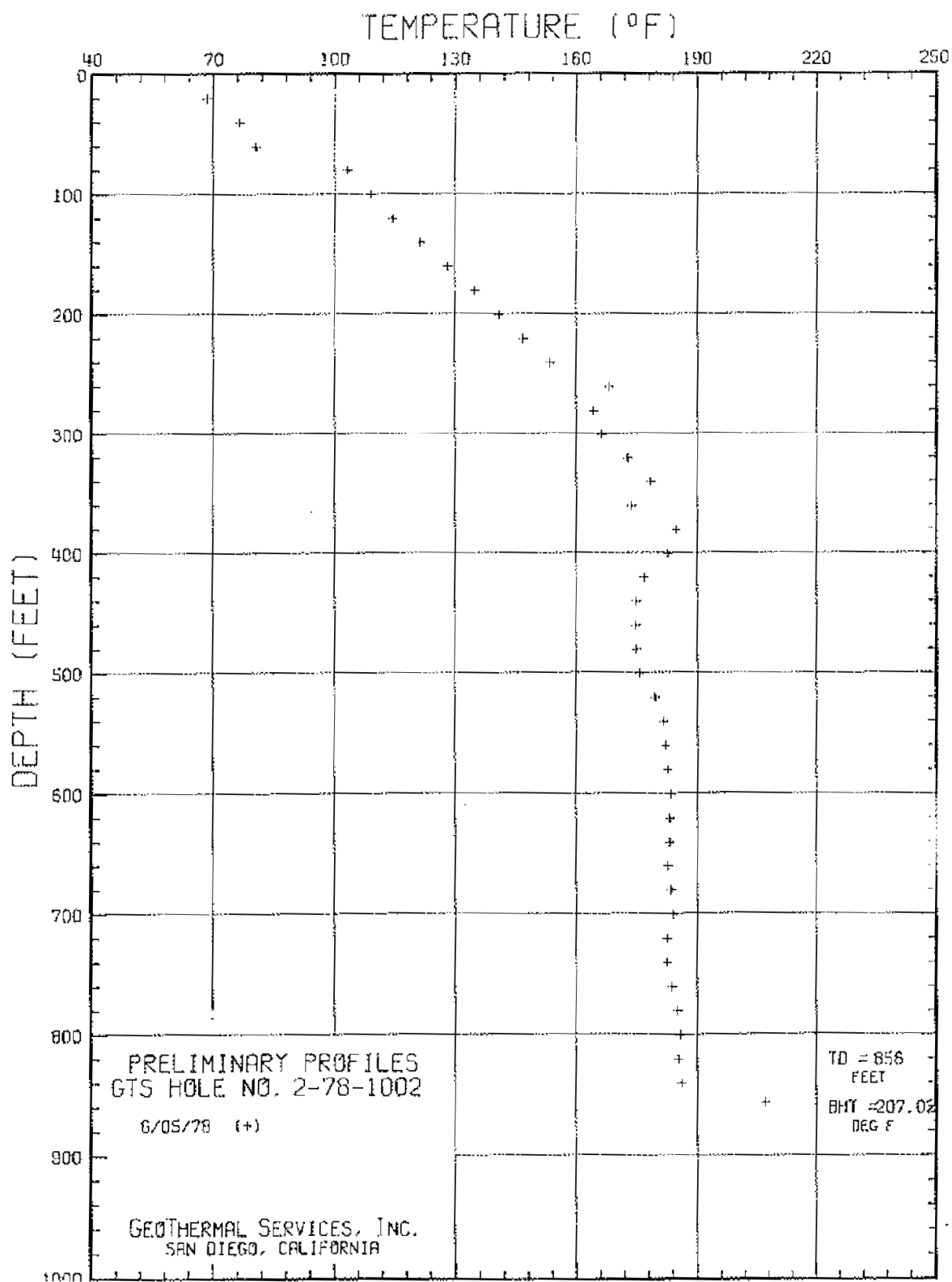


Figure 3.20. Temperature gradient profile for Sunedco test well 2-78-1002.

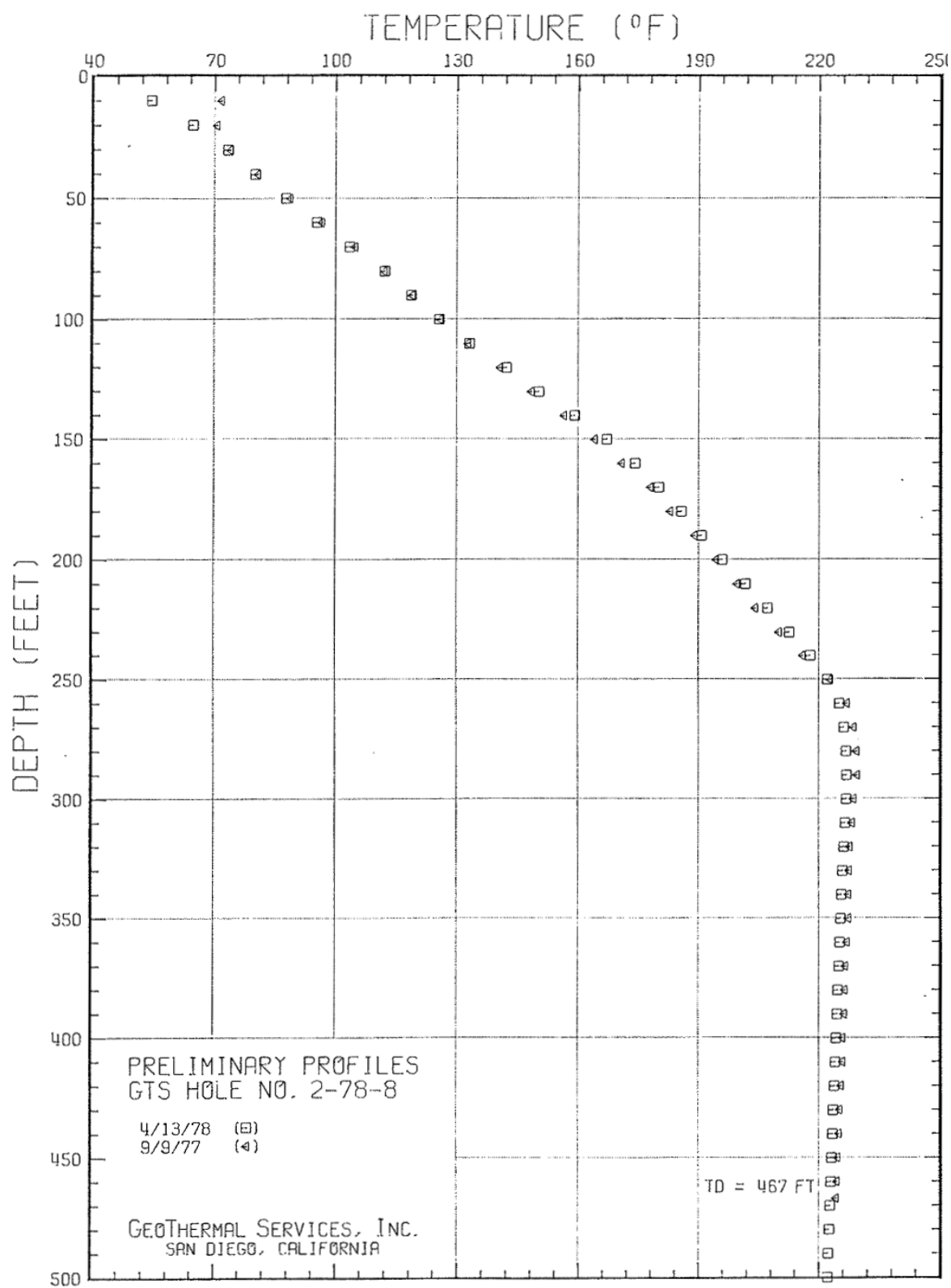


Figure 3.21. Temperature gradient profile for Sunedco test well 2-78-8.

From these temperature gradient profiles, it can be inferred that a permeable zone of lateral flow exists between 250 and 450 ft below ground surface. The thermal reservoir feeding an outflow plume may be anywhere between 2 and 20 km up gradient from the hot spring at the end of the plume trace (Goff et al, 1988). If Squaw hot springs is indeed located at the end of the plume, then the reservoir could be located anywhere along a 20 km long, northwest trending line originating at Squaw hot springs.

PERMEABLE FAULT STRUCTURES

Permeability in fault systems that host geothermal reservoirs is often increased at the intersection and/or overlap of faults. Such favorable structural settings are critically stressed causing these areas to persist as pathways for fluid flow (Faulds et al, 2011). For example “step-over” or relay ramp faults (Figure 3.22). These series of faults translate stress between larger faults and in the process create highly permeable inter-fault zones. In the study area, such structures may exist in multiple areas (Figure 3.23).

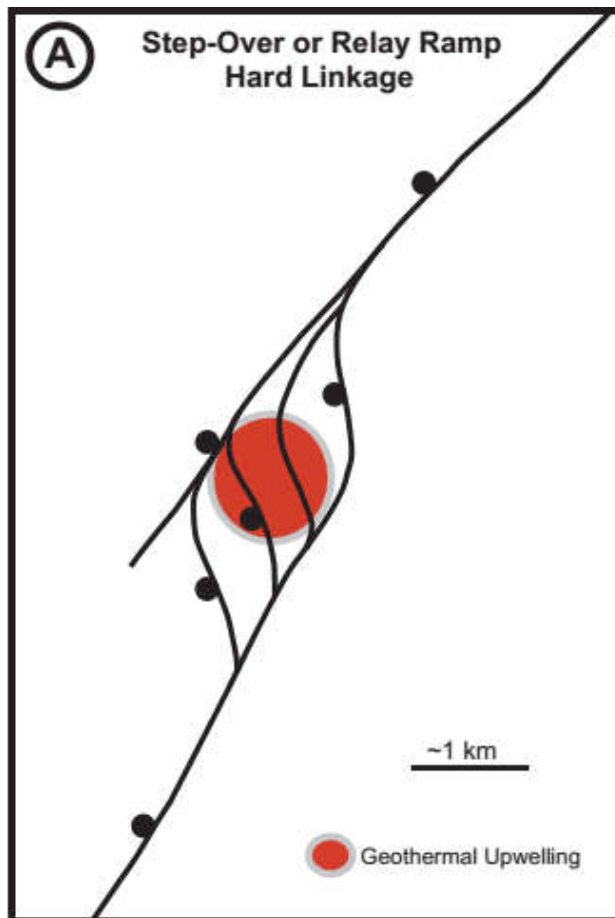


Figure 3.22. Example of step-over faults, a favorable structure of permeability caused by small faults translating stress from one fault to another. Modified from Faulds et al, 2011.

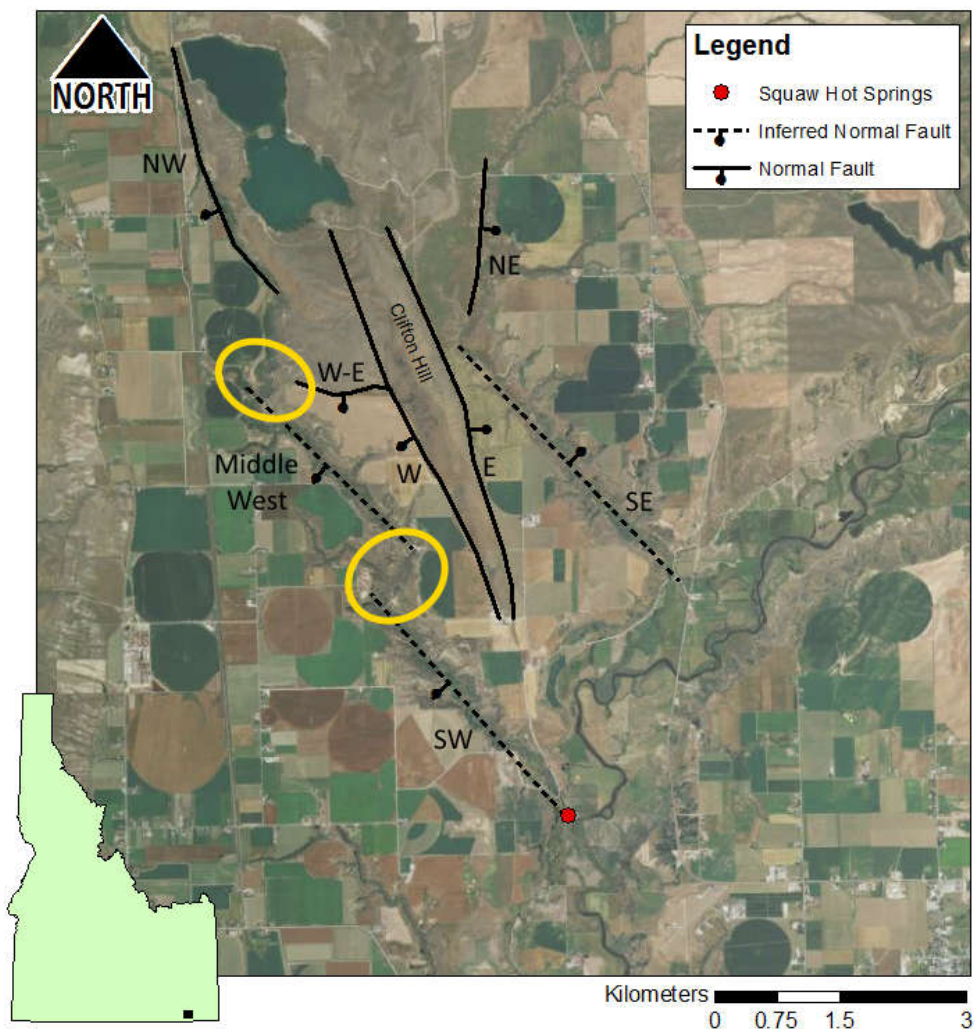


Figure 3.23. Yellow ovals indicates possible location of step-over faults. These faults increase permeability in the shallow subsurface while translating stress from one fault to another. Geothermal fluids often use these permeable zones as flow conduits. Labels correspond to the faults: NW – Northwest fault, Middle West – Middle West fault, SW – Southwest fault, NE – Northeast fault, SE – Southeast fault, W-E – West-East trending bounding fault, W – West bounding fault, E – East bounding fault.

These locations are both located up gradient from well 2-78-7. Squaw hot springs is positioned at the end of the southernmost fault, which may be the terminus of the previously discussed outflow plume. Evidence for step over faults being the cause of the thermal anomalies is not conclusive but the available data support this interpretation.

An alternative theory is that one or more of the Clifton Hill bounding faults may go listric with depth and encounter a deep thermal reservoir or a fault carrying thermal fluids upwards. Horst bounding faults in basin and range settings often behave this way, the angles of the

faults decreasing with depth until they are almost horizontal. In this manner, the fault would need to have an open and permeable fault plane to transmit water from depth.

Another theory suggested by Mitchell (1976) is that the hot springs along the Bear River are the result of the interaction of the southern extension of the Clifton Hill bounding faults with the Mink Creek-Bear River lineament (Figures 1.6 and 3.24). *“The intersection of this Mink Creek-Bear River lineament and the Clifton Hill boundary faults could be the controlling structure or focal point for the hot spring activity in this area.”* (Mitchell, 1976). Mitchell

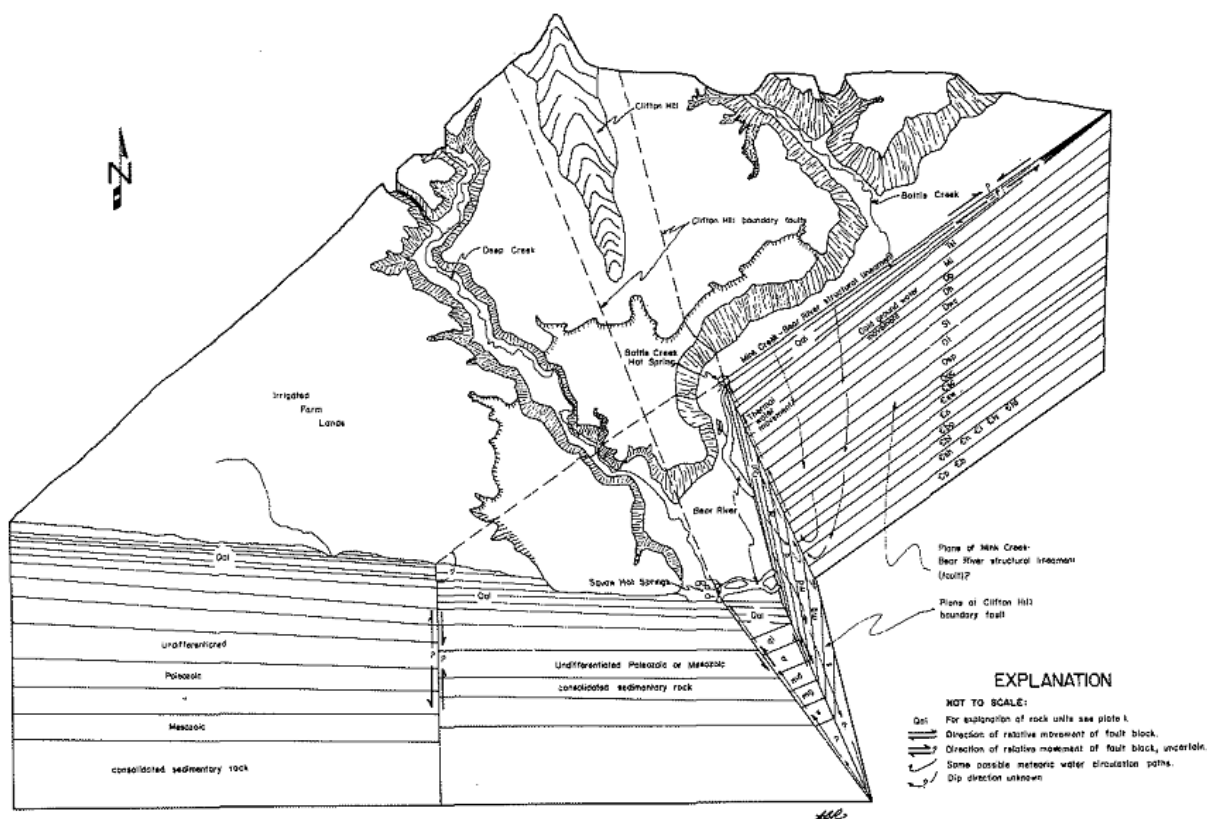


Figure 3.24. Conceptual model of the interaction of the Mink Creek-Bear River lineament with the southern extension of the Clifton Hill bounding faults. Here the structure of the lineament is depicted as being nearly vertical, and the type and direction of movement is unknown. After Mitchell, 1976.

There exists still, a substantial amount of uncertainty regarding the source of the thermal water that travels upward from depth along unknown flow pathways. At this time, without additional data, it is impossible to reduce this level of uncertainty regarding the reservoir and the flow pathway(s). The favored explanation for the source of geothermal waters in the vicinity of Clifton Hill is that heat from a deep thermal reservoir is traveling convectively upwards in the yellow areas indicated in Figure 3.23. As thermal water nears the phreatic

surface it encounters highly permeable horizontal zones. Here, thermal water leaves the vertical fault system and begins traveling horizontally down gradient. The thermal waters create the reversed thermal gradient as observed in wells 2-78-7, 2-78-9, 2-78-1002 and ultimately the thermal water is discharged at Squaw and Hot springs. It is also plausible that thermal waters from the same reservoir are traveling from depth along permeable extents of the listric portions of the Clifton Hill western bounding fault, expressing themselves in the shallow subsurface near the Stock 1 and 2-78-3 wells (Figures 1.3 and 1.4).

Water may also be derived from compaction and dewatering of the Salt Lake formation and the Quaternary Lake Bonneville sediments. Such water, known as connate fluids, can be released into the subsurface from the pore spaces of sediment and young sedimentary rocks as compaction and lithification progresses. Recharge to local aquifer systems and springs from connate sources has been found to occur in Death Valley, CA (Anderson et al, 2006).

Table 3.2. Names of wells and respective temperatures and elevations included in the deep temperature range.

Name	Max Temp (C)	Elevation (m)	Name	Max Temp (C)	Elevation (m)
2-78-3	105.9	1351.2	BR-78-10	25.4	1259.8
2-78-4	67.4	1335.7	BR-78-35	44.6	1264.3
2-78-5	19.1	1294.5	Jason Bunderson	16.5	1342.1
2-78-6	27.6	1293.3	Randy Moore	2	1351.2
2-78-9	36.8	1258.2	Dave Scott	20.2	1339.3
2-78-8	108.2	1290.2	E Gregorson 2	13	1258.8
2-78-11	14.1	1335.1	Jack Choules	13	1289.6
2-78-7	94.9	1287.2	Ernest Buetler	16	1303.4
BR-78-24	26.5	1313.1	Bert Winn #1	77.8	1260.4
BR-78-22	20.9	1332.3	2-78-1002	101.2	1294.2
BR-78-21	76.7	1305.8	Stock 1	106.3	1264
BR-78-3	16.7	1338.4	Stocks 1-A	68.6	1261.9

Table 3.3. Names of wells and respective temperatures and elevations included in the shallow temperature range.

Name	Max Temp (C)	Elevation (m)	Name	Max Temp (C)	Elevation (m)
2-78-1	31.2	1363.1	Clifton Village	12	1411.3
2-78-3	102.9	1357.3	Leonard Povey	12	1400.3
2-78-4	55.8	1354	C A Mortensen	13	1385.1
2-78-5	16.3	1355.5	M Hollingsworth	13	1415.9
2-78-6	21.4	1354.3	Dave Johnson	12	1425.3
2-78-13	54	1354	E D Bergeson	17	1381.1
2-78-9	26.8	1355.8	G Housley	19	1409.1
2-78-8	44.5	1357.3	Dale Ralphs	14	1416.2
2-78-11	9.8	1359.5	A C Wardell	14	1425.3
2-78-7	70.2	1354.3	Richard Ballif	12	1390.2
BR-78-26	15.7	1367.1	Bruce Naylor	11	1439
BR-78-31	13.5	1384.5	John Jackson	12	1422.9
BR-78-24	22.2	1355.8	Dayton Cemetary	14	1437.2
BR-78-22	19.3	1356.7	William Hawkes	12	1433.2
BR-78-20	14.8	1361.9	U. S. Bureau of Reclamation	13	1434.5
BR-78-21	58	1354.6	Frank Mitchell	12	1362.2
BR-78-4	25	1284.8	Williard Gailey	17	1384.1
BR-78-14	16.2	1357.6	Byron Tanner	16	1410.1
BR-78-3	15.2	1356.7	John Vaterlaus	14	1373.2
BR-78-10	13.4	1357.3	Ariel Meek	17	1376.2
BR-78-35	29	1355.8	Ward Nielson	13	1433.8
David Bosen	102.78	1365.2	T Schvaneveldt	12	1438.7
Kevin Jepperson	16.5	1397	Hepworth Well	10.7	1437.8
Swain Family Trust	16.3	1416.8	Battle Creek (Wayland) Hot Springs	84	1368.3
Brandon Schaffer	11.9	1433.3	Squaw Hot Springs Well	84	1361.3
Emil Tasso	13	1416.2	2-78-1002	49.9	1355.14
Lavon Porter 1	13	1385.7	Stock 1	107.2	1306.7
Pas Martinez 1	13	1398.8	Stocks 1-A	41.7	1357.9
E Gregorson	12	1366.8	Bert Winn #1	62.2	1354
Dennis Ralphs	12	1407.6			

CHAPTER 4 SUMMARY AND RECOMMENDATIONS

This thesis has collected new potential field data that has refined the locations and orientations of the Clifton Hill bounding faults. Newly collected water temperature and water level data and data from previous studies were used to improve the understanding of ground water flow in the shallow aquifer and the interaction between the shallow aquifer and the faults that are probably the conduits of hot water from the deep geothermal system. Thermal gradients from abandoned exploration wells were interpreted to provide insight into the hydrogeologic conceptual model have created new hypotheses. It is hoped that these efforts will inspire further investigations into the Clifton Hill Geothermal Prospect.

SUMMARY

The NCV has been the subject of many studies in the last sixty years. The structure of the valley was studied by Peterson and Oriol (1970) and more recently by Dr. Susan Janecke (1999, 2011) and Dr. Paul Link (1983_(1 & 2)). Between 1970 and 1981, Young and Mitchell (1973), Mitchell (1976) and Ralston (1981) studied the geochemistry of the valley's thermal waters. In 2015 these data were revisited and the reservoir temperatures reanalyzed using MEG predictive methods (Wood et al, 2015). Two Na-Cl waters of differing levels of maturity were found in the valley, the more mature of those waters samples originated near Clifton Hill. Reservoir temperature predictions of these waters range from 67°C to 227°C, with RTEst values ranging from 95±1°C to 179±9°C (Table 1.1) (Wood et al, 2015).

Commercial geothermal exploration of Preston geothermal prospect was centered on the Clifton Hill area in the late 1970s and early 1980s. Sunedco and Chevron drilled shallow test wells (Figures 1.4 and 1.5) and two deep test wells were completed by 1980 (McIntyre and Koenig, 1978 & 1979; Munoa, 2016, Figure 1.3). The exploration in the area was abandoned in the early 1980's with recommendations that high resolution geophysical surveys be completed to gain a better understanding of the fault structure(s) underlying the geothermal system.

In the spring of 2014, a well drilled to 260 ft yielded a bottom hole temperature of 217°F, elevating the attention of this area for commercial geothermal development once again.

To improve understanding of the prospect and the geothermal system, a high resolution potential field survey was conducted and the data analyzed and interpreted in the field area during the summer and fall of 2015. A local gravity base station was established in Preston, ID (Appendix A, Figures A.1-A.3). Survey lines were planned for maximum coverage of Clifton Hill's bounding fault system (Figure 2.3 and 2.4). Gravity data were collected using a LaCoste and Romberg gravimeter and nearly 300 gravity stations were occupied. Magnetic data were collected with two magnetometers, a pack-mounted G-859AP Cesium Vapor Magnetometer was used to collect data along the survey lines, and a G-857 Proton Precession Magnetometer was used to collect base station data (Figures 2.2 and 2.3). Gravity, magnetics and GPS data were reduced and processed according to USGS standards and protocols (Ponce, 2009). These data sets were then analyzed using a 2-D and in certain cases, a 2 ³/₄-D forward modeling approach. This 2 ³/₄-D method is applied through defining depths into or out of the modeled plane that geologic units extend.

A hydrogeologic temperature and phreatic surface survey was conducted in the spring of 2016. These new data were combined with legacy data from previous surveys in the area (McGreevey & Bjorklund, 1970; Ralston, 1980, Mitchell, 1976). Analysis of local groundwater flow and subsurface temperatures were made from these combined datasets and interpreted in conjunction with the geophysical models of the area's fault structure.

Based on interpretation of geophysical data, the Clifton Hill bounding faults are normal faults (Figure 3.12), the western fault dips to the west, while the eastern fault dips to the east (Figures 3.6-3.8). This supports assertions of previous studies in the area, that Clifton Hill is a secondary horst complex within the larger NCV horst-graben complex (Wood et al, 2015; Worthing et al, 2016).

The five hypothesized ancillary faults located further from Clifton Hill are not well constrained by potential field data. Of these five faults, data were only collected across the two in the northwestern and northeastern edges of the study area (Figure 3.12). Based on forward modeling of lines 7 and 8, the northwestern fault dips to the west and the northeastern fault dips to the east (Figures 3.10-3.11).

Temperature plumes centered on the southwestern edge of Clifton Hill grow larger with depth in the subsurface and are influenced by the southeastern flow of ground water in the

local aquifer. Temperature gradient data from abandoned test wells suggest that thermal fluids may be traveling in a pattern indicative of a thermal outflow plume (Figures 3.16-3.21). This thermal outflow plume is mapped in the southern portion of the study area, southwest and southeast of the toe of Clifton Hill.

The interpretation presented, herein is that geothermal fluids rise along localized permeable sections of the faults and associated fractures. Permeable, geothermal conduits have been found where faults intersect and interact, creating highly permeable subsurface conditions, such as step-over faults or relay ramps (Faulds, 2011). We have identified structures in the area which suggest these conditions could exist up-gradient of thermal plumes and may be responsible for transporting hot water from depth to the shallow subsurface (Figures 3.22 and 3.23).

In order to better define the Preston Geothermal prospect, more data are needed.

Recommendations are described in the following section.

RECOMMENDATIONS

Additional geophysical exploration should be conducted to better constrain the extent and orientations of ancillary faults (dashed lines in Figure 3.23), and to determine if step over faults are associated with them. These ancillary faults differ from the Clifton Hill bounding faults in that they likely do not separate sedimentary units from much older, denser metamorphic rock. Therefore, strong contrasts are not expected in the magnetics and gravity signals across these faults. Seismic refraction is better suited to this situation because of the velocity contrast produced by the fault plane and its associated permeable zones. Velocity contrasts provide good targets for seismic imaging.

Electrical resistivity is recommended to image the Middle-West and Southwest ancillary faults on the west side (Figure 3.23). Electrical resistivity surveys are useful in determining depth to water, and in this situation the water in the area of interest is likely highly saline (from water collected from the Bosen well). Highly saline waters are highly conductive and image well using electrical resistivity, if these southern faults are transporting conductive thermal fluids along sections of the fault planes, it may be discernable using electrical resistivity methods. Resistivity and seismic data should be used to conduct slip and dilation

tendency analysis. Such analysis may help to quantify high and low stress sections of the fault plane and constrain areas of permeability (Faulds et al, 2011).

Based upon the results of the seismic and surface resistivity surveys, nine to fifteen shallow (250 - 450 ft) geothermal gradient wells should be drilled to gather temperature gradient data. Drilling locations can be chosen from a combination of the fault mapping presented here, the seismic and resistivity surveys and real time measurements of temperature while drilling. From these temperature data, the origin of the thermal outflow plume can be located. A geometric spread or spacing of the drilling locations is required for defining the hydraulic gradient, but some wells should be reserved for defining the exact location of the thermal upwelling. A preliminary area of interest for the installation of these wells is presented in figure 4.1, although the recommended geophysical surveys will help to constrain this area (Figure 4.1). Also from these wells, samples for geochemical analyses should be collected. These data, along with hydraulic head data will be used to generate a 3-D thermal, hydrogeologic model. Discharge from Squaw and Wayland Springs will need to be carefully measured for calibration of the hydrogeologic model.

Determination of requirement for a deep exploration well can be made based on calculated and measured maximum temperatures, volumes of thermal water discharge and geothermometry predictions in areas of thermal upwelling.

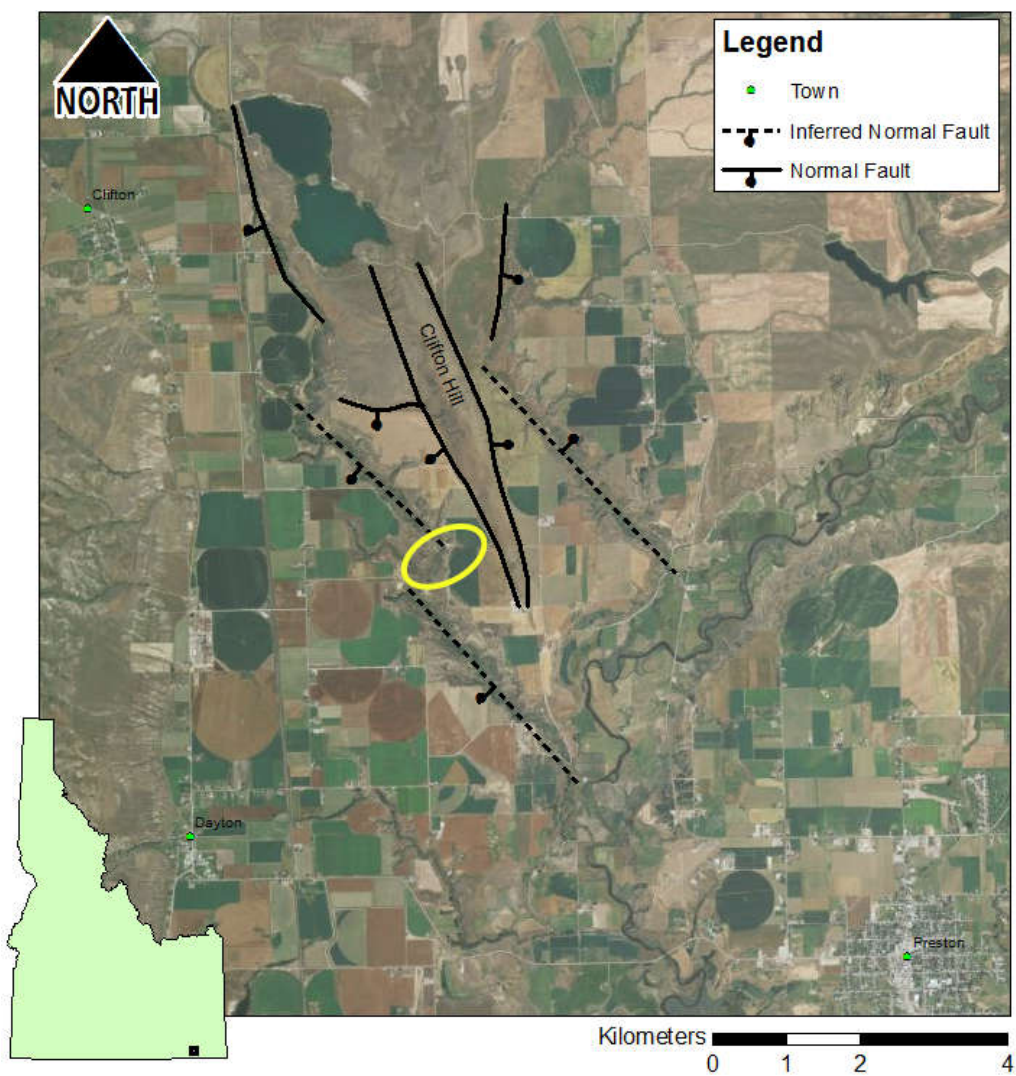


Figure 4.1. Current interpretation of fault positions and orientations surrounding Clifton Hill. Yellow circle indicates recommended location of new shallow temperature wells.

REFERENCES

- Anderson, K., Nelson, S., Mayo, A., Tingey, D.: "Interbasin flow revisited: The contribution of local recharge to high-discharge springs, Death Valley, CA." *Journal of Hydrology*, 323 (2006) 276-302
- Austin, C. F.: "The Preston Geothermal Prospect - An Evaluation." (2008)
- Avery, C.: "Chemistry of Thermal Water and Estimated Reservoir Temperatures in Southeastern Idaho, North-Central Utah, and Southwestern Wyoming." *Wyoming Geological Association Guidebook, Thirty-Eighth Field Conference*. (1987) p.347-353.
- Browne, P. R. L.: "Hydrothermal Alteration in Active Geothermal Field." *Annual Review of Earth and Planetary Sciences*, 6: (1968) p.229-250.
- Carney, S. M., Janecke, S. U.: "Excision and the Original Low Dip of the Miocene-Pliocene Bannock Detachment System, SE Idaho: Northern Cousin of the Sevier Desert Detachment?" *Geological Society of America Bulletin* vol 117, no. 3-4, (2005), p. 334-353.
- Cook, K. L., Carter, J. A.: "Precision Leveling and Gravity Studies at Roosevelt Hot Springs KGRA, Utah." Department of Geology and Geophysics, University of Utah, Salt Lake City, Utah 84112 (1978)
- Coulter, H. W.: "Geology of the Southeast Portion of the Preston Quadrangle, Idaho." (1956).
- Currey, D. R., Oviatt, C. G.: "Durations, average rates, and probable causes of lake bonneville expansions, stillstands, and contractions during the last deep-lake cycle, 32,000 to 10,000 years ago." *Problems of and prospects for predicting Great Salt Lake levels*. (1985), p.9-24
- de Vries, J. L.: "Evaluation of Low-Temperature Geothermal Potential in Cache Valley, Utah." *Utah Geological and Mineral Survey Report*, (1982).
- DeCelles, P. G.: "Late Jurassic to Eocene Evolution of the Cordilleran Thrust Belt and Foreland Basin System, Western U.S.A." *American Journal of Science* vol 304 (2004) p.105-168

- Dion, N. P.: "Hydrologic Reconnaissance of the Bear River Basin in Southeastern Idaho." *United States Geological Survey Water Information Bulletin* 13, (1969).
- Erickson, 2014, Email message from Nathan Erickson to Tom Wood dated August 20, 2014.
- Evans, J. P., Oaks, R. Q.: "Three-dimensional Variations in Extensional Fault Shape and Basin Form: the Cache Valley Basin, Eastern Basin and Range Province, United States." *Geological Society of America Bulletin* 108, 12 (1996), 1580-1593.
- Fournier, R. O.: "Chemical geothermometers and mixing model for geothermal systems." *Geothermics*, 5 (1977), p.41-50.
- Fournier, R. O., Potter R. W.II.: "Magnesium correction to Na-K-Ca geothermometer." *Geochim. Cosmochim. Acta*, 43 (1979), p.1543-1550.
- Fournier, R. O., and Truesdell, A.H.: "An empirical Na-K-Ca geothermometer for natural waters." *Geochim. Cosmochim. Acta*, 37 (1973), p.1255-1275.
- Grubbs, K. L., Van Der Voo, R.: "Structural Deformation of the Idaho-Wyoming Overthrust Belt (U.S.A), as determined by Triassic Paleomagnetism." *Tectonophysics*, 33 (1976), p.321-336
- Hayden, F. V.: "Preliminary Field Report of the U.S. Geological Survey of Montana and Portions of Adjacent Territories." (1872), p.18-21.
- Henley, R. W. and Ellis, A.J.: "Geothermal Systems Ancient and Modern – a Geochemical Review". *Earth-Science Reviews*, 19(1) (1983): p.1-50.
- Idaho Office of Energy: "Preston, Idaho, site specific development analysis: Idaho Office of Energy", Boise, Idaho, undated, 40 p.
- Janecke, S. U., Evans, J. C.: "Folded and Faulted Salt Lake Formation Above the Miocene to Pliocene New Canyon and Clifton Detachment Faults, Malad and Bannock Ranges, Idaho: Field Trip Guide to the Deep Creek Half Graben and Environs", Guidebook to the Geology of Eastern Idaho: Pocatello, Idaho Museum of Natural History, (1999), p. 71-96
- Karingithi, C. W.: "Chemical Geothermometers for Geothermal Exploration." (2009).
- Link, P. K., LeFebre, G. B.: "Upper Proterozoic Diamictites and Volcanic Rocks of the Pocatello Formation and Correlative Units, Southeastern Idaho and Northern Utah." *Utah Geological and Mineral Survey Special Studies* 60, Guidebook Part 2 – GSA

- Rocky Mountain and Cordilleran Sections Meeting, Salt Lake City, Utah – May 2 – 4, (1983).
- Link, P. K.: “Glacial and tectonically influenced sedimentation in the Upper Proterozoic Pocatello Formation, southeastern Idaho.” Geological Society of America, Memoirs; 157 (1983); p. 165-182.
- Liu, L., Spasojevic, S., & Gurnis, M.: “Reconstructing Farallon Plate Subduction Beneath North America Back to the Late Cretaceous.”, *Science* vol 322 (2008).
- Mattson, E.D., Smith, R.W., Neupane, G., Palmer, C.D., Fujita, Y., McLing, T.L., Reed, D.W., Cooper, D.C., and Thompson, V.S.: Improved geothermometry through multivariate reaction-path modeling and evaluation of geomicrobiological influences on geochemical temperature indicators: Final Report No. INL/EXT-14-33959, Idaho National Laboratory (INL), Idaho Falls, Idaho, (2015).
- Mariita, N. O.: “The Gravity Method.” *Short Course II on Surface Exploration for Geothermal Resources*, Lake Naivasha, Kenya, 2-17 November, 2007.
- Mariita, N. O.: “The Magnetic Method.” *Short Course II on Surface Exploration for Geothermal Resources*, Lake Naivasha, Kenya, 2-17 November, 2007.
- McGreevy, L. J., & Bjorklund, L. J.: “Selected Hydrologic Data Cache Valley, Utah and Idaho.” (1970).
- McGreevy, L. J., & Bjorklund, L. J.: “Geohydrologic Sections Cache Valley, Utah and Idaho.” (1971).
- McIntyre, J. R., & Koenig, J. B.: “Geology of Sunedco C. H. Stock 1-A Geothermal Test, Franklin County, Idaho.” (1978).
- McIntyre, J. R., & Koenig, J. B. (1980). “Geology and Thermal Regime of Bert Winn #1 Geothermal Test, Franklin County, Idaho.”
- Mitchell, J. C.: “Geothermal Investigations in Idaho, Part 5, Geochemistry and Geologic Setting of the Thermal Waters of the Northern Cache Valley Area, Franklin County, Idaho.” *Idaho Department of Water Resources Water Information Bulletin* 30, (1976).
- Murray, A. S., Tracey, R.M.: “Best Practice in Gravity Surveying.” Geoscience Australia, Australian Government, (2001).
- Neupane, G., Mattson, E.D., McLing, T.L., Palmer, C.D., Smith, R.W., Wood, T.R., and Podgorney, R.K.: Geothermal reservoir temperatures in southeastern Idaho using

- multicomponent geothermometry. Proceedings, World Geothermal Congress 2015, Melbourne, Australia, 19-25 April 2015, (2015).
- Neupane, G., Mattson, E.D., McLing, T.L., Palmer, C.D., Smith, R.W., Wood, T.R., and Podgorney, R.K.: Geothermometric evaluation of geothermal resources in southeastern Idaho. *Geoth. Energ. Sci*, 4(1), (2016), 11-22.
- Nowell, D. A. G.: “Gravity terrain corrections – an overview.” *Journal of Applied Geophysics* 42, (1999), p. 117-134.
- Palmer, C. D.: “Installation manual for Reservoir Temperature Estimator version 2.5 (RTEst).” *Idaho National Laboratory*, Idaho Falls, ID, (2014).
- Parsons, T.: “The Basin and Range Province, in Continental Rifts: Evolution, Structure and Tectonics”, Olsen, K., ed., Amsterdam, Elsevier, ISBN 044489-566-3, (1995), p. 277-324.
- Peterson, D. L., & Oriel, S. S.: “Gravity Anomalies in Cache Valley, Cache and Box Elder Counties, Utah, and Bannock and Franklin Counties, Idaho.” *United States Geological Survey Professional Paper* 700-C. (1970), C114-C118
- Picha, F., & Gibson, R. I.: “Cordilleran hingeline: Late Precambrian rifted margin of the North American craton and its impact on the depositional and structural history, Utah and Nevada.” *Geology*, vol 13, (1985), p.465-468.
- Sbar, M. L., Barazangi, M., Dorman, J., Scholz, C. H., Smith, R. B.: “Tectonics of the Intermountain Seismic Belt, Western United States: Microearthquake Seismicity and Composite Fault Plane Solutions.” *Geological Society of America Bulletin* 83, no. 1 (1972), p.13-28.
- Smith, R., & Sbar, M.: “Contemporary Tectonics and Seismicity of the Western United States with Emphasis on the Intermountain Seismic Belt.” *Geological Society of America Bulletin*, 85 (1974), p.1205-1218.
- Smith, R. B.: “Intraplate Tectonics of the western North American Plate.” *Tectonophysics* 37 (1976), p.323-336.
- Ralston, D. R., Arrigo, J. L., Baglio, J. V. Jr., Coleman, L. M., Hubbell, J. M., Souder, K., Mayo, A. L.: “Geothermal Evaluation of the Thrust Zone in Southeastern Idaho.” (1981).

- Robbins, S. L., Oliver, H. W.: "On Making Inner-zone Terrain Corrections to Gravity Data." United States, Geological Survey, In-House Memorandum, (1970).
- Ribe, N. M., Smith, R. B., Lowry, A. R.: "Dynamic elevation of the Cordillera, western United States." *American Geophysical Union*, (2000).
- Utah Geological Survey, (n.d.). Utah geologic map with multiple scales – Logan UT Quadrangle. Retrieved November 13, 2014, from <http://geology.utah.gov/maps/geomap/interactive/viewer/index.html>
- Unknown. "Geologic Provinces of the United States: Basin and Range Province" (2014). Retrieved November 18, 2014, from <http://geomaps.wr.usgs.gov/parks/province/basinrange.html>
- Unknown. Introduction to Idaho Geology Web Course, (undated). Retrieved October 2, 2014, from http://geology.isu.edu/Digital_Geology_Idaho/
- Unknown. "Lake Bonneville: A Brief History - Utah Geological Survey" (undated). Retrieved October 2, 2014, from http://geology.utah.gov/utahgeo/gsl/flash/lb_flash.htm
- Unknown. "Lake Bonneville and the Bonneville Flood" (undated). Retrieved October 2, 2014, from <http://hugefloods.com/Bonneville.html>
- Unknown. "Placement of Basin and Range Faulting" (undated). Retrieved January 14, 2015, from http://geology.isu.edu/Alamo/devonian/basin_range.php
- Unknown. "Preston, Idaho, Site Specific Development Analysis" (undated).
- Unknown. "The Lake Bonneville Flood" (undated). Retrieved October 2, 2014, from <http://imnh.isu.edu/digitalatlas/hydr/lkblood/lbf.htm>
- Willard, P. D.: "Tertiary Igneous Rocks of Northeastern Cache Valley (Franklin County), Idaho." MS thesis, Utah State University, (1972).
- Williams, J. S.: "Lake Bonneville: Geology of Southern Cache Valley, Utah." (1962).
- Winester, D.: Salt Lake City BM8, (1998). Retrieved from http://www.gis.utep.edu/subpages/states/documents/Utah/salt_lake_dity_bm8.pdf
- Winter, M. B.: "Geology and Petrology of the Cub River Diabase, a Late Pliocene Differentiated Mafic Intrusion, Northeastern Cache Valley, Idaho." Utah Geologic Association, publication 14, (1985), p. 215-225.

- Wood, T. R., Worthing, W., Cannon, C., Palmer, C., Neupane, G., McLing, T. L., Mattson, E., Dobson, P. F., Conrad, M.: “The Preston Geothermal Resources; Renewed Interest in a Known Geothermal Resource Area.” Proceedings, Fortieth Workshop on Geothermal Reservoir Engineering Stanford University, Stanford, California, January 26-28, (2015).
- Young, B., Shervais, K., Ponce-Zepeda, M., Rosove, S., & Evans, J.: “Hydrogeochemistry, Geothermometry, and Structural Setting of Thermal Springs in Northern Utah and Southeastern Idaho.” (2013).
- Young, H. W., & Mitchell, J. C.: “Geothermal Investigations in Idaho, Part 1, Geochemistry and Geologic Setting of Selected Thermal Waters.” *Idaho Department of Water Administration Water Information Bulletin* 30, (1973)

APPENDIX A : GRAVITY BASE STATION ESTABLISHMENT

Gravity base stations are reference points where the value of gravity has been carefully determined and which may be occupied as a check against errors made in a new gravity survey (Murray & Tracey, 2001). The Preston, ID gravity base station was established on September 11th and 12th, 2015. Establishing a base station involves making a relative gravity measurement at the proposed base station site, then another measurement at an established base station used to “tie-in” the new one. This process is repeated until a “loop” between the proposed and the previous station has been completed at least 3 times. The location proposed for the new base station was the Federal Post Office in Preston, ID (Figure 1). The base station that it would be initially tied to was the Salt Lake City BM8 gravity base station, located in President’s Circle at the University of Utah in Salt Lake City, UT (Figures 1-2).

The initial measurement at the Preston, ID post office was made on September 11th, 2015 at 9:37am, and the first measurement at the Salt Lake City BM8 station was made at 12:52 pm, see table 1 for all tie-in measurement values, times and dates (Figure A.3, Table A.1).

Tie in measurements were corrected for tidal variations and closures calculated. A relationship between gravity measurement at the Salt Lake City BM8 and Preston, ID stations could then be developed, and an accurate value of the gravitational field computed for the new Preston, ID gravity base station. This value would be used later in post processing of the gravity data.

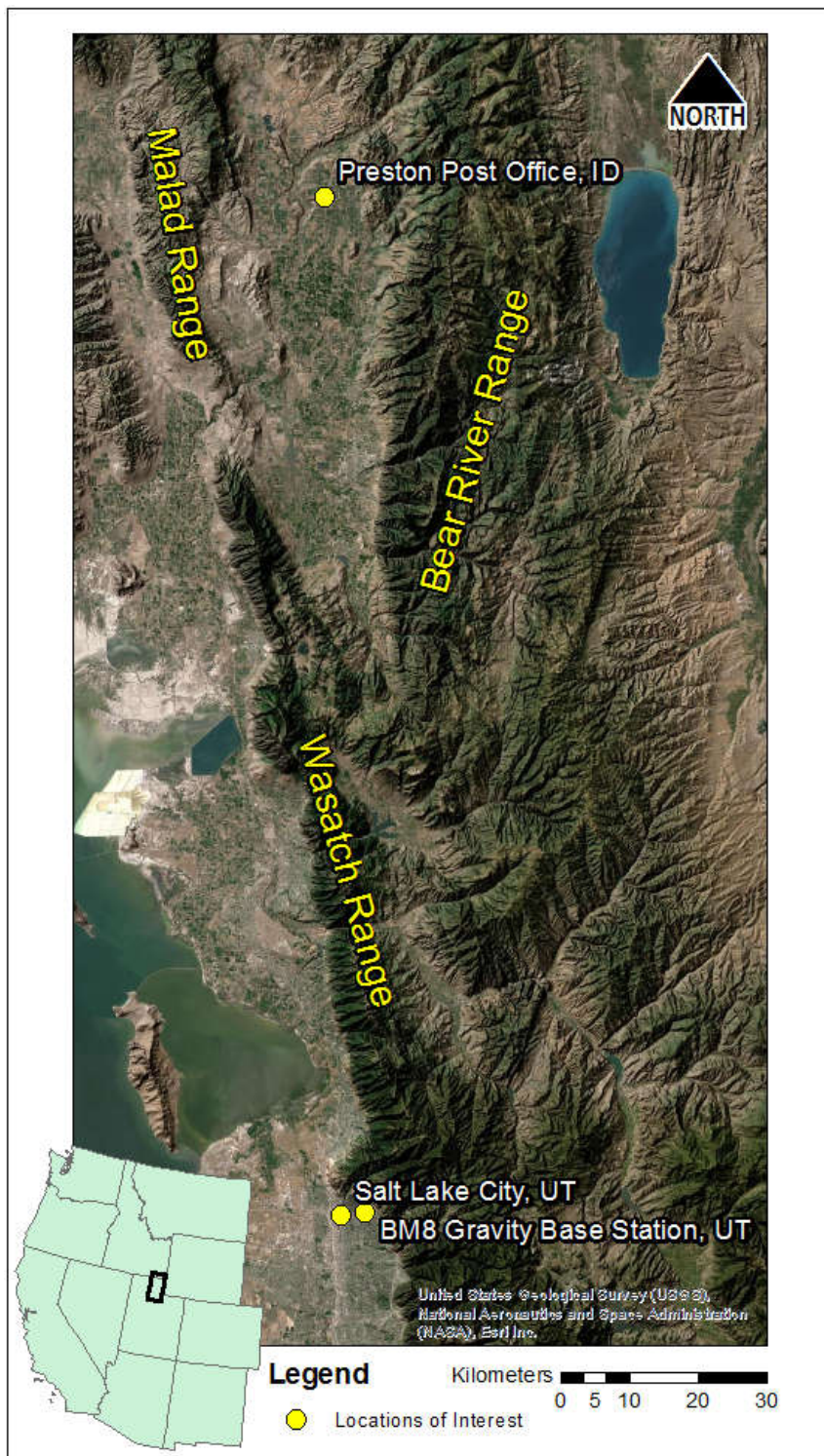


Figure A.1. Locations of the Preston, ID Federal Post Office and the Salt Lake City BM8 base station, relative to one another.

GRAVITY STATION DESCRIPTION		STATION TYPE	STATION DESIGNATION
		Absolute Excenter	SALT LAKE CITY BM8
COUNTRY	United States	STATE/PROVINCE-COUNTY	Utah - Salt Lake
LATITUDE	40° 45' 53.9" N	LONGITUDE	111° 51' 00.3" W
GRAVITY STATION MARK	Benchmark Disk	AGENCY	USC&GS & state survey
POSITION/ELEVATION REFERENCE	Topo Map	POSITION/ELEVATION SOURCE	USGS 1:24000
POSITION/ELEVATION REMARKS		GRAVITY VALUE/SOURCE/DATE	
Contour Interval = 10 feet		g = 979 772.407 ± 0.003 mGals (NGS,6/98)	
DESCRIPTION/CONTACT Station is in Presidents' Circle at the University of Utah, Salt Lake City, UT. It is 2.2 mi E of Meridian Monument in Temple Square. To access from Exit 126 of I-80 (E of I-15), go N on 1300 East (= UT 181) for 3.1 mi to 200 South. Turn E (right), go 1 block, dog-leg right onto Presidents' Circle (= 220 South). Go E for 0.27 mi, around head of Circle at Administration Bldg. to station in lawn at left. Station is 18.0 m NNW of flagpole, 21.9 m NE of 6-way sidewalk intersection, 45.7 m SSE of center of intersection of 1400 East and Presidents' Circle and 4.6 m WSW of 0.55 m diameter Crimean Linden tree. Disk at center of 0.35 m square concrete post, level with lawn and sidewalk and at SE edge of NE-trending sidewalk. Center of W ₂ , NE, SW, NW, Sec 4, T1S, R1E.			
OTHER STATION DESIGNATIONS: DOD 0471-5, IGB 15601, UNIVERSITY OF UTAH BASE, NN 326			
DIAGRAM/PHOTOGRAPH			
DESCRIPTION BY	Daniel Winester	AGENCY	NOAA/NOS/NGS
		DATE	17 June 1998

Figure A.2. Information sheet for the Salt Lake City BM8 gravity base station.


NAME	CITY/STATE
Preston Base Station	Preston, Idaho
LATITUDE/LONGITUDE/ELEVATION	Agency
42.096448, -111.875303 1439 meters	University of Idaho
DESCRIPTION	
<p>Base station is located at the Preston, ID post office (55 E Onieda St, Preston, ID 83263). On the East side of the buiding, up the side entrance ramp, at the outside corner of the landing outside the door. Location is not marked with an official disk, base station was set up for the purposes of a gravity survey in the Clifton Hill region, north west of Preston (Worthing et al, 2016).</p>	
PHOTOS	
	

Figure A.3. Information sheet for Preston, ID gravity base station.

Table A.1. Base station tie-in data. Time is in military time, Reading, Tidal Correction and Corrected Reading values are in mGal.

Station Id	Date	time	Reading	Tidal Correction	Corrected Reading
Preston BS	9/11/2015	0950	3438366	16.4	3438382.4
SLC BM8	9/11/2015	1300	3344852	81	3344933
Preston BS	9/11/2015	1554	3438368	-1.34	3438366.66
SLC BM8	9/11/2015	1830	3344990	-78.4	3344911.6
Preston BS	9/11/2015	2123	3438441	-45.89	3438395.11
SLC BM8	9/12/2015	0010	3344991	23.9	3345014.9
Preston BS	9/12/2015	0233	3438362	10.16	3438372.16
SLC BM8	9/12/2015	0458	3344956	-57.34	3344898.66

APPENDIX B : ROCK SAMPLING AND SUSCEPTIBILITY FIELD MEASUREMENTS

Geophysical modeling of the subsurface involves the inclusion of rock parameters such as density and susceptibility. In order to obtain a more accurate range of values which could be applied to the rock units in my models, rock samples were collected in November, 2015 for laboratory density analysis. Susceptibility measurements were made in the field in January, 2016.

On November 12th, 2015 I traveled to the area of study, northwest of Preston, ID, to collect rock samples representative of the geologic units which comprise Clifton Hill. Beginning at the southern end of the Clifton Hill horst, the Bosen well, I hiked up along the ridge line towards the northwest. Rock samples were collected periodically, whenever a change in lithology was encountered. Pictures and descriptions of the units were also collected. Instances of samples, pictures and descriptions were marked with GPS coordinates (Figure 1).

Two samples were collected after ascending the first hill at the toe of the horst. These are rock samples 001 and 002 (Figure B.1: RS-001 & RS-002). These samples appear to be igneous, or possibly metamorphosed igneous rocks, specifically diabase or a slightly metamorphosed diabase. The rock has an abundance of green minerals, likely chlorite or actinolite. Samples 001 & 002 also display an abundance white crystals which may be feldspars. Farther along the ridge (450 ft) I took three pictures of the same type of rocks (Figures B.2-B.4), and 900 ft beyond that point I collected another sample (RS-003). Sample 003 was found just before there was a significant change in the topography, and a clear shift in rock type (Figure B.1: RS-003).

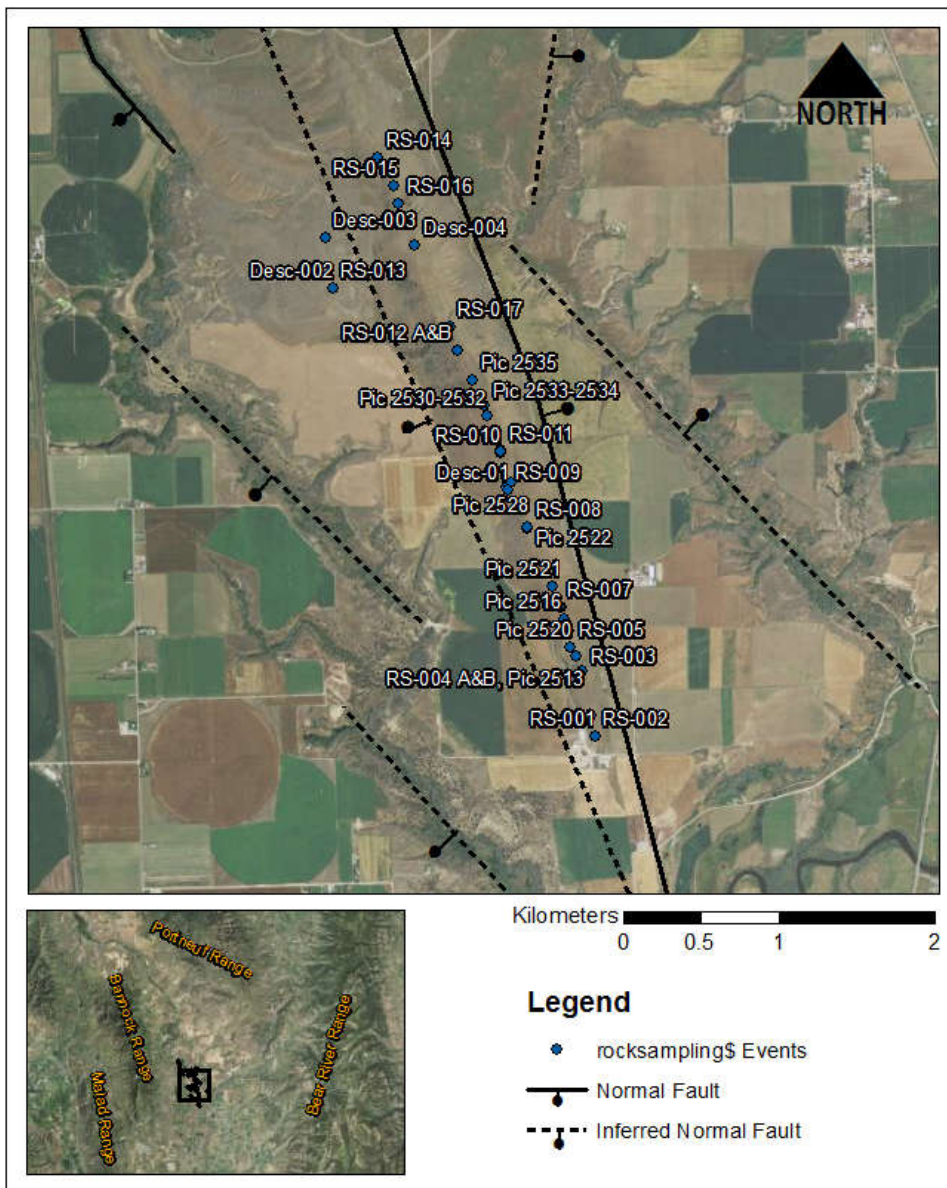


Figure B.1. Locations where rock samples (RS-####) and pictures (Pic#####) were taken and descriptions incorporated into the appendix were observed (Desc-###).



Figure B.2. Meta-diorite, samples 001, 002 & 003 are of this type (Figure B.1: picture 2508).



Figure B.3. Meta-diorite, samples 001, 002 & 003 are of this type (Figure B.1: picture 2509).



Figure B.4. Meta-diorite, samples 001, 002 & 003 are of this type (Figure B.1: picture 2511).

North of RS-003 there is a steep downward change in the topography. The ridge descends to a saddle, and gradually rises back up again on the northern side. In this saddle, two samples were collected, RS-004A & RS-004B, which appear to be a mudstone, likely Argillite (Figure B.4). This implies that the marked change in topography is a contact between the Meta-diorite intrusive unit and the Scout Mountain member of the Pocatello Formation. The Scout Mountain unit is comprised of differing metasedimentary rocks, one of which is Argillite. There is a lot of float on the saddle from the previous rock type (Meta-diorite) and from the hill to the north. The argillite was fairly hidden except in the middle of the saddle, downslope to the western side where much of the topsoil and float had been worn off by cattle traffic.



Figure B.5. Emplaced Argillite of the Scout Mountain Member of the Pocatello Formation (Figure B.1: picture 2513).

Another 250ft north along the ridge I encountered more meta-dabase, here I took another sample, RS-005, for comparison with samples 001-003. This unit is exposed for another 580 ft northward along the ridge (Figures B.5-B.6).



Figure B.6. Meta-diorite float and possible outcrop along ridgeline of Clifton Hill (Figure B.1: picture 2514).



Figure B.7. Close up of Meta-diorite along ridgeline of Clifton Hill (Figure B.1: picture 2515).

Approximately 330 ft beyond where sample 005 was found, the lithology changes to slate. At first appearing as small pieces and the occasional large chunk scattered among other rock talus (Figure B.7). On top of a bench further onward, I found much more slate and in larger chunks. At this point it was still hard to tell if the imbedded pieces were insitu though. I took two samples, RS-006A&B, here (Figures B.8-B.9).



Figure B.8. Small pieces of slate scattered among larger chunks of meta-diorite (Figure B.1: picture 2516).



Figure B.9. Large chunk of slate (Figure B.1: picture 2517).



Figure B.10. Broken piece of slate that sample 006A&B were taken from (Figure B.1: picture 2519)

Another 250ft up the hill and I encountered what appears to be basalt, representing another shift from the Scout Mountain member to the Bannock Volcanic member of the Pocatello Formation. Though I am unsure if it was insitu or just a large boulder (Figure B.10). Sample 007 (RS-007) was taken just up the hill from this point. Approximately 475 ft from sample 007, argillite was again seen outcropping (Figure B.11).



Figure B.11. Basalt of the Bannock Volcanic member of the Pocatello Formation, southernmost outcrop seen on Clifton Hill (Figure B.1: picture 2520).



Figure B.12. Argillite (Figure B.1: picture 2521).

From where the photo in figure 11 was taken to the next sample and photo, the slope of the ridge is very gradual, and apart from the occasional chunk of argillite sticking out of the ground, no rocks were to be found. This seems to me to be a good indication of the underlying unit being a softer metasedimentary unit of the Scout Mountain member. When I first encountered argillite on Clifton Hill, it was forming a fairly flat section of a saddle and seemed to form a fairly smooth slope. Approximately 1400 feet from the rock pictured in figure 11, I collected an interesting sample, RS-008, from an outcrop of argillite complete with iron pyrite crystals (Figure B.12).



Figure B.13. Argillite with iron pyrite crystals (Figure B.1: picture 2522).

Sample 008 (RS-008) was found where the ridgeline was beginning to slope downwards, approximately 600 ft from the point Line 3, of the magnetics and gravity surveys, crossed the ridge. At a point 300 ft beyond where line 3 crosses the ridge, on the western flank a sample, RS-009, was found among large boulders of a metamorphosed volcanic rock from the Bannock volcanic member (Figures B.13-B.18).



Figure B.14. Bannock Volcanic Member outcrop near the ridgeline where magnetic and gravity line 3 crosses over Clifton Hill (Figure B.1: picture 2523).



Figure B.15. Bannock Volcanic member boulder (Figure B.1: picture 2524).



Figure B.16. Bannock Volcanic Member outcrop (Figure B.1: picture 2525).



Figure B.17. Bannock Volcanic Member outcrop (Figure B.1: picture 2526).



Figure B.18. Close up of Bannock volcanic member outcrop (Figure B.1: picture 2527).



Figure B.19. Bannock Volcanic member outcrop (Figure B.1: picture 2528).

Another 650 ft along the ridge I encountered what appeared to be volcanic breccia (Bannock Volcanic Member). There are large angular clasts/inclusions of different types in a matrix of a fine grained mafic rock, probably basalt. Sample 010 was collected here (Figure B.1: RS-010).

About 30 feet north of that, I encountered what I believe is either an example of metagraywacke or argillite (Scout Mountain Member) and collected sample 011 (RS-011) (Figure B.19). This unit was located between a barbed wire fence and another outcrop of volcanic breccia. Only another 35 ft beyond this point is what appears to be metamorphosed volcanic boulder-sized chunks of rock next to another outcrop of volcanic breccia, both I believe are Bannock Volcanics.



Figure B.20. Metagreywacke or Argillite (Figure B.1: picture 2529).

The volcanic breccia continues for 750 ft, when basalt becomes the new dominant lithology. In the basalt, there is a differentiation of mineral structure and crystal size from the outside inward, and outer surfaces display a “hummocky” or “rounded” and “wavy” texture and appearance (Figure B.20-B.24).



Figure B.21. Basalt (Figure B.1: picture 2531).



Figure B.22. Basalt (Figure B.1: picture 2532).



Figure B.23. Basalt (Figure B.1: picture 2533).



Figure B.24. Basalt displaying "hummocky" surface texture (Figure B.1: picture 2534).



Figure B.25. Basalt displaying "hummocky" surface texture (Figure B.1: picture 2535).

Northward along the ridgeline 650 ft from where the outcrop in figure B.24, another sample of basalt was taken collected, RS-012A & B. To the west of where sample 012A & B were found, down slope from the ridgeline, there are huge amounts of basalt float. Most of the whole hillside on the western flank is made up of large clasts of loose basalt (skree face). This is where I stopped for the day.

I returned on Monday, November 16th, 2015 to finish hiking the length of the ridge to where magnetics and gravity line 6 crested the ridgeline. I decided to travel this distance in reverse, from North to South; to hike up to the crossing point of line 6 along the same path taken when data was collected. This meant following the more gradual route to the west of where RS-012 was collected, heading Northeast until I hit the ridgeline then coming back south along the ridge.

Line 3 (Figure 2.3 and 2.4) begins in the field to the west of Clifton Hill, where there are no outcrops to be seen. After transitioning to sagebrush the slope increases, and small rock fragments are visible, but the first large amount of talus is that of the Bannock Volcanic member. From which I collected sample 013 (RS-013), there were no obvious outcrops though. I did not encounter another rock type until reaching the ridge. Near the top of the ridge I found more of the same rock that was collected then. This was meta-diorite (Miocene, metamorphosed igneous intrusive), similar to the first three samples (RS-001, 002 & 003). Another sample, RS-015, of this type was collected, 700 ft further south along the ridge. Then approximately 365 ft beyond that, metagraywacke (Scout Mountain Member) was found and collected, RS-016 (Figure B.1: RS-0016). This unit remained fairly constant until I found more volcanic breccia 900ft south of sample 016. The breccia appeared as sedimentary clasts imbedded in a matrix of mafic volcanic rock. Finally the last sample, RS-017, was taken just 550 ft north of where sample 012 was collected (Figure B.1: RS-017). It too to be a basalt of the Bannock Volcanics.

SUSCEPTIBILITY FIELD MEASUREMENTS

Magnetic susceptibility measurements were made in the field during January, 2016. Beginning at the southern end of the Clifton Hill horst, measurements were made on rock outcrops using a Terraplus KT-10 susceptibility meter. Measurements were made at 29 locations on outcrops from all the geologic units encountered when collecting samples for

density analysis (Figure B.26). Values ranged from 0.019×10^{-3} to 0.923×10^{-3} , SI units (Table 1).

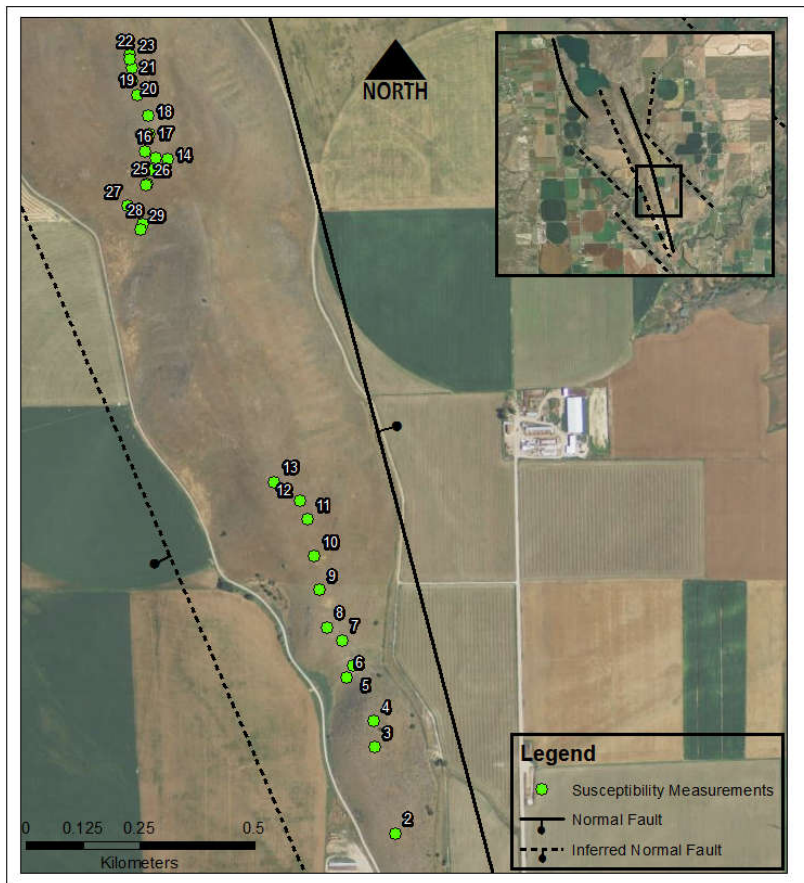


Figure B.26. Locations of susceptibility field measurements taken along Clifton Hill.

Table B.1. Susceptibility measurements and average measurements organized by unit, taken in the field. The diabase rock type refers to the meta-diabase intrusive seen in the area. Color codes are green for meta-diabase, blue for Scout Mountain member of the Pocatello formation and red for the Bannock member of the Pocatello formation. Susceptibility units are SI.

Waypoint	Susceptibility (x10 ⁻³)	Rock Type	Avg Susc (x10 ⁻³)
1	0.86	Diabase	0.821625
2	0.769	Diabase	
3	0.827	Diabase	
4	0.762	Diabase	
5	0.494	Argillite	0.355
6	0.487	Argillite	
7	0.766	Diabase	
8	0.898	Diabase	
9	0.768	Diabase	
10	0.923	Diabase	
11	0.298	Shale	
12	0.019	Shale	
13	0.553	Bannock	0.546266667
14	0.469	Bannock	
15	0.569	Bannock	
16	0.559	Bannock	
17	0.524	Bannock	
18	0.687	Bannock	
19	0.432	Bannock	
20	0.504	Bannock	
21	0.71	Bannock	
22	0.56	Bannock	
23	0.103	Argillite	
24	0.527	Bannock	
25	0.58	Bannock	
26	0.566	Bannock	
27	0.487	Bannock	
28	0.467	Bannock	
29	0.336	Shale	

APPENDIX C : LABORATORY DENSITY MEASUREMENTS

In order to obtain accurate values of density of the geologic units that make up Clifton Hill, rock samples were collected from the field (Appendix B). These samples were then measured in the following fashion in a laboratory setting in to determine appropriate density values to use during geophysical modeling of the structure of Clifton Hill. Based on recommendations by Dr. Jonathan Glen and Brent Ritzinger of the United States Geologic Survey (USGS), Dr. Tom Wood of the University of Idaho and Travis McLing of the Idaho National Laboratory (INL), rock samples were first dried in a Cascade TEK TFO-28 forced air lab oven at 80° Celsius (176° Fahrenheit) for 24 hours. Once dry, the samples' masses were measured using a Denver Instrument XL6100 scale and the values recorded (dry mass). Between each measurement, the scale was tared. Then the samples were submerged in deionized water for 72 hours to allow all pore spaces to become saturated with water.

After 72 hours the samples were presumed to be saturated and their masses were measured again (saturated mass) using the same scale but this time modified so that the samples could be measured while submerged in deionized water (Figures C.1 and C.2).



Figure C.1. Denver Instrument XL6100 scale modified to make saturated mass measurements.

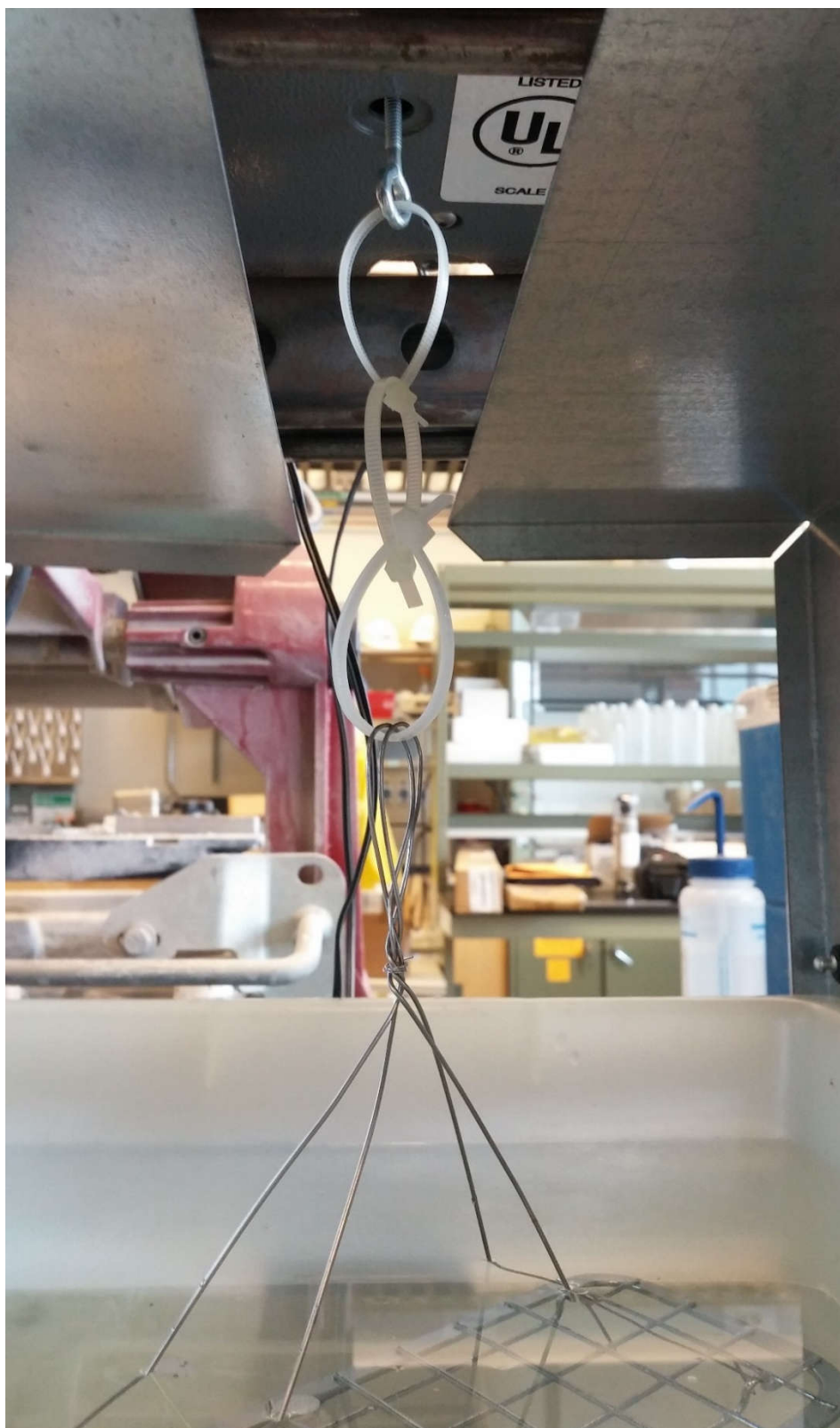


Figure C.2. Suspension linking the platform holding the saturated, submerged sample to a connection hook on the underside of the scale.

Samples were positioned on a wire platform while submerged in water so that the entire mass of the sample was supported by the platform connected to the scale. The platform and sample were not allowed to touch the sides of the container. Again, between each measurement the scale was tared.

To determine the density of the samples, an equation using the saturated and dry masses of the samples was utilized (Figure C.3, Table C.1).

$$\rho = \frac{m}{V} = \frac{m_{dry}}{\frac{m_{dry} - m_{wet}}{\rho_{water}}}$$

Figure C.3. Equation used to calculate the density of rock samples, where m_{dry} is the mass of the dry sample and m_{wet} is the mass of the saturated sample. Value of water density used was 1.0 g/cm³.

Procedure:

1. Dry rock samples in oven at 80° C for 24 hours
2. Measure and record the masses of the dried samples
3. Submerge samples in deionized water for 72 hours
4. Measure and record the masses of the saturated samples
5. Using the equation from Figure 3, determine the densities of the samples

Materials Used:

1. Cascade TEK TFO-28 Forced Air Lab Oven
2. Metal oven trays
3. Denver Instrument XL6100 scale
4. Deionized water

Table C.1. Density values calculated for rock samples collected from Clifton Hill, near Preston, ID.

Sample	Rock Name	Dry Mass (g)	Wet Mass (g)	Density (g/cubic m)	Group
1	Meta-dabase	1545.4	1038.9	3.051135242	Miocene intrusive diabase
2	Meta-dabase	3464.1	2306.9	2.993518839	Miocene intrusive diabase
3	Meta-dabase	2364.3	1585.4	3.035434587	Miocene intrusive diabase
4A	argillite	822.7	519	2.70892328	Scout Mountain Member, argillite
4B	argillite	1306.7	821.7	2.694226804	Scout Mountain Member, argillite
5	Meta-dabase	3178	2097.2	2.940414508	Miocene intrusive diabase
6A	Slate	510.6	327.8	2.79321663	Scout Mountain Member, slate
6B	Slate	1064.5	682.3	2.785190999	Scout Mountain Member, slate
7	Pillow Basalt	1715.5	1047.3	2.567345106	Basalt (Bannock Volcanic)
8	argillite	952.1	580.7	2.563543349	Scout Mountain Member, argillite
9	Bannock Volcanic	1412.9	911.4	2.817347956	Bannock Volcanic
10A	Volcanic Breccia	2173.9	1410	2.845791334	Bannock Volcanic
10B	Volcanic Breccia	735.4	469.8	2.768825301	Bannock Volcanic
11	argillite	1810.9	1147.7	2.730548854	Scout Mountain Member
12A	Basalt	1868.8	1259.2	3.065616798	Bannock Volcanic
12B	Basalt	735.4	489.5	2.990646604	Bannock Volcanic
13	Bannock Volcanic	1743.8	1098.4	2.701890301	Bannock Volcanic
14	Meta-dabase	1726.5	1163.4	3.066062866	Miocene intrusive diabase
15	Meta-dabase	1543.3	1037.6	3.051809373	Miocene intrusive diabase
16	Bannock Volcanic	2962.1	1860.8	2.689639517	Bannock Volcanic
17	Meta-dabase	2623.3	1687.4	2.802970403	Miocene intrusive diabase